CHEMICAL REVIEWS

Review

pubs.acs.org/CR

Formation of Urban Fine Particulate Matter

Renyi Zhang,*[,†,§] Gehui Wang,[†,∥] Song Guo,[†,§] Misti L. Zamora,[†] Qi Ying,[‡] Yun Lin,[†] Weigang Wang,[†,⊥] Min Hu,[§] and Yuan Wang[#]

[†]Departments of Atmospheric Sciences and Chemistry and [‡]Department of Civil Engineering, Texas A&M University, College Station, Texas 77843, United States

[§]State Key Joint Laboratory of Environmental Simulation and Pollution Control, College of Environmental Sciences and Engineering, Peking University, Beijing 100871, People's Republic of China

[∥]Key Laboratory of Aerosol Physics and Chemistry, State Key Laboratory of Loess and Quaternary Geology, Institute of Earth Environment, and [⊥]State Key Laboratory for Structural Chemistry of Unstable and Stable Species, Beijing National Laboratory for Molecular Sciences (BNLMS), Institute of Chemistry, Chinese Academy of Sciences, Beijing 100864, People's Republic of China

[#]Jet Propulsion Laboratory, California Institute of Technology, Pasadena, California 91125, United States

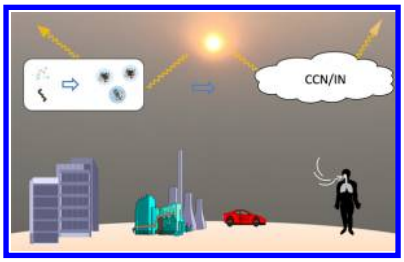

CONTENTS

1. Introduction 3803
2. Historical Perspectives 3806
2.1. London Fog 3806
2.2. Los Angeles Smog 3806
2.3. Beijing Haze 3806
3. Origins of Urban Fine PM 3807
3.1. Primary Emissions 3807
3.2. New Particle Formation 3808
4. Growth Processes 3809
4.1. Gas–Particle Partitioning of Organic Matter 3810
4.2. Particle-Phase Reactions of Organic Matter 3812
4.2.1. Hydration Reactions 3812
4.2.2. Acid-Catalyzed Reactions 3813
4.2.3. Reactions with Basic Species 3814
4.3. Sulfate Formation 3816
4.4. Nitrate Formation 3817
4.5. Aging of Primary Particles 3819
5. Atmospheric Measurements 3821
5.1. Analytical Techniques 3821
5.1.1. Gaseous Aerosol Precursor Measurements 3821
5.1.2. PM Measurements 3822
5.2. Analysis Approaches 3823
5.3. Spatial and Temporal Characteristics of the Number Concentration, Size, Chemical Composition, and Other Properties of Urban Fine PM 3825
5.3.1. Houston, TX 3825
5.3.2. Los Angeles, CA 3826
5.3.3. Mexico City, Mexico 3828
5.3.4. Beijing, China 3829
6. Atmospheric Modeling 3833
6.1. Primary PM and Gas Precursor Emissions 3833
6.2. Gaseous and Multiphase Chemistry 3834
6.2.1. Gas-Phase Photochemical Oxidation Mechanism 3834
6.2.2. New Particle Formation 3834
6.2.3. Multiphase Processes 3834
6.3. Regional Transport and Removal Processes 3835
7. Future Directions and Conclusions 3836
Author Information 3837
Corresponding Author 3837
Notes 3837
Biographies 3838
Acknowledgments 3839
Glossary of Acronyms 3840
References 3841

1. INTRODUCTION

Urban air pollution represents one of the greatest environmental challenges facing mankind in the 21st century.[1,2] Noticeably, many developing countries, such as China and India, have experienced severe air pollution because of their fast-developing economy and urbanization. Globally, the urbanization trend is projected to continue: 70% of the world population will reside in urban centers by 2050, and there will exist 41 megacities (with more than 10 million inhabitants) by 2030.[3] Air pollutants consist of a complex combination of gases and particulate matter (PM). In particular, fine PM (particles with the aerodynamic diameter smaller than 2.5 μm or $PM_{2.5}$) profoundly impacts human health, visibility, the ecosystem, the weather, and the climate,[1] and these PM effects are largely dependent on the aerosol properties, including the number concentration, size, and chemical composition. PM is emitted directly into the atmosphere (primary) or formed in the atmosphere through gas-to-particle conversion (secondary) (Figure 1).[4,5] Also, primary and secondary PM undergoes chemical and physical transformations and is subjected to transport, cloud processing, and removal from the atmosphere. The mechanisms leading to urban fine PM formation remain highly uncertain,[4−10]

Special Issue: 2015 Chemistry in Climate

Received: February 2, 2015
Published: May 5, 2015

DOI: 10.1021/acs.chemrev.5b00067
Chem. Rev. 2015, 115, 3803−3855

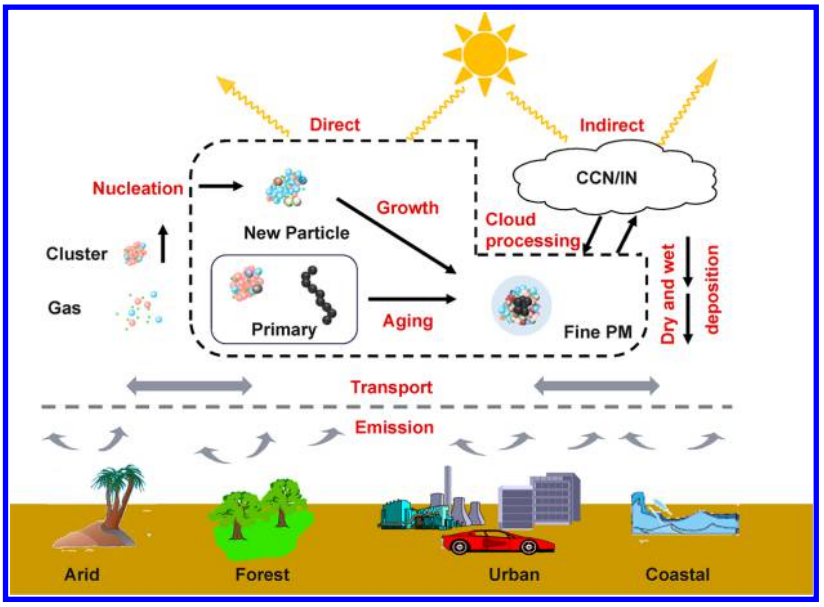

Figure 1. Schematic representation of the formation, growth, and processing of atmospheric aerosols.

particularly for the processes related to the PM origin and growth. For example, the chemical constituents of organic carbon (OC), sulfate, nitrate, ammonium, trace metals, and elemental carbon (EC) have been commonly identified in urban fine PM, reflecting the diverse primary and secondary sources from the traffic, industry, biosphere, and other anthropogenic activities, along with regional components from biomass burning and agricultural activities.[6,11,12] Since there exist a large number of natural and anthropogenic emission sources for urban PM, source apportionments are difficult and the currently available methodologies are rather inaccurate and often produce conflicting results.[6−8] The deficiencies in our understanding of urban fine PM formation hinder the developments of predictive atmospheric models to simulate urban pollution episodes and efficient mediation policies to minimize its local, regional, and global impacts.

Urban fine PM has been unequivocally associated with adverse human health impacts.[2] The human health effects of fine PM range from aggravating allergies to the development of serious chronic diseases and premature death.[13−17] Both epidemiological and toxicological studies have indicated that smaller particles are more closely linked with adverse health outcomes than larger ones.[18] Although ultrafine particles (less than 100 nm) contribute negligibly to the total ambient PM mass, they are typically present in high number concentrations under urban environments and have a higher probability than larger particles to deposit in the pulmonary region after inhalation. In addition, fine PM can enter extrapulmonary tissues (e.g., the heart, reproductive tract, and intestine) through blood circulation. For ultrafine particles, organs beyond the lungs, such as the heart, reproductive tract, intestine, brain, and liver, are also considered as targets.[19] A large surface area of ultrafine PM, a high redox capacity, and the ability to form radical species are thought to induce inflammatory effects, cause cellular DNA damage, or inhibit the anti-inflammatory capacity of plasma high-density lipoprotein and macrophage phagocytosis.[20,21]

The PM toxicity derives not only from the physical presence of particles on biological tissues, but also from the toxic effects of PM chemical constituents, including hygroscopic inorganic electrolytes, polycyclic aromatic hydrocarbons (PAHs), polychlorinated biphenyls (PCBs), EC (i.e., soot), crustal materials, and metals. For example, EC as a pervasive component in urban fine PM exhibits significant toxicity[22] and is routinely considered by epidemiological studies in evaluation of the PM adverse health effects.[23−26] Knowledge of detailed chemical compositions and physical properties of particles is crucial to assess the health impacts, since the biological responses to PM are not always linked with major constituents, but rather with toxicologically potent minor components.[18]

Presently, residents in urban areas around the world frequently experience severe asthma and a decreased lifespan among many other health issues.[27−29] Long-term exposure to fine PM has been associated with a 6% increase in the risk of premature death.[15,30] In China, more than 20 million cases of respiratory illnesses were reported in 2007.[31] The World Health Organization indicated that globally over 800 000 deaths occurred as a result of poor outdoor air quality in 2005.[32] Other estimated numbers of global premature deaths are substantially higher, i.e., 1.4 million for 2010 and rising to 3.6 million by 2050 (ref 33) and 2.8−3.6 million in 2010 (ref 34).

Aerosols originated from the urban regions also exhibit a broad range of impacts on the atmosphere, directly by interfering with the solar radiative transfer and indirectly by influencing cloud formation.[1,2] Specifically, those particles modify the lifetime and albedo of clouds, precipitation, and lightning,[35−41] modulate photochemistry,[42−44] promote multiphase chemistry,[5,46−48] degrade local, regional, and global air quality,[48,49] and ultimately impact the Earth energy budget.[1] By serving as cloud condensation nuclei (CCN) or ice nuclei (IN), aerosols influence the macro- and microphysical properties of clouds[50−52] and regulate the cloud lifetimes and the precipitation efficiency.[53−58] Atmospheric measurements and modeling studies have revealed invigorated convective clouds resulting from elevated aerosol levels over urban regions.[50,53] Also, the aerosol effects on urban precipitation have been shown to increase the rainfall rate under clean conditions but decrease the rainfall rate under polluted conditions, suggesting a plausible distinction of the aerosol effects on precipitation between developed and developing countries.[50] Presently, the estimates of the cloud adjustment by aerosols range from 0.06 to 1.33 W

DOI: 10.1021/acs.chemrev.5b00067
Chem. Rev. 2015, 115, 3803−3855

Figure 2. View of the Los Angeles Civic Center masked by smog in 1948. (Photo: Los Angeles Times; Photographic Archive/UCLA, http://digital2.library.ucla.edu/viewItem.do?ark=21198/zz0002tsmb). Copyright 1948 Los Angeles Times (http://creativecommons.org/licenses/by/4.0/).)

m^{-2} in the global radiative forcing budget on the top of the atmosphere, representing the largest uncertainty in climate projections of anthropogenic activities.[1] In addition, long-range transport of urban and regional PM from Asia has been implicated in climatically altered midlatitude cyclones over the Pacific Ocean.[59−61] Furthermore, anthropogenic aerosols have been illustrated to result in delayed development, weakened intensity, and early dissipation, but an enlarged rainband and increased precipitation for tropical cyclones under polluted conditions.[62]

The aerosol−cloud interaction corresponds to one of the most poorly represented processes in atmospheric models, because of largely varying aerosol properties under diverse environmental conditions. For example, the CCN activation efficiency of aerosols to form cloud droplets is dependent on hygroscopicity, which is related to the particle size and chemical compositions.[63−65] In addition, atmospheric aging of primary and secondary PM considerably modifies the hygroscopicity, because of increased coating by inorganic and organic species from the secondary formation processes.[66] A change in the particle hygroscopicity also impacts the atmospheric lifetime of aerosols, since wet deposition represents one of the key removal processes for aerosols. On the other hand, cloud-processing of gaseous species has been suggested to account for an important fraction of the tropospheric aerosol loading.[5,45]

The optical effects of aerosols also impact visibility and air quality. In addition to scattering light, certain aerosol types, such as black carbon (BC), mineral particles, and brown carbon, are light absorbing.[67,68] Enhanced light absorption and scattering by aerosols stabilize the atmosphere, resulting in a negative feedback on air quality and inhibition of cloud formation.[69] Furthermore, the direct and indirect effects of urban aerosols on clouds often operate in the opposite directions.[36]

Although there have existed several comprehensive reviews on the topic of formation and growth of atmospheric aerosols,[4,5,9,10,70,71] few have been focused specifically on the subject of urban fine PM. This review emphasizes the fundamental chemical aspects relevant to urban PM formation, particularly the processes governing the particle number, size, and chemical compositions. The similarities and differences in urban fine PM between different world regions and compared to those of pristine environments are discussed and attributed to the distinct aerosol formation and growth mechanisms under diverse environmental conditions.[4] Since there is a large body of literatures in the area of atmospheric urban aerosols, we do not attempt to be inclusive to cover all available publications on this subject. Instead, we intend in this review to focus on the studies that contribute to the most important advances in the understanding of the urban PM formation.

In section 2, we briefly introduce a historical perspective of urban PM pollution, including those that occurred in London, Los Angeles, and Beijing. The similarities and differences in the severe PM episodes between the three locations are compared, and some regulatory implications are discussed. The various origins contributing to the number concentrations of urban fine PM, including from primary emissions and new particle formation, are described in section 3. The mechanisms contributing to the secondary growth of urban fine PM are presented in section 4, emphasizing the formation of organic matter, sulfate, nitrate, and basic species. Section 5 summarizes atmospheric measurements of urban PM properties, including the analytical techniques, analysis methods, and aerosol characteristics in four urban regions (i.e., Houston, Los Angeles, Mexico City, and Beijing). Those locations are selected not only to reflect the diverse geography, economic developing stages, and PM emission sources, but also to represent the sites where some of the most intensive atmospheric chemistry field measurements have been conducted. Section 6 summarizes the current numerical approaches to quantitatively simulate urban fine PM in atmospheric models. Section 7 contains the concluding remarks and describes future research needs. A glossary of acronyms is provided at the end of the review.

DOI: 10.1021/acs.chemrev.5b00067
Chem. Rev. 2015, 115, 3803−3855

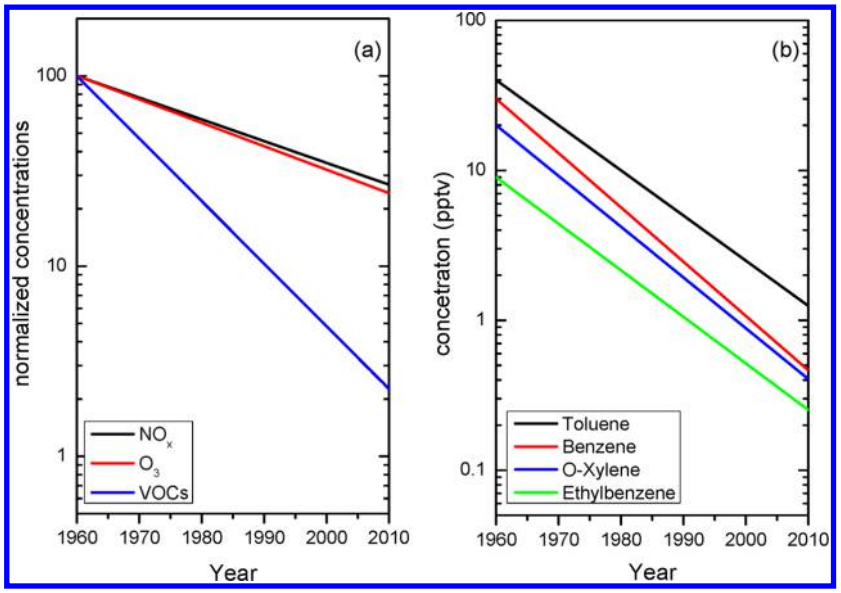

Figure 3. Long-term trends of ambient concentrations of VOCs, NO_x, and O_3 in Los Angeles. (a) NO_x (black line), O_3 (red line), and VOCs (blue line) are linear least-squares fits to log-transformed data. The data are normalized so that the linear fits intersect 100 in 1960. (b) Toluene (black line), benzene (red line), *o*-xylene (blue line), and ethylbenzene (green line) are linear least-squares fits to the measurements, representing the long-term trends in the abundances of aromatics. All data and fitted slopes are taken from refs 79 and 80.

2. HISTORICAL PERSPECTIVES

2.1. London Fog

The Great Fog of London during Dec 5−8, 1952, was one of the first-recognized and most severe air pollution episodes in the world.[72] Extremely high levels of PM (2−4 mg m^{-3}) and SO_2 (1 ppm), which were emanated from coal burning of house heating and power generating, were estimated during the London Fog episode.[73] The lethal London Fog of 1952 was initially estimated to result in over 4000 premature deaths and more than 10 000 illnesses.[74] A reassessment of the toxic 1952 London Fog further revealed that about 12 000 excess deaths occurred from December 1952 through February 1953 due to acute and persisting effects of the fog.[75] In response to the 1952 Great Fog in London, a Clean Air Act (CAA) was promulgated by the Parliament of the United Kingdom in 1956, introducing a number of regulatory measures to reduce air pollution. The 1956 CCA was extended in 1968, and both acts were repealed and consolidated in 1993. The 1952 London Fog represents one of the most significant environmental events, in terms of its effects on environmental research, government regulation, and public awareness of the relationship between air quality and human health.

Although pollutants emitted from coal combustion have been significantly reduced since the 1950s, air pollution in London and other cities in England persists. For example, sharp growth in road traffic resulted in another pollution episode in December 1991, with measurable increased mortality and hospital admissions.[75] An intensive observation conducted in 2006−2007 showed that the major part (~65% in mass) of PM_{10} (particles with the aerodynamic diameter smaller than 10 μm) in London is composed of $PM_{2.5}$, with sulfate, nitrate, and carbonaceous materials as the dominant species and largely formed from traffic related emissions.[76,77]

2.2. Los Angeles Smog

As early as in 1940, Los Angeles had more than a million vehicles, and that number was more than doubled 10 years later as the postwar population and economy boomed. The first recognized smog episode in Los Angeles occurred in 1943, and severe air pollution episodes with high levels of PM and ozone occurred regularly in the summer seasons of the 1940s and 1950s (Figure 2). Air pollution in Los Angeles is often refereed to as the photochemical smog, which is formed in the presence of sunlight from the chemical reactions involving nitrogen oxides (NO_x = NO + NO_2) and volatile organic compounds (VOCs), both of which are mainly produced from traffic emissions.

Since the 1950s, the summertime photochemical smog in Los Angeles has been the subject of extensive air pollution control efforts.[78] Because vehicular traffic represents the major sources in the Los Angeles Basin, control strategies on VOCs and NO_x emissions from the vehicular sources have the greatest potential to reduce the PM and ozone levels. Figure 3 shows that normalized NO_x and VOC concentrations have been reduced by 70−80% and more than 90% from 1960 to 2010, respectively.[79,80] Warneke et al.[81] analyzed the decadal trend of different VOC types in Los Angeles between 1960 and 2010, showing reduced concentrations of aromatic hydrocarbons (i.e., benzene, toluene, and xylenes) from several tens of to a few parts per billion from 1960 to 2010 and reduced VOC emissions by nearly an order of magnitude from gasoline-fueled vehicles in Los Angeles since 1960. Those atmospheric measurements have clearly demonstrated the efficacy of the implementation of the major federal, state, and local regulations on vehicle emission control in Los Angeles.[82] Over the past decade, the annual mean level of $PM_{2.5}$ in Los Angeles has decreased from 20 μg m^{-3} in 2000 to 11 μg m^{-3} in 2013.[79,80] However, the annual mean level of ozone only exhibits a slight decline (Figure 3), with values of 88 ppb in 2000 and 74 ppb in 2013. Nevertheless, the experience in successfully mediating fine PM in Los Angeles by reducing traffic-related VOC and NO_x emissions yields invaluable hints for many developing countries in development of regulatory policies to control urban fine PM levels.

2.3. Beijing Haze

Beijing has undergone rapid expansions in economy and urbanization over the past several decades. From 2009 to 2013,

DOI: 10.1021/acs.chemrev.5b00067
Chem. Rev. 2015, 115, 3803−3855

Figure 4. Campus view of Peking University on clean and polluted days.

Table 1. Comparison between the Historical Pollution Episodes in London, Los Angeles, and Beijing

	London	Los Angeles	Beijing
type of smog	sulfurous	photochemical	photochemical
observed	1800s to 1950s	1940s to present	1990s to present
meteorological conditions	strong inversion layer, low winds, cloudy, cold, winter	sunny, warm, dry, inversion layer, summertime	low winds typically from the south, year-round
pollutants	SO_2, soot, and PM	NO_x, VOCs, ozone, and PM	NO_x, VOCs, SO_2, and PM
source of pollutants	coal burning from house heating and power generation	vehicles	vehicles and industrial sources

the gross domestic product (GDP) in Beijing increased from $203 to $325 billion, and vehicles in the city have increased from 4.0 to 5.4 million.[6,83] Beijing has suffered from deteriorated air quality since the 1990s, with exceedingly high PM levels (Figure 4).[6,7,84,85] For example, in 2013 the annual level of $PM_{2.5}$ in Beijing was 102 $\mu g\ m^{-3}$, with the daily maximum $PM_{2.5}$ value reaching 568 $\mu g\ m^{-3}$; there were more than half of the days when the daily maximum $PM_{2.5}$ concentration exceeded 300 $\mu g\ m^{-3}$ in January. Haze in Beijing occurs in all seasons; the occurrence of haze episodes is more frequent and severe in wintertime, because of increased pollutant emissions from coal combustion for house heating and unfavorable meteorological conditions. Since the 1990s, the Chinese government has implemented major measures to improve air quality in Beijing, by relocating power plants and industrial factories away from the city, replacing coal by clean energy such as electricity and natural gas, and promulgating stricter traffic emission standards.[83] Primary PM emissions from industry have been significantly reduced, but secondary fine PM has remained elevated, because of the presence of high levels of gaseous precursors from urban transportation and regional industrial facilities.[6] As summarized in Table 1, the characteristics of air pollution in Beijing are distinct from those occurring in London, but exhibit a similarity to those in Los Angeles. It has been suggested that regulatory controls of gaseous emissions for VOCs and NO_x from local transportation and SO_2 from regional industrial sources represent the key steps to reduce the urban PM level in Beijing.[6]

3. ORIGINS OF URBAN FINE PM

3.1. Primary Emissions

The primary PM emissions are wide-ranging, from both natural sources and anthropogenic sources, although urban primary PM is mainly from anthropogenic sources (Figure 5).[86−96] For

DOI: 10.1021/acs.chemrev.5b00067
Chem. Rev. 2015, 115, 3803−3855

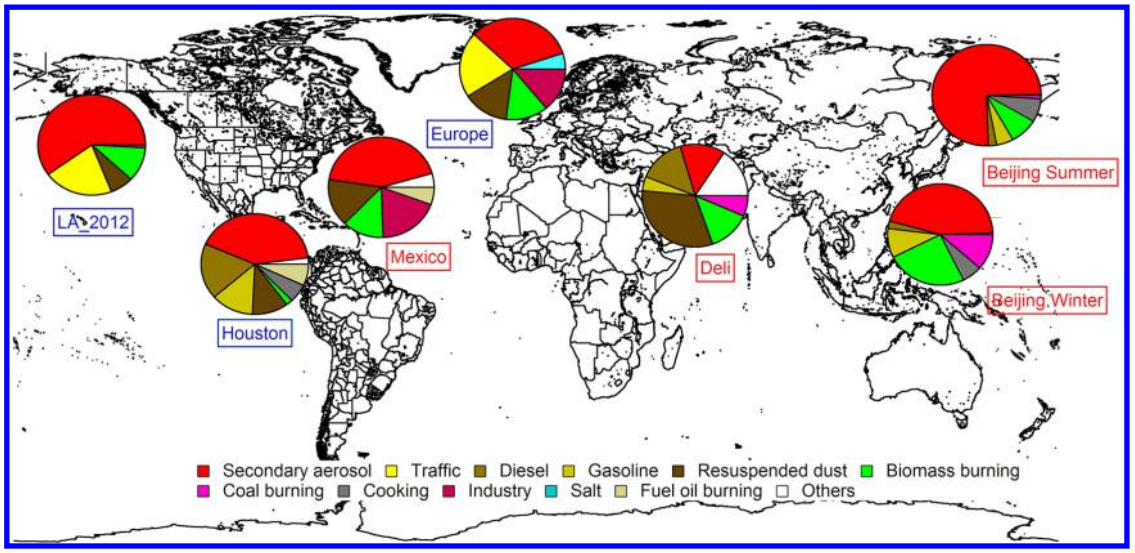

Figure 5. Source contributions of fine urban PM at several cities of developed and developing countries, including Houston, Los Angeles, Mexico City, and Beijing. The results in Europe and Deli are also shown for comparison. The data are taken from refs 86−96.

instance, over 70 primary PM sources have been identified in Los Angeles,[86] including vehicle emission, industrial fuel combustion, domestic heating, meat cooking, and biomass burning. Some of the primary PM sources are further divided: vehicle emissions are divided into gasoline and diesel vehicles, and biomass burning includes fireplace wood burning, open wood burning, and straw burning.

An early study by Schauer et al.[87] apportioned the $PM_{2.0}$ (particles smaller than 2 μm) sources in Los Angeles from 1982 by using chemical mass balance (CMB) modeling. Primary PM emissions were found to be the dominant source of ambient fine PM (about 60%). Diesel exhaust, paved-road dust, and gasoline-powered vehicle exhaust were the major contributors to primary fine PM in Los Angeles, followed by cooking and wood smoke, and other sources, including cigarette smoke, tire wear debris, and vegetative detritus. A recent study summarized the source apportionment results of the ambient fine PM in Los Angeles from 2002 to 2012:[88] Secondary inorganic formation, i.e., sulfate, nitrate, and aged sea salt, represents the major contributor to fine PM, and in some months the secondary contribution is more than 70%. Traffic emissions are the most important primary PM source, accounting for about 31% of the primary organic PM. However, the traffic contribution exhibits a significant decrease after 2007, due to the implementation of major regulations. Wood burning also represents a significant source of primary PM.

Fraser et al.[89] analyzed aerosol samples collected during the course of one year in Houston and apportioned the fine PM sources using CMB. Secondary inorganic aerosols are found to contribute 42% of the particles, followed by vehicle emissions (diesel car, 18%; gasoline car, 13%). Due to the large amount of vehicles, road dust represents another important fine PM source in Houston, accounting for 11% of the total $PM_{2.5}$ mass.

Aiken et al.[90] compared the source apportionment results of organic aerosols in Mexico City by aerosol mass spectrometry−positive matrix factorization (AMS−PMF) and CMB of organic molecular markers (CMB-OMM). Both results indicate that secondary organics are dominant in organic aerosols (58%). Another source apportionment study by using PMF also suggested that secondary formation is important to fine PM in Mexico City, accounting for 43% of PM_1 (i.e., particles smaller than 1 μm).[91] Vehicle emission and wood burning represent the important fine primary PM sources, accounting for 29% and 12% of the particulate organic matter. Road dust is also an important source of PM due to the presence of unpaved roads and a high volume of vehicles. Industrial sources are also found to significantly contribute to the PM_1 mass.[90,91]

Guo et al.[92] summarized the source apportionment results from 2000 to 2008 in Beijing: secondary formation represents the major fine PM source, except in the winter heating period when the primary PM contribution is comparable to the secondary formation. Traffic emissions represent the most important primary PM sources in Beijing in the early part of the decade; however, several control measures of vehicle emissions have been implemented since the 2008 Olympic Games, resulting in a decreased total vehicle contribution. Coal combustion also significantly contributes to the ambient fine PM, particularly during the winter. Cooking emission contributes up to 10% of fine PM.[93] The contribution of biomass burning is highly seasonal and may be important during the harvest seasons (i.e., spring and fall).

3.2. New Particle Formation

Aerosol nucleation has been measured under diverse environmental conditions, and globally new particle formation (NPF) accounts for about 50% of the aerosol number production in the troposphere.[4,97] Atmospheric field measurements have revealed that NPF is responsible for a major fraction of particle number concentrations observed under urban environments.[6,98−100] A comprehensive review on the subject of NPF can be found elsewhere,[4] and we focus below on the aspects relevant to aerosol nucleation under urban conditions.

NPF occurs in two distinct stages, i.e., nucleation to form a critical nucleus and subsequent growth of the freshly nucleated particle to a larger size. On the basis of thermodynamic and kinetic considerations, aerosol nucleation includes two major limitations: a free energy barrier needs to be overcome prior to spontaneous transformation to the new phase, and the growth of freshly nucleated particles is limited by the Kelvin effect because of significantly elevated equilibrium vapor pressures over nanoparticles. In addition, the growth process competes with capture/removal of nanoparticles by coagulation with pre-existing aerosols.[101] The nucleation rate is related to the chemical

DOI: 10.1021/acs.chemrev.5b00067
Chem. Rev. 2015, 115, 3803−3855

composition of the critical nucleus and the gaseous concentrations of the nucleating species,[102] representing an important variable in simulations of urban fine PM number concentrations in atmospheric models.[103]

Much of the earlier research has focused on nucleation of sulfuric acid, since sulfate represents an important component of the nucleation mode aerosols.[104] The presence of sulfuric acid in concentrations exceeding 10^5–10^7 molecules cm^{-3} has been shown as a necessary condition to observe NPF in the atmosphere.[105] Field measurements in an urban location reveal a weak dependence of the nucleation rate on sulfuric acid concentrations, implying that only 1–2 H_2SO_4 molecules are present in the critical clusters.[106] From the available laboratory measurements, binary H_2SO_4 nucleation has been recognized as incapable of explaining atmospheric nucleation events, and several alternative nucleation mechanisms have been proposed, including ternary nucleation of sulfuric acid with ammonia and water, ion-induced nucleation, and nucleation involving iodine species.[4,107] However, none of those mechanisms provide a consistent explanation of aerosol nucleation under a wide range of environmental conditions.

A number of more recent studies have suggested that other stabilizing species are involved in aerosol nucleation and are present in the critical nucleus.[4,5] For instance, organic compounds from anthropogenic and biogenic sources may assist the nucleation process directly, e.g., by amines,[108−110] or following atmospheric photo-oxidation, such as by organic acids from aromatics[111,112] and monoterpenes.[113] The presence of 10^8–10^9 molecules cm^{-3} levels of organic acids considerably enhances nucleation of the water–sulfuric acid system via formation of strongly hydrogen-bonded clusters containing one organic molecule and several molecules of sulfuric acid and water.[113,114] The contribution from organic acids likely explains the high aerosol concentrations observed in polluted urban environments,[103] where large concentrations of organic acids can be produced by direct emissions and by photochemical oxidation of hydrocarbons. It has been further suggested that organic aerosol nucleation through the formation of stable dimers from monocarboxylic acids alone under atmospherically relevant concentrations may not occur in the absence of sulfuric acid,[113] because monocarboxylic acid dimers have no vacant hydrogen acceptor/donor groups to promote subsequent cluster growth and cannot be stabilized by forming strongly bonded hydrates.[114,115] Most recently, experiments conducted at the Cosmics Leaving Outdoor Droplets (CLOUD) chamber have also shown the important role of oxidized organic compounds in atmospheric aerosol nucleation.[116]

Typically, severe urban PM pollution inhibits the occurrence of aerosol nucleation events, since high levels of pre-existing particles suppress the nucleation and growth of freshly nucleated particles through capture via coagulation or providing a large surface for removal of the aerosol nucleating precursors. Aalto et al.[117] concluded that NPF hardly occurs under a polluted condition when the aerosol surface area exceeds 100 μm^2 cm^{-3}. Wang et al.[118] showed that reduced PM pollution during the 2008 Olympic Games enhanced the frequency of NPF events due to fewer pre-existing particles. Interestingly, NPF events have been frequently observed in many urban areas of China.[119] The efficient occurrence of NPF in urban regions may be explainable because of the presence of high levels of aerosol nucleation precursors, such as sulfur dioxide, ammonia, amines, and anthropogenic VOCs.[4,6,100,103]

In addition to primary emissions and NPT, two other processes exist which also regulate the PM number concentrations, i.e., coagulation and cloud-processing.[4,5] While coagulation represents a sink for the PM number concentration, cloud-processing either increases or decreases the PM number concentration. By acting as CCN and IN or through in- and below-cloud scavenging, aerosols are incorporated into atmospheric hydrometeors (i.e., fog and cloud droplets, rain drops, and ice crystals). Also, uptake of gaseous reactive or water-soluble organic and inorganic compounds by clouds can significantly shift their partitioning toward the condensed phase. For precipitating clouds, cloud-processing leads to irreversible removal of both gaseous and PM pollutants from the atmosphere, but PM is re-emitted or generated from evaporation of non-precipitating clouds. The mechanisms of cloud-processing for gases are similar to those of multiphase chemical processes for organic and inorganic species (except for close to neutral pH conditions), to be discussed in the next section.

4. GROWTH PROCESSES

Atmospheric measurements have revealed that urban fine PM typically consists of large amounts of secondary constituents, including organic matter, sulfate, nitrate, and ammonium.[6,8] The formation of the particle-phase organic matter, sulfate, and nitrate is attributable to emissions of VOCs, SO_2, and NO_x, respectively.[6] Under the urban environments, there exist high VOC emissions from anthropogenic and biogenic sources, and photochemical oxidation of VOCs leads to formation of a variety of semi- and nonvolatile products,[120−125] some of which engage in the gas-to-particle conversion processes to contribute to the growth of particle organic matter.[5] The gas-phase oxidation of VOCs is initiated by reactions with radicals (e.g., OH, NO_3, or ozone). In particular, VOC oxidation initiated by OH during the daytime produces a number of organic products of oxygenated functional groups, such as aldehyde, ketone, alcohol, carboxylic acid, hydroperoxide, percarboxylic acid, and peroxyacyl nitrate groups.[126,127] The relative abundance of these product formations is dependent on the VOC structure, NO_x level, temperature, relative humidity (RH), and solar intensity.[5] Some compounds formed in the first oxidation step undergo further oxidation reactions, yielding additional functional groups and resulting in multigenerations of products that are of lower volatility and higher solubility in comparison with their parent compounds.

For example, aromatic hydrocarbons (i.e., toluene, xylenes, and trimethylbenzenes) constitute an important fraction (20% or higher) of the total VOCs in the urban atmosphere.[5,6,128] Emissions of aromatic hydrocarbons are primarily from anthropogenic sources, i.e., from automobiles, fuel-based vehicles, and industry. Depending on the locations and emission sources, the urban toluene concentration ranges from 1 to 200 ppb.[6,128,129] Aromatics react exclusively with the OH radical, with a lifetime of 0.5–2.5 days.[130−134] Previous experimental and theoretical studies have indicated the OH–aromatic reactions lead to the formation of a variety of ring-opening (e.g., glyoxal and methylglyoxal) and ring-retaining (e.g., benzaldehyde and cresol) products.[130−136] Secondary organic aerosol (SOA) formation on pre-existing ammonium sulfate aerosols from toluene–OH oxidation products has been evaluated with an SOA yield of 30% in low-NO_x conditions, independent of the initial toluene concentration.[137] In addition, the oxidation products of aromatics alter the composition and properties of

DOI: 10.1021/acs.chemrev.5b00067
Chem. Rev. 2015, 115, 3803−3855

BC particles and lead to increased particle density, hygroscopicity, and optical properties.[138]

Formation of organic matter is a complex multiphase process and represents one of the most poorly understood topics and a frontier area in atmospheric chemistry research. A conventional view is that SOA formation is dominated by absorptive partitioning of low-volatility and semivolatile oxidation products associated with VOC emissions.[139,140] Atmospheric models, however, greatly underestimate the SOA mass measured in field studies.[141,142] Several factors have been suggested to explain the observed inconsistencies between modeled and measured SOA yields, including incorrect emission inventories, missing precursors, and unaccounted processes of gas-to-particle conversion. The latter topic has received particularly close attention because of the evidence from laboratory[143−146] and field[147] studies showing that heterogeneous reactions of oxygenated organics, such as α-dicarbonyls and large aldehydes, produce functionalized and higher molecular weight species with lower saturation vapor pressures and shift the physical partitioning equilibrium to increase SOA yields. Some of those aqueous-phase reactions (such as aldol condensation of large aldehydes) require catalysis by a strong acidic medium,[46,148] while others occur in low-acidity or even pH-neutral solutions (such as oligomerization of α-dicarbonyls).[145,149] In addition, the multiphase reactions of organic species considerably modify the hygroscopicity and contribute to browning of the organic matter.[67,150]

In this section, the currently recognized pathways leading to the formations of secondary organic matter, sulfate, and nitrate relevant to urban environments are discussed.

4.1. Gas−Particle Partitioning of Organic Matter

Semivolatile organic compounds (SVOCs) undergo partitioning between the gas and particle phases. The gas−particle partitioning includes two processes: physical adsorption and absorption. The absorptive partitioning is typically important in urban areas, except for that the OC to TSPs (total suspended particles) ratio is low. The SVOCs can partition into the condensed phase, even though the ambient gas-phase concentrations are lower than their saturation vapor pressures in accordance with the Raoult's law.

The flux of gaseous species diffusing toward a particle is calculated from[47]

$$J = \frac{\rho_p}{M_A}\frac{d}{dt}\left(\frac{4}{3}\pi R_p^3\right) \tag{4.1}$$

where ρ_p is the density of the particle, M_A is the molecular weight of the gaseous species, and $R_p = {}^1/_2 D_p$ is the radius of the nanoparticle. For fine PM, the kinetic regime applies to the growth equation, since the Knudsen number, Kn, which is defined as the ratio between the mean free path (λ) and R_p, is significantly larger than unity:[5]

$$J = J_k = \pi R_p^2 \omega \gamma (c_\infty - c_s) \tag{4.2}$$

where c_∞ is the molar concentration at an infinity distance from the particle, c_s is the molar concentration near the particle surface, ω is the thermal speed, and γ is the uptake coefficient of the gas species. Combining eqs 4.1 and 4.2 yields the particle growth rate

$$\frac{dR_p}{dt} = \frac{\gamma \omega M_A}{4\rho_p}(c_\infty - c_s) \tag{4.3}$$

When Kn is significantly smaller than 1, the particle can be treated with the continuum mechanics, and the growth rate is expressed as

$$\frac{dR_p}{dt} = \frac{D_g M_A}{\rho_p R_p}(c_\infty - c_s) \tag{4.4}$$

where D_g is the gas-phase diffusion coefficient. If $Kn \approx 1$, the particle is in the transition regime, and both the mass uptake and gas-phase diffusion need to be considered. The c_∞ and c_s concentrations of the gas species decrease and increase with time, respectively. At sufficiently longer times, the two quantities equal each other, and the particle growth ceases. Typically, because of efficient gas-phase diffusion, equilibrium between gaseous species and aerosols is closely maintained.[151,152]

Pankow developed an absorption model for partitioning of organic compounds between the gas and particle phases based on the thermodynamic equilibrium principle.[153,154] At equilibrium, the chemical potentials of species i in the gas phase ($\mu_{i,g}$) and particle phase ($\mu_{i,om}$) are equal:

$$\mu_{i,g} = \mu_{i,om} \tag{4.5}$$

Assuming all the components in the particle phase are well-mixed (i.e., no phase separation in the particle phase), the chemical potentials of species i in the gas and particle phases are expressed respectively as

$$\mu_{i,g} = \mu_{i,g}^0 + RT \ln\left(\frac{P_i}{P_{i,L}^0}\right) \tag{4.6}$$

$$\mu_{i,om} = \mu_{i,pure}^0 + RT \ln(\zeta_i X_{i,om}) \tag{4.7}$$

where P_i is the vapor pressure for i, $P_{i,L}^0$ is the saturation vapor pressure of i over its pure liquid state, ζ_i is the activity coefficient, and $X_{i,om}$ is the mole fraction of component i in the particle phase. Under the chemical equilibrium for the pure component i between the gas and particle phases, the following equation holds:

$$\mu_{i,g}^0 = \mu_{i,pure}^0 \tag{4.8}$$

Combining eqs 4.5, 4.6, 4.7, and 4.8 leads to the following equation (i.e., the modified Raoult's law):

$$\frac{P_i}{P_{i,L}^0} = \zeta_i X_{i,om} = \frac{n_{i,g}}{VP_{i,L}^0}RT = \zeta_i \frac{n_{i,om}}{n_{om}} \tag{4.9}$$

where $n_{i,g}$ is the number of moles of i in the gas phase, $n_{i,om}$ is the number of moles of i in the particle phase, and n_{om} is the total number of moles of the organic compounds in the particle phase. Further arrangement of the above equation with the ideal gas law yields

$$\frac{n_{i,g}}{VP_{i,L}^0}RT = \frac{A_i}{P_{i,L}^0 MW_i}RT \tag{4.10}$$

$$\zeta_i \frac{n_{i,om}}{n_{om}} = \zeta_i \frac{F_{i,om}}{MW_i}\frac{1}{(TSP)f_{om}/MW_{om}} \tag{4.11}$$

where A_i is the mass concentration of i in the gas phase, $F_{i,om}$ is the mass concentration of i in the aerosol phase, TSP is the mass of total suspended particulate, MW_{om} is the average molecular weight of the aerosol phase, and f_{om} is the soluble mole fraction in

DOI: 10.1021/acs.chemrev.5b00067
Chem. Rev. 2015, 115, 3803−3855

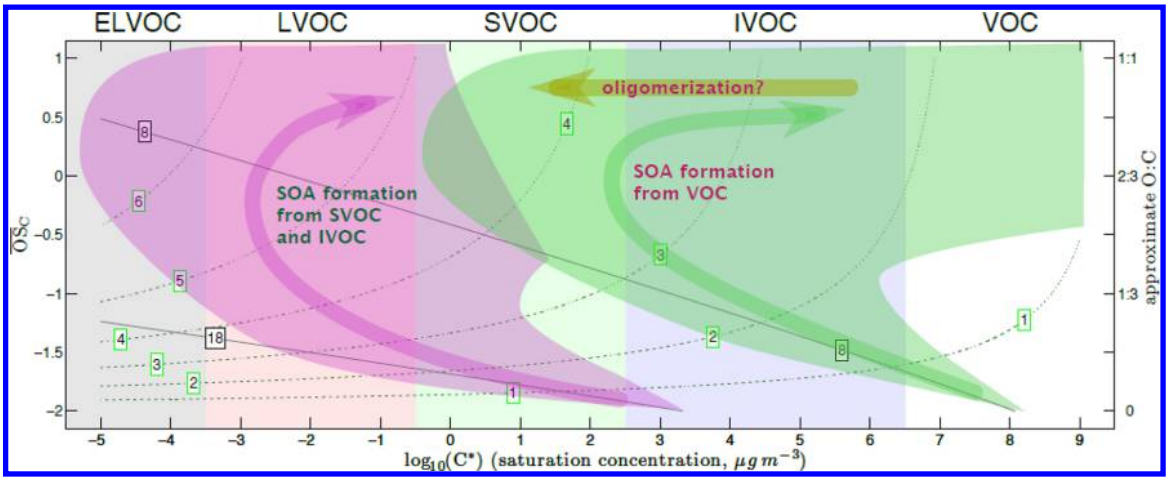

Figure 6. Two reaction trajectories in 2D space. Contours are the carbon number (gray) and oxygen number (dashed green). SOA formed from VOCs (shown at C_8) moves rapidly upward in $\overline{OS}_C$ but reaches a minimum in C^* only barely sufficient to form any SOA in the atmosphere. SOA formed from SVOCs and IVOCs (shown at C_{18}) moves more slowly upward in $\overline{OS}_C$ but reaches very low C^* values. Both trajectories ultimately result in complete fragmentation (in the limit where the chemistry is allowed to continue to completion), and both consist of a cloud of individual reaction pathways initially centered on the mean carbon contour for the parent carbon number. A potential oligomerization trajectory is shown as well. Reprinted with permission from ref 157. Copyright 2012 Copernicus Publications.

the aerosol phase (i.e., the fraction of the particle mass for the dissolved gas). Combining eqs 4.10 and 4.11 yields

$$\frac{A_i}{P^0_{i,\mathrm{L}}\mathrm{MW}_i}RT = \zeta_i\frac{F_{i,\mathrm{om}}}{\mathrm{MW}_i}\frac{1}{(\mathrm{TSP})f_{\mathrm{om}}/\mathrm{MW}_{\mathrm{om}}} \tag{4.12}$$

The partitioning coefficient ($K_{\mathrm{p},i}$) for species i is given by

$$K_{\mathrm{p},i} = \frac{F_{i,\mathrm{om}}/\mathrm{TSP}}{A_i} = \frac{f_{\mathrm{om}}RT}{\mathrm{MW}_{\mathrm{om}}\zeta_i P^0_{i,\mathrm{L}}} \tag{4.13}$$

Odum et al.[155] employed the absorption partitioning model to evaluate the SOA formation in environmental chamber studies and developed the expression for the fractional aerosol yields (Y):

$$Y = \frac{\Delta M_{\mathrm{o}}}{\Delta\mathrm{VOC}} \tag{4.14}$$

where ΔM_{o} is the organic aerosol mass concentration produced from the reaction of a given amount of VOC consumed (ΔVOC). One of the important assumptions in the partitioning approach is that the concentrations of different products produced from photo-oxidation are proportional to the total amount of VOCs reacted. The overall yield is connected with the partitioning coefficient by using the multicomponent absorptive partitioning:

$$Y = \sum_i Y_i = M_{\mathrm{o}}\sum_i\left(\frac{\alpha_i K_{\mathrm{om},i}}{1 + K_{\mathrm{om},i}M_{\mathrm{o}}}\right) = M_{\mathrm{o}}\sum_i\left(\frac{\alpha_i K_{\mathrm{p},i}/f_{\mathrm{om}}}{1 + K_{\mathrm{p},i}M_{\mathrm{o}}/f_{\mathrm{om}}}\right) \tag{4.15}$$

where M_{o} is the organic aerosol mass concentration and α_i is one mass-based stoichiometric coefficient. $K_{\mathrm{om},i}$ is the partitioning coefficient of species i, which equals the ratio of $K_{\mathrm{p},i}$ to the absorbing organic mass concentration. The two-product yield method has been used to fit the SOA yield from photo-oxidation of different individual and mixture VOCs (by adjusting the saturation vapor pressures) and performs well with the smog chamber experiments.[155] However, the chamber results need to be carefully evaluated, when extrapolated to atmospheric conditions, because of higher precursor concentrations, wall effects, and a shorter time (i.e., mainly for first-generation products) in smog chamber experiments. Also, only two kinds of compounds are defined in the two-product scheme, and little information on the molecular structures of the products is provided. In addition, the assumption of a constant ratio of products is invalid with the changes in temperature and oxidant levels.

To treat both semivolatile primary OC and SOA and continuing oxidation of SVOCs, Donahue et al.[140] have developed a partitioning method using the volatility basis set (VBS). The expression by Pankow[153,154] is modified using C^* to replace the partitioning coefficient as the x axis in the one-dimensional volatility basis set (1D-VBS) framework, which is the inverse of $K_{\mathrm{p},i}$ from eq 4.13:

$$C_i^* = \frac{C_i^{\mathrm{vap}}C_{\mathrm{OA}}}{C_i^{\mathrm{aer}}} = \frac{1}{K_{\mathrm{p},i}} \tag{4.16}$$

where C_{OA} is the total organic aerosol concentration, C_i^{aer} is the mass concentration of component i in the aerosol phase, and C_i^{vap} is the mass concentration of component i in the gas phase. Assuming that the total concentration of component i in the gas and particle phases is $C_i^{\mathrm{aer+vap}}$, eq 4.16 is transferred to[47]

$$C_i^{\mathrm{aer+vap}} - C_i^{\mathrm{aer}} = C_i^{\mathrm{vap}} = \frac{C_i^{\mathrm{aer}}/C_{\mathrm{OA}}}{K_{\mathrm{p},i}} = \frac{K_{\mathrm{p},i}^{-1}C_i^{\mathrm{aer}}}{C_{\mathrm{OA}}(..., C_i^{\mathrm{aer}}, ...)} \tag{4.17}$$

$$C_{\mathrm{OA}}(..., C_i^{\mathrm{aer}}, ...) = \sum_i C_i^{\mathrm{aer}} \tag{4.18}$$

Dividing both sides of eq 4.17 by $C_i^{\mathrm{aer+vap}}$ leads to the following equations:[47]

$$f_i^{\mathrm{aer}} = \frac{C_i^{\mathrm{aer}}}{C_i^{\mathrm{aer+vap}}} = \frac{1}{1 + \frac{K_{\mathrm{p},i}^{-1}}{C_{\mathrm{OA}}(..., C_i^{\mathrm{aer}}, ...)}} = \frac{1}{1 + \frac{C_i^*}{C_{\mathrm{OA}}(..., C_i^{\mathrm{aer}}, ...)}} \tag{4.19}$$

DOI: 10.1021/acs.chemrev.5b00067
Chem. Rev. 2015, 115, 3803−3855

$$C_{OA}(..., C_i^{aer}, ...) = \sum_i f_i^{aer} C_i^{aer+vap} \quad (4.20)$$

where f_i^{aer} is the fraction of component i in the aerosol phase compared to the total concentration. Under the VBS framework, the compounds with similar C_i^* values are grouped into one bin, and a new $C_i^{aer+vap}$ is defined. The quantity f_i^{aer} is calculated for a given organic aerosol concentration. This grouping method, however, does not alter the formulations for eqs 4.19 and 4.20. After grouping of the compounds, $C_i^{aer+vap}$ is the total concentration for the ith bin. The overall partitioning of the organic compounds is represented using several bins, and each bin has a fixed C^* value (mass-equivalent effective saturation concentration). The key assumption is that an organic aerosol mixture is expressed by the bulk average properties, and the respective unique property of an individual organic compound may be unimportant. Since it is easier to determine the value of C^* than to determine the identities of organic compounds in the atmosphere, it is convenient to group compounds via their volatility to reduce the complexity of partitioning. A uniform basis set (C^*) ranging from picograms per cubic meter to kilograms per cubic meter is used to map the different primary organic aerosol and SOA, and the C^* values are separated by an order of magnitude. However, the 1D-VBS fails to treat compounds with similar volatility but significantly different chemical properties and reactivities. Donahue et al.[156] have further developed a two-dimensional volatility basis set (2D-VBS) from 1D-VBS, by adding the average oxidation state of carbon ($\overline{OS}_C$) as the y axis. The composition information (the carbon, hydrogen, and oxygen numbers) of organic aerosols is correlated with the volatility (Figure 6).[157] The 2D-VBS approach considers the multigenerational aging, i.e., with a factor of 10 reduction in C^* and a ~15% increase in the mass due to oxygen addition at each step. For ambient aerosols, the bulk properties of organic aerosols are constrained by only two parameters, which can be readily measured or estimated. The average oxidation state is expressed by $\overline{OS}_C \approx 2(O/C) - (H/C)$, when the deviations introduced by peroxide groups and heteroatoms are insignificant.[158] The bulk oxidation state based on measurements of the O/C and H/C atomic molar ratios can be directly derived from AMS data,[159] even though the structures for thousands of individual molecular species are unknown. The volatility can be measured by several different methods, such as dilution and the use of a thermodenuder. The thermodenuder is composed of a heated flow reactor, which is used widely in determining volatility on the basis of the change of C^* under different temperatures. Two alternative 2D approaches consider the carbon number vs polarity, as proposed by Pankow and Barsanti[160] and in the statistical oxidation model (SOM) by Cappa and Wilson.[161]

The treatment of partitioning including the influence of water and inorganic constituents, which are typically mixed with the organic compositions in ambient aerosols, is presently not included in 2D-VBS. Also, phase separation has been identified in aerosols with organic and inorganic compounds and significantly influences gas–particle partitioning.[162,163] Other techniques, such as aerosol inorganic–organic mixture functional group activity coefficients (AIOMFAC), have been developed to remedy such a deficiency.[164] However, the AIOMFAC model requires the functional group information on organics as the input information or at least a reasonable estimation of a series of representative compounds, which are difficult to obtain from ambient measurements. Since the partitioning approach is based on the thermodynamic equilibrium consideration, the kinetic and mechanistic processes related to the formation of secondary organic matter are not adequately and accurately represented, including the rate of growth or aging of particles for the different types of anthropogenic and biogenic VOCs.[5] Furthermore, particle-phase reactions leading to polymerization/oligomerization also change the O/C and H/C atomic molar ratios measured by AMS, making it difficult for interpretation of ambient measurements by considering the thermodynamic equilibrium alone.

4.2. Particle-Phase Reactions of Organic Matter

4.2.1. Hydration Reactions. Photo-oxidation of aromatics (toluene, xylenes, or trimethylbenzenes) and isoprene leads to significant production of small α-dicarbonyls, i.e., glyoxal and methylglyoxal, in the urban and regional atmospheres. For example, the molar molecular yield of methylglyoxal is about 0.9 from 1,3,5-trimethylbenzene oxidation and 0.16 for toluene oxidation,[144] and the molar molecular yield for glyoxal is 40% from OH-initiated oxidation of p-xylene.[165] Concentrations of glyoxal and methylglyoxal up to a few parts per billion levels have been measured in polluted air,[166−169] and the global sources of glyoxal and methylglyoxal are estimated at 45 and 140 Tg year^{-1}, respectively.[45] In the gas phase, photolysis or reaction with the OH radical is identified as the major loss process for small α-dicarbonyls, with a corresponding lifetime of a few hours. In Mexico City, the measured glyoxal concentrations have been shown to be significantly below those predicted, indicating a possible missing sink for gas-phase glyoxal that is likely linked to SOA formation.[170]

Small α-dicarbonyls engage in facile hydration reactions in water, initially yielding a diol and a tetrol (Figure 7). For

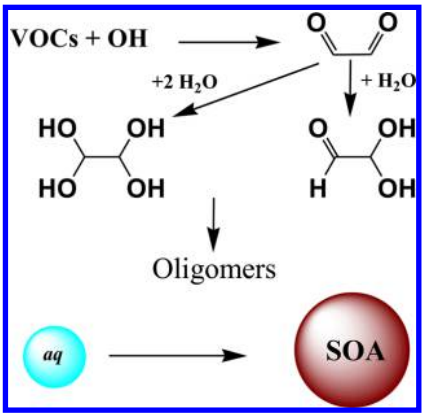

Figure 7. Schematic representation of glyoxal oligomerization. Reprinted from ref 146. Copyright 2015 American Chemical Society.

methylglyoxal, for example, these two hydrates have been identified as the major forms in pure water solution, consisting of 56−62% monohydrate (diol) and 38−44% dihydrate (tetrol).[171] Several laboratory studies have investigated the heterogeneous interaction of glyoxal with atmospheric PM.[149,172−180] A previous study by Ip et al.[172] reported the effective Henry law constant (H^*) of 1.6×10^6 M atm^{-1} for glyoxal in water at neutral pH and at 278 K, whereas the H^* value decreases with increasing temperature. Previous laboratory studies have also measured γ values of 8×10^{-4} to 7.3×10^{-3} on aqueous inorganic aerosols[179] and 1×10^{-3} to 2×10^{-2} on cloud droplets/ice crystals,[180] with a larger γ on more acidic particles and at lower temperatures.

DOI: 10.1021/acs.chemrev.5b00067
Chem. Rev. 2015, 115, 3803−3855

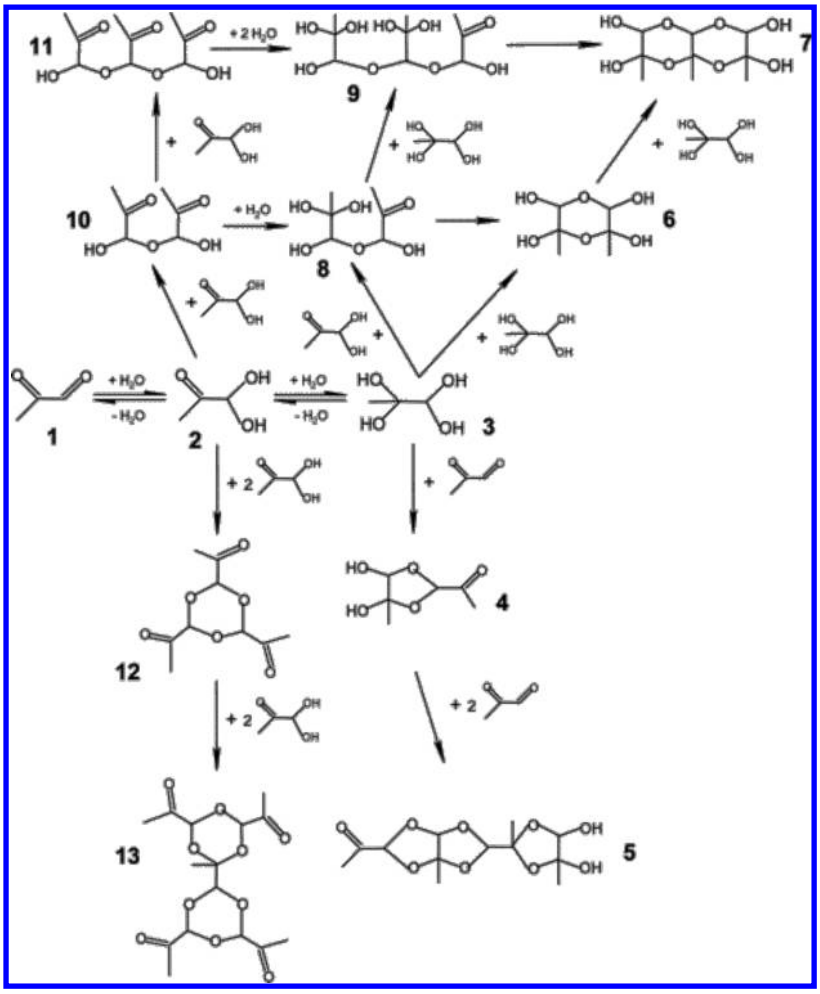

Figure 8. Possible aqueous reaction mechanism of methylglyoxal in H_2SO_4. Reprinted from ref 145. Copyright 2006 American Chemical Society.

Two experimental studies of the uptake of glyoxal and methylglyoxal on sulfuric acid solutions have revealed that the heterogeneous reactions of the smaller α-dicarbonyls on aqueous solutions correspond to hydration, followed by oligomerization, even in the absence of an acidic medium (Figure 8).[145,146] For methylglyoxal, for example, the initial dissolution and hydration result in diol formation, and further hydration produces a tetrol. Subsequent reactions among methylglyoxal, diols, and tetrols lead to formation of various oligomers. The experimentally measured uptake coefficients and Henry law constant show more efficient aqueous reactions of glyoxal than methylglyoxal on sulfuric acid, suggesting that the effect of methyl substitution for α-dicarbonyls likely inhibits hydration and oligomerization.[146] The measured dependence of the γ and H^* values on the acidity for both glyoxal and methylglyoxal indicates that the reactions of hydration and oligomerization for smaller α-dicarbonyls are unlikely to be acid-catalyzed, in contrast to the results of several previous studies.[172,180] For glyoxal, the experimentally measured uptake coefficient (γ) ranges from $(1.2 \pm 0.06) \times 10^{-2}$ to $(2.5 \pm 0.01) \times 10^{-3}$ for 60−93 wt % H_2SO_4 at 253−273 K, and the measured effective Henry law constant (H^*) ranges from $(98.9 \pm 4.9) \times 10^5$ to $(1.6 \pm 0.1) \times 10^5$ M atm^{-1} for 60−93 wt % H_2SO_4 at 263−273 K.[146]

Experimental studies of H_2SO_4 nanoparticles exposed to glyoxal vapor show that glyoxal enhances the growth of nanoparticles.[181,182] The nanoparticle growth after glyoxal exposure increases with RH, indicating the occurrence of hydration. For example, on H_2SO_4 particles of 20 nm the measured growth factor is 1.93 at 20% RH, but decreases to 1.53 at 7% RH. The analysis of particle chemical compositions using thermal desorption ion drift chemical ionization mass spectrometry (TD-ID-CIMS) reveals the coexistence of various oligomers, including the linear, branched, and cyclic forms in the particle phase.

Hence, the available experimental results indicate that oligomerization of glyoxal and methylglyoxal leading to SOA formation is largely dependent on the particle hygroscopicity.[145,146,181,182] Since oligomerization of α-dicarbonyls corresponds to second- or higher-order reactions with respect to the organics to form high-molecular-weight species, the rates of these particle-phase reactions are strongly dependent on the gaseous concentrations of glyoxal and methylglyoxal under ambient environments. Furthermore, cloud-processing of glyoxal and methylglyoxal has been suggested to represent a major source of the global SOA.[45]

4.2.2. Acid-Catalyzed Reactions. In acidic aqueous media, carbonyl (i.e., aldehyde and ketone) compounds engage in acid-catalyzed reactions, such as polymerization, hemiacetal/acetal formation, aldol condensation, or cationic rearrangement.[183,184] The carbonyl is a polar group with a partial charge on the carbon, which is prone to nucleophilic attack (a common nucleophile is H_2O). For example, alcohols can be added to carbonyls in acidic media, analogous to H_2O addition, to form hemiacetals or acetals. Reactive or physical uptake of various carbonyl

DOI: 10.1021/acs.chemrev.5b00067
Chem. Rev. 2015, 115, 3803−3855

compounds has been measured using a droplet train reactor, a flow tube reactor, and environmental chambers (e.g., by Jayne et al.,[185] Zhao et al.,[46] and Jang et al.,[186] respectively).

Aldol condensation has also been proposed to contribute to SOA growth. Jang and co-workers performed a series of smog chamber and flow tube experiments to measure particle growth by acid-catalyzed reactions of oxygenated organic compounds, such as octanal and 2,4-hexadienal, and suggested that the reactions of aldehydes increase the SOA mass production.[143,186−189] However, little aerosol growth was measured in a chamber study by Kroll et al.,[190] when H_2SO_4 particles were exposed to much lower concentrations of different carbonyls, including formaldehyde, 2,4-hexadienal, octanal, 2,3-butanedione, 2,4-pentanedione, glutaraldehyde, and hydroxyacetone. Hemiacetal formation from the uptake of hexanal on moderately concentrated sulfuric acid submicrometer aerosols (30%) was experimentally measured, although high concentrations of hexanal (up to 0.009 atm) were used.[191] An electrodynamic balance study on the reaction between octanal vapor and single levitated H_2SO_4 droplets also suggested that the reactive uptake of aldehydes into acidic particles may not be an important pathway in SOA formation under typical tropospheric conditions.[148]

An experimental study using bulk sulfuric acid solutions shows that large aldehydes, such as 2,4-hexadienal, while having negligible hydration rates, undergo protonation and enolization followed by aldol condensation and formation of large unsaturated polymers at high acidity.[46] Octanal is shown to be physically absorbed by sulfuric acid without undergoing irreversible reaction, and the measured Henry constant decreases with decreasing acidity and increasing temperature. Irreversible uptake is observed for 2,4-hexadienal, and the uptake coefficient increases with increasing acidity. For large aldehydes, initial protonation and enolization result in aldol condensation, which in high acidity leads to formation of long-chain unsaturated polymers (Figure 9), responsible for the increasing reactivity

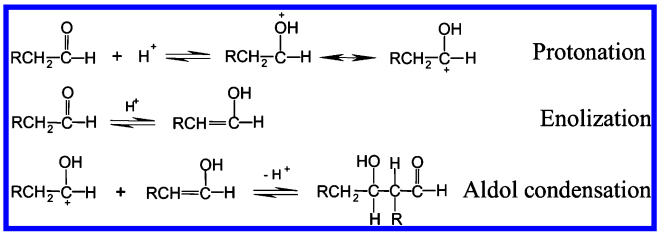

Figure 9. Acid-catalyzed reactions of large aldehydes. Reprinted with permission from ref 46. Copyright 2005 American Geophysical Union.

with increasing acidity. The conjugated 2,4-hexadienal is more reactive than octanal in H_2SO_4, because protonation of conjugated carbonyls leads to resonance stabilization and increases the basicity.

It has also been shown that exposure of 2,4-hexadienal to nanoparticles contributes to particle growth.[181,182] For H_2SO_4 particles of 20 nm, the measured growth factor is 1.13, 1.09, and 1.01 at 7%, 12%, and 20% RH, respectively, showing an acid-catalyzed reaction. Analysis of the particle chemical compositions using TD-ID-CIMS reveals that the products of aldol condensation in collected nanoparticles exposed to 2,4-hexadienal are evident in the desorption spectra, showing the protonated aldol and its dehydrated form (with a loss of H_2O).

The uptake of a series of alcohols by bulk H_2SO_4 solutions has also been investigated.[192−196] In dilute sulfuric acid, alcohols interact mostly through a reversible physical absorption, with the Henry law constant increasing with acidity. In concentrated sulfuric acid, the uptake of alcohols occurs due to the reversible formation of alkyl hydrogen sulfate ($ROSO_3H$) and/or dialkyl sulfate ($(RO)_2SO_2$). Furthermore, the previous experimental studies indicate that the uptake of octanal and 2,4-hexadienal is not enhanced in the presence of butanol or decanol, suggesting that the aldehydes and alcohols react independently in acidic media to form aldol condensation and alkyl sulfate products, respectively.[194] The growth factor of H_2SO_4 nanoparticles exposed to ethanol, 1-butanol, 1-heptanol, and 1-decanol is measured using a nano tandem differential mobility analyzer (n-TDMA); the measured growth factor is close to unity when nanoparticles are exposed to those species, indicating no apparent growth within the experimental uncertainty.[182] The significant difference in the uptake of alcohols on H_2SO_4 nanoparticles from those on bulk solutions are explained jointly by their high volatility and a large curvature effect on nanoparticles.

It should be pointed out that the acid-catalyzed heterogeneous reactions of alcohols and large aldehydes typically require high acidity. While their occurrence may be non-negligible in the upper troposphere where RH is lower and sulfate aerosols are more concentrated, formation of aldol condensation products and alkyl sulfate species may not significantly contribute to SOA formation in humid lower tropospheric conditions, since the aerosol acidity is typically small.

Recently, epoxides, especially isoprene epoxydiols (IEPOXs), have been suggested to be produced with a large yield from the oxidation of biogenic hydrocarbons (e.g., isoprene) and to contribute to SOA formation.[197−212] Also, methacrylic acid epoxide has been suggested to be produced from methacryloyl peroxynitrate oxidation (with a yield of 8−32%),[207] likely explaining SOA formation from isoprene under high-NO_x conditions.[198] Recent field studies have indicated that the epoxides derived from 2-methyl-3-buten-2-ol oxidation are important for SOA and organosulfate formation.[200,209] While recent chamber experiments have shown organosulfate formation from reactive uptake of gas-phase epoxides (α- and β-pinene oxides) by acidic aerosols,[197] the reactive uptake for α-pinene oxides has been suggested unlikely to represent a major route to formation of aerosols or organosulfates in the atmosphere, since high particle acidity is required.[211]

The size-dependent growth factors of 4−20 nm nanoparticles exposed to three model epoxides (i.e., isoprene oxide, α-pinene oxide, and butadiene diepoxides) at various RHs and reactant concentrations have been recently measured using an n-TDMA.[213] Large size growth is measured when sulfuric acid nanoparticles of 4−20 nm are exposed to the epoxide vapors, dependent on the particle size and RH. For example, the measured growth factors for 20 nm particles exposed to isoprene oxide are 1.91 and 1.50 at RH values of 4% and 30%, respectively. Chemical composition analysis of sulfuric acid nanoparticles after epoxide exposure using TD-ID-CIMS indicates that both α-pinene oxide and butadiene diepoxides form organosulfates, while isoprene oxide only forms polymers. Organosulfates are formed only in low-RH or high-acidity conditions, but isoprene-derived polymers are formed in both low- and high-RH conditions by the acid-catalyzed reaction (Figure 10).

4.2.3. Reactions with Basic Species. Ammonia is the most abundant basic gas and the most important neutralization agent for atmospheric PM. While the concentrations of low-molecular-weight alkylamines are expected to be at least an order of

DOI: 10.1021/acs.chemrev.5b00067
Chem. Rev. 2015, 115, 3803−3855

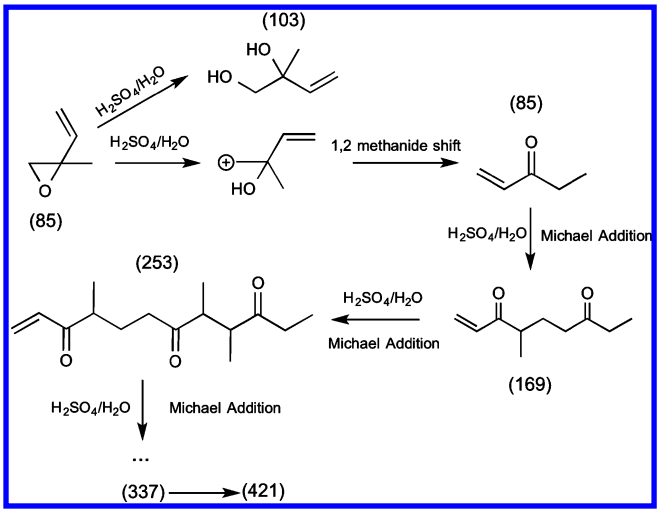

Figure 10. Heterogeneous reaction mechanism of isoprene oxide on sulfuric acid nanoparticles. Reprinted from ref 213. Copyright 2014 American Chemical Society.

magnitude lower than that of ammonia in the atmosphere, amines have stronger basicity than ammonia and are more likely to participate in acid−base reactions in the condensed phase, because of substitution by one or more organic functional groups. Although ammonia and alkylamines are highly volatile, both engage readily in multiphase reactions with organic species, contributing to aerosol nucleation and growth.[4] For example, the multiphase reactions of basic species leading to SOA growth include acid−base neutralization, interaction with carbonyls, and particle-phase oxidation reactions.[214]

The importance of the interaction between organic acids and basic species to aerosol nucleation has recently been recognized.[215,216] Quantum chemical calculations reveal that alkylamines bind to organic acids with a large bonding energy, and hydration promotes proton transfer from organic acids to alkylamines and consequently increases the interaction strength. The free energies of formation for hydrated clusters consisting of alkylamines and organic acids reveal that the interaction likely exerts a synergetic effect on atmospheric aerosol nucleation by the formation of aminium carboxylate ion pairs. In a flow tube study, it has been shown that NPF is considerably enhanced in the mixture of methanesulfonic acid, amines, and water, and the particle formation is quantitatively reproduced by a semi-empirical kinetic model by considering the relevant intermediate clusters.[217] By considering equilibrium partitioning of organic acids, bases and their salts, amines have been suggested as an important contributor to organic salt formation, likely explaining field and laboratory measurements of the coexistence and accumulation of low-molecular-weight organic acids and bases in the nucleation mode particles.[218]

Gaseous ammonia and amines react efficiently with organic acids via the acid−base reactions in the particle phase:

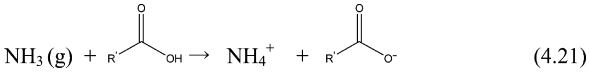

(4.21)

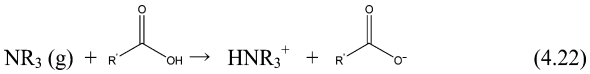

(4.22)

the acid−base reactions of ammonia and amines considerably alter the particle volatility, optical properties, and hygroscopicity.[214]

Recently, the saturation vapor pressure and enthalpy of vaporization of ammonium oxalate and adipate have been measured using a TDMA and a thermodenuder (TDMA−TD) to investigate the effects of ammonia on the partitioning of oxalic and adipic acids.[219] Ammonia is shown to considerably reduce the vapor pressure of oxalic acid (by 4 orders of magnitude), because of ammonium oxalate formation, while the vapor pressures between ammonium adipate and adipic acid do not change appreciably.[219] Those results reveal that the salt formation represents an important step for oxalate concentrations measured in ambient aerosol. In an environmental study of α-pinene ozonolysis in dry and humid conditions,[220] the addition of ammonia is shown to increase the particle number and volume concentrations (by 15% and 8%, respectively) and the averaged particle size (from 242 to 248 nm). In particular, a dramatic increase in the number and volume concentrations of *cis*-pinonic acid occurs with ammonia addition to the chamber, supporting that NH_3 interacts with gas-phase organic acids to form condensable salts and enhance SOA formation.

The kinetics of the acid−base reactions between methylamine, dimethylamine, and trimethylamine on citric acid and humic acid has been investigated using a Knudsen cell reactor.[221] Citric acid, as a stronger acid, shows a higher reactivity than humic acid for amines, while the steric effect of amines regulates the reactivity of amines with the organic acids.

Barsanti and Pankow[222] have developed a theoretical approach to evaluate the thermodynamics for accretion reactions for four mono- and dicarboxylic acids (acetic, malic, maleic, and pinic) to form esters and amides. For all organic acids considered, ester and amide formations are thermodynamically favored, and for malic, maleic, and pinic acids, and likely for similar mono- and dicarboxylic acids, organic matter formation via ester and amide formation can be significant in the atmosphere.

A recent measurement of the volatility of alkylaminium carboxylate salts shows high thermal stability from the organic acid−amine reactions;[223] the measured vapor pressure of alkylaminium dicarboxylate salts is $\sim 10^{-6}$ Pa, and the vaporization enthalpy ranges from 73 to 134 kJ mol^{-1}.[223] The experimental results indicate that alkylaminium monocarboxylates behave as protic ionic liquids at room temperature and are more hygroscopic than ammonium sulfate, suggesting that alkylaminium carboxylate salts contribute importantly to new particle formation and particle growth under ambient conditions and significantly enhance the CCN activity of mixed particles in areas where SO_2 emissions are limited.

The carbonyl group also reacts with primary and secondary amines (such as monomethylamine and dimethylamine) to form imine and enamine compounds, respectively, and the reactions are likely acid-catalyzed. The reaction between monomethylamine and glyoxal has been measured in both bulk solution and the particle phase.[224] Imidazole compounds are identified, and the presence of monomethylamine in the particle phase enhances the self-oligomerization of glyoxal.[224] A similar reaction has been measured for glyoxal and ammonium sulfate aerosols.[149,225,226] Experimental studies on the heterogeneous reactions between glyoxal and ammonium sulfate/amino acid particles[226,227] show that the uptake of glyoxal on ammonium sulfate and glycine aerosols increases the particle size by 1.7- and 1.6-fold at 50% RH, respectively. Aerosols containing a mixture of ammonium sulfate and glycine with a molar ratio of 100:1 grow more efficiently when exposed to glyoxal vapor.[227] In addition, field measurements have indicated urban aerosols containing high-molecular-weight constituents with a large fraction of carbon−

DOI: 10.1021/acs.chemrev.5b00067
Chem. Rev. 2015, 115, 3803−3855

nitrogen bonds, suggesting that the carbonyl−amine reaction represents an important source of nitrogen-containing compounds in the aerosol phase.[228]

The reactions between glyoxal and ammonium sulfate/amine aerosols depend strongly on the RH, suggesting more efficient occurrence on hygroscopic particles. For example, a minimum RH of 35% is identified for the occurrence of the reaction of glyoxal on ammonium sulfate, and this RH value overlaps with the efflorescence point of ammonium sulfate.[226] The reaction between glycine and glyoxal occurs only when the RH is close to 25% or above, which is slightly lower than the 35% RH required for ammonium sulfate−glyoxal reaction.[227]

Particle-phase amines also react with gas-phase oxidants, including ozone and OH radicals, yielding more oxidized compounds.[71] The reactions between ozone and aliphatic amines with long-chain alkyl groups[229] form products containing organo-nitrites and -nitrates. Ozone exposure of particles consisting of a mixture of aliphatic amines and oleic acid leads to the formation of amides and imines.[229] The ozone uptake on protein compounds shows that the reaction kinetics depends on the property of the semisolid phase of proteins, and the uptake is controlled by ozone diffusion in the bulk phase and described by a kinetic multilayer flux model.[230]

4.3. Sulfate Formation

In the atmosphere, the gas-phase oxidation of SO_2 is dominated by the reaction with OH radical:[5]

$$SO_2 + OH + M \rightarrow HOSO_2 + M \quad (4.23)$$

$$HOSO_2 + O_2 \rightarrow HO_2 + SO_3 \quad (4.24)$$

$$SO_3 + H_2O + M \rightarrow H_2SO_4 + M \quad (4.25)$$

The reaction rate for reaction 4.23 is 8.9×10^{-13} cm^3 molecule^{-1} s^{-1}.[5] At the typical atmospheric level of OH radical, the lifetime of SO_2 from the reaction with OH is about 1 week.[5] Therefore, SO_2 oxidation into sulfate may proceed during long-range transport.[231]

SO_2 is also oxidized into sulfate via heterogeneous reactions in the aqueous phase of clouds, fog, and aerosols. The aqueous-phase conversion of dissolved SO_2 to sulfate is probably the most important chemical formation pathway in cloudwater. In the urban atmosphere, sharply increased sulfate is often accompanied by a high RH,[232,233] suggesting the importance of the aqueous-phase oxidation of SO_2. The aqueous-phase oxidation process consists of two steps, i.e., dissolution of SO_2 and subsequent reactions in the aqueous phase. The dissolution of SO_2 leads to three chemical species, i.e., hydrated SO_2 ($SO_2 \cdot H_2O$), the bisulfite ion (HSO_3^-), and the sulfite ion (SO_3^{2-}). The dissolved SO_2 exists mostly in the form of HSO_3^- in the pH range of 2−7, but dominantly as $SO_2 \cdot H_2O$ at pH < 2. At pH larger than 7, SO_3^{2-} is the major form:

$$SO_2(g) + H_2O \rightleftharpoons SO_2 \cdot H_2O(aq) \quad (4.26)$$

$$SO_2 \cdot H_2O(aq) \rightleftharpoons H^+ + HSO_3^- \quad (4.27)$$

$$H^+ + HSO_3^- \rightleftharpoons SO_3^{2-} + 2H^+ \quad (4.28)$$

The equilibrium constant (i.e., the Henry law constant) for reaction 4.26 is 1.23 M atm^{-1} at 298 K.[5] There are several additional pathways for the transformation of dissolved SO_2 (referred to as S(IV)) to sulfate (referred to as S(VI)) involving typical atmospheric oxidants, i.e., ozone, hydrogen peroxide, organic perioxides, oxygen, OH radical, and nitrogen dioxide:

$$HSO_3^- + H_2O_2 \rightleftharpoons SO_2OOH^- + H_2O \quad (4.29)$$

$$SO_2OOH^- + H^+ \rightarrow H_2SO_4 \quad (4.30)$$

$$S(IV) + O_3 \rightarrow S(VI) + O_2 \quad (4.31)$$

$$HSO_3^- + CH_3OOH + H^+ \rightarrow SO_4^{2-} + H^+ + CH_3OH \quad (4.32)$$

$$S(IV) + {}^1/_2O_2 \xrightarrow{Mn^{2+},Fe^{3+}} S(VI) \quad (4.33)$$

$$S(IV) + OH \rightarrow S(VI) + H_2O \quad (4.34)$$

$$2NO_2 + HSO_3^- \rightarrow 3H^+ + 2NO_2^- + SO_4^{2-} \quad (4.35)$$

Hydrogen peroxide (H_2O_2) is one of the most effective oxidants for S(IV) in the aqueous phase. S(IV) oxidation by dissolved H_2O_2 (reactions 4.29 and 4.30) represents the dominant pathway for sulfate formation at pH values of less than 4−5.[5] When the pH is larger than 5, oxidation by ozone (reaction 4.31) is also important; at pH 6, this oxidation is 10 times faster than that by H_2O_2. The dissolved S(IV) may also be oxidized by organic peroxides (reaction 4.32). Oxidation of S(IV) with dissolved oxygen is negligible, but can be significantly catalyzed by Fe(III) and Mn(II) (reaction 4.33). This catalytic effect is inhibited by the ionic strength and sulfate. Thus, oxidation of S(IV) by O_2 catalyzed by Fe and Mn may be important under high-pH conditions. The oxidation rate of S(IV) by OH radical in the aqueous phase depends on the S(IV) and OH concentrations and the propagation and termination rates of the radical chain (reaction 4.34). Nitrogen dioxide has limited water solubility, and its resulting aqueous-phase oxidation of HSO_3^- to SO_4^{2-} (reaction 4.35) is of minor importance. However, for foggy conditions in urban areas with high NO_2 concentrations, this reaction can be a significant pathway for conversion of SO_2 into sulfate, resulting in a higher level of sulfate formation.[5]

The inhibition of most oxidation of SO_2 in fog and aerosols at low pH values results from the low solubility. Because bisulfite is a weak acid, when enough neutralizing materials such as ammonia are available, the dissolved SO_2 is completely dissociated as SO_3^- and thus significantly enhances the oxidation rate of S(IV). Lee and Schwarz investigated the oxidation of S(IV) by NO_2 at a pH of ∼7 and found that SO_3^- is rapidly oxidized to sulfate.[234] Behra et al. found that the aqueous-phase oxidation of SO_2 in the atmosphere is influenced by the presence of NH_3, and the enhancing effect of NH_3 is especially pronounced if the oxidation occurs with an oxidant such as O_3, for which the reaction rate increases strongly with increasing pH.[235] Hence, elevated NH_3 may significantly enhance the aqueous-phase oxidation of SO_2, leading to high levels of ammonium sulfate under high-RH conditions.

Oxidation of sulfur dioxide on transition metals has also been identified as a dominant in-cloud oxidation pathway.[236] Transition-metal ions, i.e., Fe(III) and Mn(II), are common species in dust particles. The catalytic oxidation of S(IV) to S(VI) by transition metals is possibly important in the urban cities of East Asia, especially in China, because dust/soil is an important component of fine particles in spring due to the frequent occurrence of dust storms.[237,238] He et al. suggested an alternative mechanism of sulfate formation on hazy days, in which the coexistence with NO_x reduces the environmental capacity for SO_2 and leads to rapid conversion of SO_2 to sulfate, because NO_2 and SO_2 likely exert a synergistic effect on the surfaces of mineral dust.[239]

DOI: 10.1021/acs.chemrev.5b00067
Chem. Rev. 2015, 115, 3803−3855

Several recent studies have highlighted the potential importance of SO_2 oxidation by Criegee intermediates (CIs), which are produced from ozonolysis of olefins. The initial addition of ozone to the double bond of an alkene yields an excited primary ozonide, which subsequently undergoes unimolecular decomposition to produce the chemically activated biradical CI, also known as the carbonyl oxide.[240−243] A recent laboratory kinetic study has shown unexpectedly efficient rate constants between the reactions of stabilized CIs with SO_2, indicating a potential role of CIs in tropospheric sulfate formation.[244] In addition, an atmospheric field study has suggested that CIs enhance sulfuric acid production over a forested site.[245]

Sulfuric acid may be neutralized by basic gases, including NH_3 and amines. The uptake coefficient for the particle-phase reaction of NH_3 on sulfate-containing particles increases as a function of acid concentration and reaches unity at >55 wt % H_2SO_4.[246,247] The reaction products include NH_4^+, HSO_4^-, and SO_4^{2-} in the aqueous phase. In addition to neutralization reactions, amines displace ammonium cations in ammonium sulfate salts. The experimentally measured uptake coefficient varies in the range from 10^{-4} to near unity on molecular clusters, nanoparticles, or bulk surfaces.[248−253] For ammonium bisulfate, the competition between the substitution and the acid−base neutralization is dependent on the particle size: neutralization is more favorable with an increasing cluster size,[248,249] and the process becomes dominant on bulk surfaces.[252] The dissolution of amines into sulfate particles considerably modifies the particle physiochemical properties, including volatility and hygroscopicity (Figure 11).[214,254,255] For example, the displacement reaction of alkylamines with ammonium sulfate aerosols leads to a transition from a crystalline to an amorphorous phase and improved water uptake.

4.4. Nitrate Formation

NO_2 reacts with OH to form nitric acid, which is the dominant homogeneous formation pathway for nitric acid during the daytime in the troposphere:[231,256]

$$NO_2 + OH + M \rightarrow HNO_3 + M \quad (4.36)$$

The reaction rate of NO_2 with OH radical (reaction 4.36) is 8×10^{-12} cm^3 $molecule^{-1}$ s^{-1} at 298 K,[231] which is about 10 times larger than the reaction rate of SO_2 with OH radical[231] and corresponds to a lifetime of about 1 day for NO_x. Although weaker and more volatile than sulfuric acid,[257−259] nitric acid can be transformed into nitrate salts via the reactions with ammonia, amine, dust, and sea salts in the aerosol phase. In the urban atmosphere, NH_4NO_3 is the major chemical form of nitrate in fine PM. The heterogeneous reaction between HNO_3 and NH_3 in the particle phase to form ammonium nitrate represents an important process to modulate the gaseous HNO_3 concentration:

$$HNO_3(g) + NH_3(g) \leftrightarrow NH_4NO_3(s) \quad (4.37)$$

Depending on the RH, ammonium nitrate formed in the above reaction exists as a solid or an aqueous solution of NH_4^+ and NO_3^-. The equilibrium constant, K_p, depends on the temperature:[5]

$$\ln K_p = 84.6 - (24220/T) - 6.1 \ln(T/298) \quad (4.38)$$

A field study during the MILAGRO/MCMA-2006 campaign in Mexico City suggested that such an equilibrium explains the correlation between measured gaseous HNO_3 and particle nitrate (Figure 12).[260]

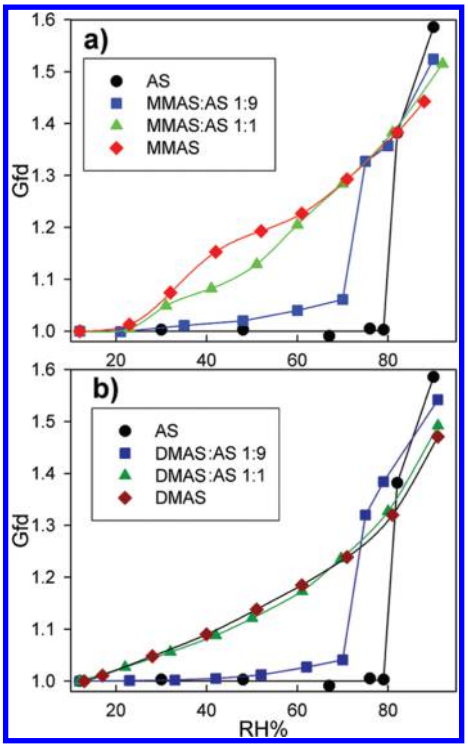

Figure 11. Deliquescent profiles for alkylaminium−ammonium sulfate mixtures. (a) Hygroscopic diametric growth factor (HGfd) profiles for monomethylaminium sulfate (MMAS) and ammonium sulfate (AS) mixtures: black circles, AS; blue squares, mixture with MMAS:AS = 1:9 by mass; green triangles, mixture with MMAS:AS = 1:1 by mass; red tilted squares, MMAS. (b) HGfd profiles for dimethylaminium sulfate (DMAS) and AS mixtures: black circles, AS; dark-blue squares, mixture with DMAS:AS = 1:9 by mass; dark-green triangles, mixture with DMAS:AS = 1:1 by mass; dark-red tilted squares, DMAS. Solid lines are connections through the experimental points. Values are averages from measurements on aerosols with initial mobility diameters of 80, 100, 150, and 240 nm with a random error of less than ±1% in HGfd. Reprinted from ref 254. Copyright 2012 American Chemical Society.

Amines also react with nitric acid and ammonium nitrate to form aminium nitrates by the acid−base and replacement reactions, respectively. The exchange kinetics and thermodynamics of amines for ammonia on small (1−2 nm) ammonium nitrate clusters have been investigated, showing a near-unity uptake coefficient and highly exothermic Gibbs free energy changes for the substitution.[248] Experimental measurements of the reaction of trimethylamine with polydisperse ammonium nitrate particles (20−500 nm) show complete exchange of trimethylamine for ammonia with high trimethylamine concentrations, but partial exchange at lower trimethylamine concentrations (less than 500 ppb for a reaction time of 23 s), with an initial reactive uptake coefficient on the order of 2×10^{-3} at 20% RH.[251] The volatility of aminium nitrates (i.e., mono-, di-, and trimethylamine, ethylamine, and monoethanolamine aminium nitrates) has been measured on laboratory-generated aerosols.[261] The estimated enthalpies of vaporization for aminium nitrates range from 54 to 74 kJ mol^{-1}, and the calculated vapor pressures at 298 K are about 10^{-4} Pa, indicating that the formation of aminium nitrates may represent an important pathway in gas-to-particle partitioning under high-NO_x conditions.[261] In addition, a field study has shown a strong seasonal dependence for gas−

DOI: 10.1021/acs.chemrev.5b00067
Chem. Rev. 2015, 115, 3803−3855

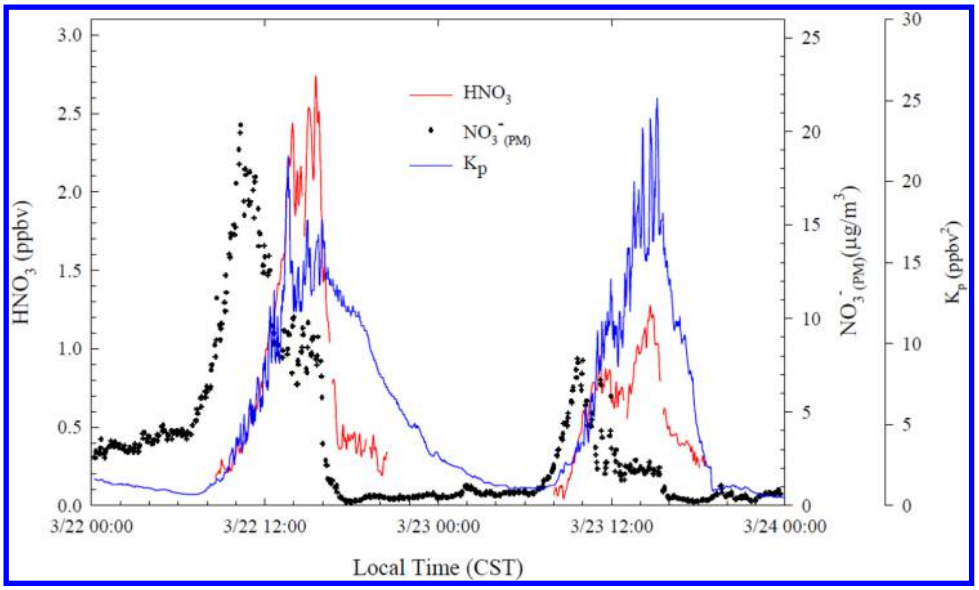

Figure 12. Gaseous HNO_3, submicrometer aerosol nitrate ($NO_3^-{}_{(PM)}$) (1 $\mu g\ m^{-3}$ nitrate under ambient pressure and temperature can contribute to 0.51 ppb gaseous HNO_3 after complete evaporation), and the calculated dissociation constant K_p for March 22 and 23, 2006. Reprinted with permission from ref 260. Copyright 2008 Copernicus Publications.

particle partitioning of alkylamines within individual ambient submicrometer aged organic carbon particles internally mixed with ammonium, nitrate, and sulfate.[262]

In addition, dinitrogen pentoxide (N_2O_5) also plays an important role at nighttime:

$$NO_2 + O_3 \rightarrow NO_3 + O_2 \tag{4.39}$$

$$NO_2 + NO_3 \overset{[M]}{\rightleftharpoons} N_2O_5(g) \tag{4.40}$$

$$N_2O_5(g) + H_2O(aq) \rightarrow 2H^+ + 2NO_3^-(aq) \tag{4.41}$$

Nitrogen dioxide reacts with ozone to produce the NO_3 radical, and the latter further reacts with NO_2, forming N_2O_5. N_2O_5 is prone to photolysis or thermal deposition and is stable at night. In addition to the daytime gas-phase formation of HNO_3, the hydrolysis of N_2O_5 with aerosols and fog is a major source of nitric acid in the urban atmosphere at night.[263] This reaction proceeds efficiently on wet surfaces but slowly in the gas phase,[264] whereas the formation of nitrate by hydrolysis of NO_2 in aerosol surfaces is of minor importance.[234,256] Hydrolysis of N_2O_5 on aqueous solution has been extensively investigated in laboratory kinetic studies.[265] The previous experimental studies indicate that the uptake coefficient of N_2O_5 on neutral electrolyte aerosols is lower than that of sulfuric acid, even on liquid aerosols containing abundant water, and the hydrolysis of N_2O_5 on solid particles is much slower than on deliquesced or supersaturated aerosols.[266]

Field measurements have found that the nocturnal hydrolysis of N_2O_5 is highly variable and depends strongly on the aerosol composition, particularly the sulfate content.[267,268] One measurement on the chemistry evolution of urban fine particles in the Pearl River Delta (PRD) region of China found that the gas-phase production of HNO_3 through the reaction of NO_2 + OH dominates during the initial rapid buildup of nitrate around noontime, but the heterogeneous production of HNO_3 via N_2O_5 hydrolysis dominates in the afternoon hours.[269] The enhanced production of nitrate aerosols due to the N_2O_5 hydrolysis has also been identified in other Chinese polluted cities.[263,270]

Efficient heterogeneous reactions of gaseous nitric acid with dust, sea salt, and fog have been intensively investigated in laboratory studies and confirmed by field measurements.[271] The heterogeneous reaction between dust and gaseous nitric acid proceeds by

$$CaCO_3(s) + 2HNO_3 \rightarrow Ca(NO_3)_2(aq) + CO_2(g) + H_2O \tag{4.42}$$

to produce the soluble and hygroscopic $Ca(NO_3)_2(aq)$ product. The reaction rate is accelerated by increasing the RH above 10%, which is the deliquescence point of calcium nitrate.[272,273] Sullivan et al.[274] investigated the reaction kinetics of nitric acid vapor with size-resolved mineral dust particles and found that calcite particles are rapidly converted into hygroscopic particles within 4 h for low HNO_3 mixing ratios (10 ppt) and in less than 3 min for 1 ppb HNO_3. Hence, the conversion of the calcite component on atmospheric mineral dust into calcite nitrate is controlled by the availability of nitric acid. Calcite is a common component of urban aerosols, and the mixing ratio of HNO_3 in the urban atmosphere is usually in the parts per billion range.[275,276] The importance of the heterogeneous reaction of nitric acid with dust has been confirmed by a field measurement on the evolution of particles in Xi'an, China, showing that during the 2009 spring dust events the urban fine particles were more acidic than in the nondust events mainly due to the fast heterogeneous formation of nitrate on dust surfaces.[237,277] The latter work suggests that sulfate aerosols during the dust events were also mostly derived from the Gobi desert rather than from heterogeneous formation.[237] Also, anthropogenic pollution has been observed near dust source regions in northwestern China.[278]

In the coastal urban atmosphere, nitric acid also undergoes a heterogeneous reaction with sea salt (NaCl) aerosols to produce $NaNO_3$ and release HCl into the air:[279]

$$HNO_3(g) + NaCl(s\ or\ aq) \rightarrow NaNO_3(s\ or\ aq) + HCl(g) \tag{4.43}$$

DOI: 10.1021/acs.chemrev.5b00067
Chem. Rev. 2015, 115, 3803−3855

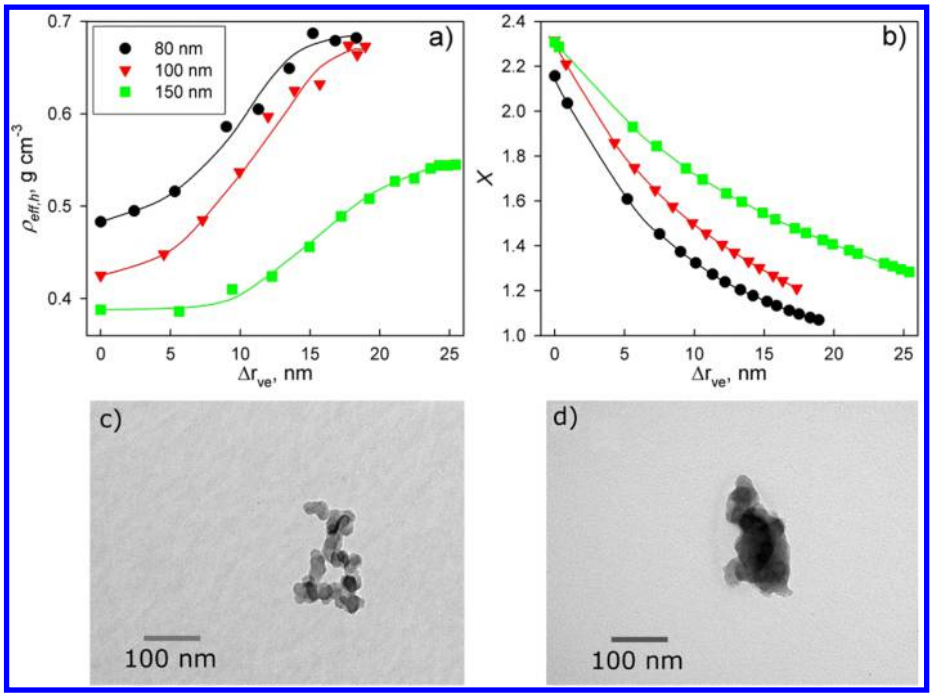

Figure 13. Morphology change and transmission electron microscopy (TEM) images of soot particles. For panels a and b, the experimental conditions are an initial toluene concentration of 250 ppb and soot particle number concentration of 750−800 cm^{-3}; the soot had an initial mobility diameter (D_p) of 80 nm (black circles), 100 nm (red triangles), or 150 nm (green squares). (a) Effective density ($\rho_{eff,h} = 6m_p/\pi D_p^3$) of the soot core (coated heated soot) as a function of the volume equivalent coating thickness (Δr_{ve}), where m_p is the particle mass. Solid lines are connections through the experimental points. (b) Particle dynamic shape factor ($\chi = (D_p/C_p)(C_{ve}/D_{ve})$) as a function of Δr_{ve}, where $D_{ve} = (6m_p/\pi\rho_m)^{1/3}$, ρ_m is the material density, and C_{ve} and C_p are the Cunningham slip correction factors for particles with diameters D_{ve} and D_p, respectively. Solid lines are the best fits of the data. (c, d) TEM images of (c) fresh and (d) coated soot particles, sampled from the experiment with an initial toluene concentration of 250 ppb and soot particles with an initial D_p of 150 nm. The initial number concentration of fresh soot is 1400 cm^{-3}. The Δr_{ve} of organics on coated soot in panel d was about 40 nm. Reprinted from ref 138. Copyright 2012 American Chemical Society.

This process represents one of the major sources of HCl vapor in the troposphere and has been studied extensively in the laboratory on both solid and aqueous substrates using various instrumental techniques (e.g., electron microscopy, X-ray photoelectron spectroscopy, infrared and Raman spectroscopy, and mass spectrometry). The presence of water in aerosols plays a critical role in this reaction. Saul et al.[280] investigated the reactive uptake of nitric acid on NaCl aerosols in a wide range of RH between 10% and 85% and found that, for RH above the efflorescence relative humidity (ERH), NaCl particles exist as liquid droplets and the uptake coefficient of HNO_3(g) ranges from 0.05 at 85% RH to >0.1 near the ERH. For RH less than the ERH, NaCl particles are nominally solid and the uptake coefficient is dependent on the amount of surface-adsorbed water. A field study of the heterogeneous reaction of HNO_3 with sea salt in the coastal region of Los Angels indicates that the displacement of chloride by nitrate on sea-salt particles is affected by several factors, including the gas-phase concentrations, particle-phase concentrations, temperature, and relative humidity.[279]

In addition to inorganic nitrate, the oxidation reactions of VOCs in the presence of NO_2 produce peroxynitrates (RO_2NO_2) and more strongly bound mono- and multifunctional alkyl nitrates ($RONO_2$). The detailed chemistry of organic nitrates has been reviewed by Perring et al.[281] There are two main pathways for the production of $RONO_2$, i.e., OH-initiated oxidation of hydrocarbons in the presence of NO_x during the daytime and nitrate radical (NO_3)-initiated oxidation of alkenes during the nighttime. The chemical lifetimes of $RONO_2$ are significantly longer than those of NO_x.[281] The saturation vapor pressures of $RONO_2$ span over several orders of magnitude, and atmospheric $RONO_2$ species have been found to exist in both the gas and aerosol phases. Large multifunctional organic nitrates generated from oxidation of alkanes and alkenes readily form SOA by partitioning to the aerosol phase due to their much lower volatility. An environmental chamber investigation on the reaction of NO_3 with α-pinene at the conditions of 1 atm, 3% RH, and 298 K identified five organic nitrates in the particle phase.[282] Experimental measurements using bulk solutions revealed that tertiary $RONO_2$ undergoes hydration reactions at low pH to yield alcohols, but is catalyzed by H_2SO_4 to form organosulfates.[203,283−286] Under high-NO_x conditions, OH-initiated oxidation of α-pinene produces $RONO_2$ with a yield of 26 ± 7%, which is dependent on both the chamber RH and seed aerosol acidity and likely results from particle-phase hydrolysis.[287] A chamber study of 1,2,4-trimethylbenzene oxidation with variable RH and VOC-to-NO_x ratios shows that tertiary $RONO_2$ hydrolysis exhibits a strong relationship between $RONO_2$ loss and relative humidity on neutral aerosols, suggesting that the particle-phase hydrolysis substantially reduces the $RONO_2$ group concentration in ambient SOA.[288]

4.5. Aging of Primary Particles

Primary PM, such as BC, dust, and biogenic particles, undergoes chemical transformation in the atmosphere, by coating with organic and inorganic constituents, commonly referred to as the aging process. The aging processes of primary PM are similar to those described above for the secondary formation of organic matter, sulfate, and nitrate. PM aging not only changes the particle mixing state (i.e., from externally to internally), but also

DOI: 10.1021/acs.chemrev.5b00067
Chem. Rev. 2015, 115, 3803−3855

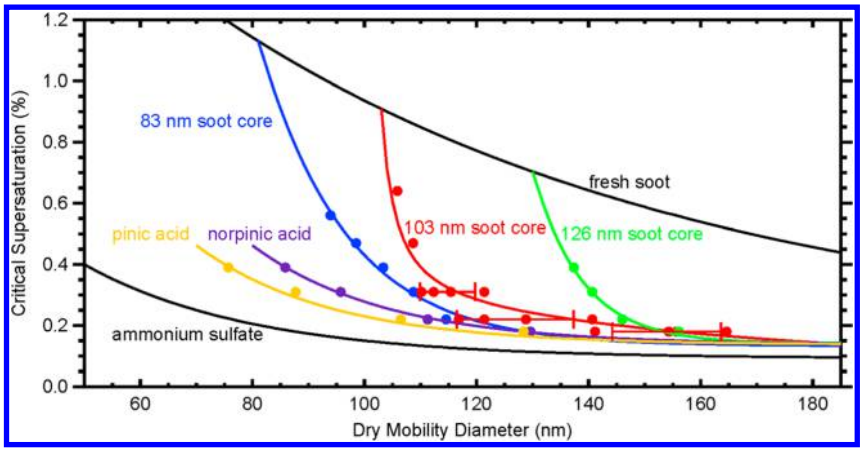

Figure 14. Critical supersaturation (%) as a function of the overall particle diameter (dry mobility diameter). Particles with an initial core of diameters 83, 103, and 126 nm coated by α-pinene ozonolysis products (37 ppb α-pinene and 20 ppb ozone) are shown in blue, red, and green, respectively. Measurements for fresh soot, pure ammonium sulfate, pinic acid (yellow), and norpinic acid (purple) are included for comparison. Reprinted with permission from ref 64. Copyright 2013 American Geophysical Union.

considerably alters the particle properties, including the morphology, hygroscopicity, and optical properties.[66]

As an important type of primary urban fine PM, BC aerosols are emitted into the atmosphere from incomplete fossil fuel combustion and biomass burning.[289,290] Fresh BC, consisting of chainlike aggregates of spherical primary particles with EC as the major component, is hydrophobic and light-absorbing. Upon entering the atmosphere, BC particles are subjected to further transformations, which involve partitioning of organic and inorganic gaseous species, heterogeneous reactions, and coagulation with other aerosol constituents.[64,138,291−298] The rate of the internal mixing for BC depends on the composition and properties of the nascent BC particles and ambient concentrations of gaseous pollutants.[66] The resulting internally mixed BC particles exhibit significantly altered properties, including the effective density, morphology, hygroscopicity, single scattering albedo (SSA), and chemical reactivity.[138,293,299−303]

The subject of BC aging by coating of inorganic and organic species has been extensively investigated.[64,138,293] The impacts of SOA formation on BC properties have been recently investigated in several well-controlled environmental chamber studies, by simultaneously monitoring the variations in the particle size, mass, organic mass faction, morphology, effective density, hygroscopicity, and optical properties of monodisperse BC particles exposed to the oxidation products of the OH-initiated reactions of toluene and isoprene and ozonolysis of α-pinene.[64,138,293] With the development of an organic coating, the BC core is changed from a highly fractal to compact form. The organic coating increases the particle density and hygroscopicity, and further exposure of coated soot to elevated relative humidity results in a more spherical particle (Figure 13). The SSA and scattering and absorption cross sections are also enhanced with the organic coating. The experimental study of BC aging from α-pinene oxidation with ozone shows that water-soluble organic acids produced from the reaction between α-pinene and ozone accumulate rapidly onto preexisting particles to form coatings of organic materials that reach a mass fraction of 80−90% within 1 h.[64] CCN measurements reveal that the initially hydrophobic aerosols are converted to efficient CCN at a supersaturation of 0.22% (Figure 14), suggesting that the changes in the activation potential of a significant fraction of the atmospheric aerosol population are controlled by the formation and composition of coatings produced during the aging process, rather than by the original particle size or composition.[64]

Hence, atmospheric transformation of both primary and secondary PM leads to multi-component chemical constituents. The cloud-forming potential of aerosols can be determined by several approaches.[63,150] For a single-component aerosol, the water supersaturation (S_w) is expressed by (i.e., the Köhler equation),[63]

$$S_w = a_w \exp\left(\frac{4\sigma M_w}{RT\rho_w D}\right) \tag{4.44}$$

where a_w is the water activity in the aerosol phase, M_w and ρ_w are the molecular weight and density of water, respectively, and D and σ are the diameter and surface tension of the aerosol, respectively. The hygroscopicity parameter (κ) is defined as,[63]

$$1/a_w = 1 + \kappa\frac{V_d}{V_w} \tag{4.45}$$

where V_d and V_w are the volumes of the dry aerosol and water, respectively. From the average molecular weight (M_d) and the density (ρ_d) for the dry aerosol, κ can be calculated,

$$\kappa = \frac{\upsilon\rho_d}{\rho_w}\frac{M_w}{M_d} \tag{4.46}$$

where υ is the number of ions per dissociating molecule. If the aerosol contains multicomponent chemical constituents, the total effective κ is expressed as the linear combination of the individual κ_i (i.e., the mixing rule),[63]

$$\kappa = \sum_i \varepsilon_i\kappa_i \tag{4.47}$$

where ε_i is the volume fraction of component i in the aerosol particle, and its molecular weight and density are M_i and ρ_i, respectively. The above equation (4.47) can be used to calculate the κ value if each κ_i and their corresponding volume fraction ε_i are known. Two alternative methods have been employed to derive the κ values, on the basis of measured CCN activity and hygroscopic growth.[150] From the measured critical supersaturation (S_c), κ is approximated as,[63]

DOI: 10.1021/acs.chemrev.5b00067
Chem. Rev. 2015, 115, 3803−3855

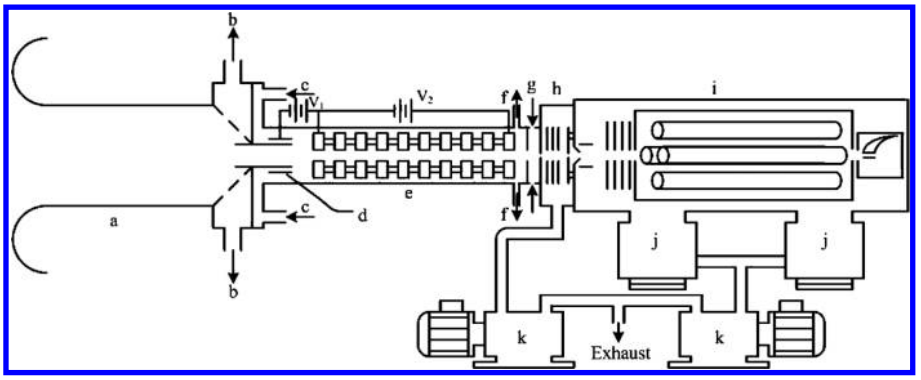

Figure 15. Schematic diagram of the AP-ID-CIMS (AP = atmospheric pressure) system: (a) 4 in. i.d. inlet; (b) flow to the sampling blower; (c) 10 slpm of N_2 carrier doped with HNO_3 and C_3H_8; (d) Am-241 holder; (e) atmospheric pressure drift tube; (f) 65 slpm drift tube flow, including 10 slpm N_2 carrier flow, pumped by a diaphragm pump, and regulated by a mass flow controller; (g) 400 sccm N_2 curtain flow to prevent water cluster formation; (h) CID chamber; (i) quadrupole mass spectrometer; (j) turbopumps; (k) oil pumps for rough pumping. Reprinted from ref 308. Copyright 2010 American Chemical Society.

$$\kappa \approx \frac{4A^3}{27D_d^3 \ln^2 S_c} \tag{4.48}$$

where $A = (4\sigma M_w)/(RT\rho_w)$ and D_d is the diameter of the dry aerosol. In addition, κ is calculated through the measured RH dependence of the hygroscopic growth factor (Gf),[47,63,150]

$$\kappa = [\frac{1}{RH}\exp(A/D) - 1](Gf^3 - 1) \tag{4.49}$$

A recent experimental study showed that for single-component aerosols the calculated κ value is close to those derived from the measured CCN activity and hygroscopic growth, but large differences exist in the κ values derived using the measured CCN and hygroscopic growth data for multi-component aerosols.[150]

Clearly, coating of inorganic salts on primary PM during atmospheric aging considerably improves their cloud-forming potential. For organic compounds, gas-phase oxidation typically leads to formation of increasingly oxidized organic species (such as organic acids) that are less volatile but more hygroscopic. The particle-phase reactions between organic acids and basic species (i.e., ammonia and amines) leading to formation of ammonium or aminium carboxylate salts also enhance the particle hygroscopicity, but oligomerization/polymerization (i.e., hydration of small α-dicarbonyls and acid-catalyzed aldol condensation of large aldehydes) decreases the particle hygroscopicity.[150]

5. ATMOSPHERIC MEASUREMENTS

5.1. Analytical Techniques

Measurements of trace gaseous and PM pollutants under urban environments represent another major challenge to quantify their abundances and decipher their chemical identity. In this section, we review several state-of-the-art analytical techniques to measure key gaseous aerosol precursors and the particle size, number, and chemical compositions.

5.1.1. Gaseous Aerosol Precursor Measurements. Most conventional offline measurements of VOCs are comprised of two steps, i.e., separation (identification) and quantification.[304] The development of gas chromatography (GC) has undoubtedly contributed to the analytical capabilities of measuring VOCs in the atmosphere. Measurements of VOCs have largely been conducted using GC analyses of air samples that are collected in canisters, on adsorbents, or in cryostats. The performance of GC in combination with flame ionization detection (FID), electron capture detection (ECD), photoionization detection (PID), and mass spectrometry (MS) has been validated for separating and quantifying VOCs at ambient concentration levels (i.e., parts per billion and parts per trillion). Such measurements are sensitive and provide a high degree of chemical speciation. However, a significant disadvantage of the offline method is the low time resolution, since VOC evolution in rapidly changing atmospheric conditions cannot be captured. To circumvent this deficiency, an online gas chromatography−mass spectrometry/flame ionization detection (GC−MS/FID) technique has been developed; VOCs are initially concentrated by a cold trap, heated until evaporation occurs, and then introduced into the GC−MS/FID system.[304]

Chemical ionization mass spectrometry (CIMS) has been widely employed in atmospheric chemistry research, including laboratory kinetic investigations and field trace gas measurements.[130,305,306] In the CIMS method, a neutral species is ionized by a reagent ion to yield a product ion, which is then analyzed by a mass spectrometer for species identification and quantification.[307] One of the advantages of the CIMS method lies in its soft ionization, which does not lead to appreciable fragmentation of the product ions.

An ion drift chemical ionization mass spectrometry (ID-CIMS) technique has been developed to detect and quantify trace gases, including VOCs and inorganic species (Figure 15).[307,308] The principle that ID-CIMS utilizes is the detection of a neutral molecule X according to the ion−molecule reaction[307,308]

$$A^{(+or-)} + X \rightarrow X'^{(+or-)} + \text{others} \qquad (k_{5.1}) \tag{5.1}$$

where A is the reagent ion, X′ is the product ion, and $k_{5.1}$ is the ion−molecule rate constant for the above reaction. The key components of the ID-CIMS system include an ionization source where the reagent ions are produced, a drift tube where the ion−molecule reaction occurs and through which the reagent and products are guided, and a mass spectrometer for analysis of the reagent and product ions. The abundance of the neutral species X in the drift tube can then be quantified from the equation[307,308]

$$[X']_{\Delta t} = k_{5.1}[A][X]\Delta t \tag{5.2}$$

where Δt represents the time for the ion−molecule reaction in the drift tube. Hence, the ID-CIMS method allows for the quantification of the gas-phase concentrations without the necessity of calibration, since the ion−molecule reaction rate constants can be accurately determined experimentally or

DOI: 10.1021/acs.chemrev.5b00067
Chem. Rev. 2015, 115, 3803−3855

theoretically.[309−313] The ID-CIMS instrument has been deployed for measurements of several key gaseous aerosol precursor species, including H_2SO_4 and HNO_3 at various urban locations.[260,314−316]

Another successful CIMS application is proton transfer reaction mass spectrometry (PTR-MS), in which VOCs are ionized by the proton transfer reactions with hydronium ions (H_3O^+) and subsequently detected by MS. The PTR-MS method was initially developed by Lindinger et al.,[309] allowing online and real-time measurements of VOCs. PTR-MS is applicable to detect VOCs with proton affinity larger than that of a water molecule (166.5 kcal mol^{-1}), which include most of the atmospheric anthropogenic and biogenic hydrocarbons and oxygenated organic species, with the exception of alkanes smaller than C5.[313] This method has been employed extensively to measure VOCs under diverse urban environments.[6,128,129] Since PTR-MS identifies species through the mass of the product ions, isomers cannot be distinguished by this method. In addition, the interpretation of mass spectra in PTR-MS can be complicated by the formation of cluster ions and the fragmentation of the product ions.

5.1.2. PM Measurements. The mobility particle size spectrometer, often referred to as the differential mobility particle sizer (DMPS) or scanning mobility particle sizer (SMPS), has been widely used to measure the particle number size distribution. Wiedensohler et al.[317] summarized the application of the mobility particle size spectrometer techniques. Most mobility particle size spectrometers consist of a sequential setup of a bipolar diffusion charger, a DMA, and a condensation particle counter (CPC). By setting different voltages in the DMA, particles of different electrical mobility are selected and passed through the DMA. The particle number concentration is then measured by a CPC. Ramping or stepping the voltage yields an electrical particle mobility distribution, which is inverted to yield the particle number size distribution.

CPCs measure the particle number concentration of particles larger than a detectable size, which is usually around 3 nm (the diameter of the particles, 50% of which can be counted). Particles are enlarged by condensing supersaturated work fluid (1-butanol or water) in a CPC. Since the nucleation mode particles have diameters of less than 3 nm, a particle size magnifier (PSM) has been developed to detect atmospheric particles as small as 1 nm in mobility diameter.[318] A cooled sample flow is mixed with heated and saturated diethylene glycol (DEG) and is cooled again to ∼0 °C. Particles are grown to a larger size in the PSM before entering into the CPC. DEG is utilized because it easily evaporates and condenses on particle surfaces at 0−100 °C, but does not nucleate during these processes. Air ion spectrometry (AIS) has been developed for in situ high-time-resolution measurements of positive and negative ions and charged particles of smaller than 1 nm in the atmosphere. Neutral cluster and air ion spectrometry (NAIS) has also been developed to measure neutral particles.[319] The NAIS system has an additional charger-filter section in the inlet to charge particles.

Filters are typically used as particle collection substrates for offline measurements of PM chemical compositions.[320] A cutoff inlet, such as an impactor and a cyclone, is usually required to select the particle size. Some size-resolved instruments are widely used for collecting particles, such as micro-orifice uniform deposit impactors (MOUDIs). Ion chromatographs (ICs) are well developed to analyze the particle water-soluble inorganic anions and cations and organic acids. Capillary electrophoresis (CE) is applied to analyze inorganic cations and low-molecular-weight organic acids. The energy-dispersive X-ray fluorescence (ED-XRF) spectrometer has been widely used for particle tracer metal measurements. Inductively coupled plasma mass spectrometry (ICP-MS) is a sensitive and an increasingly popular approach to quantify the particle tracer metals. Niu et al.[321] compared the advantages and limitations of the two approaches.

The IMPROVE (Interagency Monitoring of Protected Visual Environments) and NIOSH (National Institute of Occupational Safety and Health) thermal evolution protocols are commonly used to quantify the EC and OC concentrations. Chow et al.[322] compared the different protocols and found that the protocols are equivalent for the total carbon, but EC from NIOSH is typically less than half of that from IMPROVE. Another major problem for the thermal evolution analysis is that during the initial heating some of the OC may change to EC due to pyrolyzation. To overcome this problem, a He/Ne laser is used to correct the OC pyrolysis. By detecting the reflectance or transmission of the light during the heating, pyrolysis OC is corrected. This approach is known as the thermal−optical method, which has a time resolution of 1 h, but is not size resolved. However, the thermal−optical reflectance (TOR) method and the thermal−optical transmittance (TOT) method often yield different results. Two carbon analyzers using the different correction methods are widely applied to measure OC and EC. The Sunset carbon analyzer uses the TOT method, while the Desert Research Institute carbon analyzer uses the TOR method. Turpin et al. developed the in situ OC/EC analyzer.[323]

Several filter-based techniques have been employed to identify and quantify the PM organic species, e.g., liquid chromatography−mass spectrometry (LC−MS), Fourier transform infrared spectroscopy (FTIR), and GC−MS. GC−MS is most widely used to analyze particulate organic matter (POM).[324] Trace-level quantification of organics in airborne PM by GC−MS techniques is well developed.[325,326]

Several commercial optical instruments have been developed to measure BC in the atmosphere, e.g., the multiangle absorption photometer (MAAP), aethalometer, particle soot absorption photometer (PSAP), and single-particle soot photometer (SP2).[327−329] The various optical methods assume that BC is the only light-absorbing species in the atmosphere, so light absorption by organic compounds, i.e., brown carbon, may influence the accuracy of BC measurements. Photoacoustic techniques have been applied to BC measurements,[330] e.g., photoacoustic soot spectrometry, three wavelengths (PASS-3), and photoacoustic extinctiometry (PAX).

Recently, an integrated PM monitoring system, consisting of TDMA, aerosol particle mass analyzer (APM), cavity ring down spectrometry (CRDS), and nephelometer, has been employed to measure a comprehensive set of sized-resolved ambient aerosol properties and to infer the BC content and particle mixing state.[329,360] For example, the measured aerosol mass-size relation using the combined TDMA−APM provides the effective density, volatility, hygroscopicity, and dynamic shape factor, and the aerosol optical properties using CRDS for extinction and a nephelometer for scattering are used to derive light absorption and SSA (for example, see Figures 13, 17, 20, and 28).

Several techniques are employed to measure the particulate ionic compounds. Steam jet collection has been proven to be a successful technique, which adds steam to sampled air to generate condensation droplets; the instruments using this technique include the steam-jet aerosol collector (SJAC), monitor for aerosols and gases in ambient air (MARGA), and

DOI: 10.1021/acs.chemrev.5b00067
Chem. Rev. 2015, 115, 3803−3855

particle-into-liquid sampler (PILS).[331,332] A wet denuder system is typically used to separate gases from particles. The absorption solution is pure water or a carbonate solution, which retains all gaseous pollutants such as HNO_2, HNO_3, SO_2, and NH_3. Particles through the denuder rapidly mix with the steam inside the mixing reservoir and grow rapidly (within 0.1 s) into droplets, which are collected by a cyclone. The solution collected in the cyclone is constantly pumped to an IC to be analyzed. The PILS is similar to the SJAC or MARGA.[333]

Aerosol mass spectrometry (AMS) is capable of measuring the size-resolved particle chemical composition with a high time resolution (seconds to minutes), high sensitivity, and low detection limit.[334−340] Drewnick[341] summarized the two most common types of online AMS, laser desorption/ionization mass spectrometry (LDI-MS) and thermal desorption electron impact ionization mass spectrometry (TD-EI-MS). The major difference for these two types of MS is the method of particle vaporization and ionization. LDI-MS is used for analysis of individual aerosol particles by identification of the chemical particle classes associated with subsets of the particles. TD-EI-MS is usually used for quantitative determination of non-refractive aerosol components.

The Aerodyne AMS instrument developed by Jayne et al.[342] is widely used.[343,344] Aerosols are focused into a narrow beam by an aerodynamic lens and transmitted into a detection chamber, where they are impacted on a heated surface. Vaporized aerosol species are ionized by electron impact and analyzed via mass spectrometry. The particle time-of-flight from a mechanical beam chopper to the vaporizer is measured to obtain chemically speciated size distributions. The Aerodyne AMS instrument has been upgraded in several versions, including a high-resolution time-of-flight aerosol mass spectrometry (HR-ToF-AMS) system.[345] The HR-ToF-AMS system uses a time-of-flight mass spectrometer as the detector. The MS resolution ranges from 2500 (in V-mode) or 4500 to 5000 (in W-mode), where the V and W represent the path of the ions in the flight chamber. In V-mode ions follow a traditional reflection path, whereas in W-mode the ions are reflected three times, thereby increasing the effective drift length. The high mass resolution allows the separation of each unit mass peak into separate contributions for specific elemental compositions based on small differences in mass defects. The aerosol chemical speciation monitor (ACSM) is a simpler version of the aerosol mass spectrometer, which only measures the bulk particle chemical composition.

GC−MS has been used for in situ analysis of ambient POM. In particular, thermal desorption aerosol GC−MS/FID (TAG GC−MS/FID) has been developed to determine the organic aerosol species.[346] The principle of TAG GC−MS/FID is similar to that of offline GC−MS/FID. Particles are collected onto a metal sheet. The metal sheet is then heated, and particles are evaporated into the gas phase, which is introduced into the GC−MS/FID system for analysis. TAG GC−MS provides the data at the molecular level with a time resolution of about 1 h, but detection of highly oxygenated and polar functional groups is still challenging, since polar organic compounds cannot be separated by GC without derivatization. Thermal desorption followed by CIMS (TD-CIMS) is another technique that has been proven to be effective in analyzing complex organic aerosol particles.[181,347] Chemical ionization yields less fragmentation and is more desirable for POM identification. In particular, the addition of a drift tube to the system (TD-ID-CIMS) greatly facilitates the control of ion−molecule reactions and quantification of collected particles.[113,181] Recently developed micro-orifice volatilization impact coupled to chemical ionization mass spectrometry (MOVI−CIMS) has the capability to measure laboratory-generated particulate organic species as well as atmospheric particles.[348]

Considering the diverse organic and inorganic PM in the urban atmosphere, which is directly emitted or produced by photo-oxidation of hydrocarbons and inorganic compounds from anthropogenic and natural sources,[127] characterization of the PM chemical compositions still poses the greatest analytical challenge. In particular, the ability of contemporary instruments to provide detailed and accurate molecular information is limited, especially when dealing with multifunctional and oligomeric organic compounds, which may represent the dominant forms in urban fine PM.[349]

5.2. Analysis Approaches

The contributions of an individual emission source to ambient $PM_{2.5}$ concentrations cannot be directly measured. Three source apportionment approaches are commonly used to determine the sources, i.e., the emission inventory, the atmospheric diffusion model, and the receptor model (RM) such as CMB and PMF by using ambient $PM_{2.5}$ chemical compositions with or without localized emission source profiles. RMs employ measurements of chemical composition data for PM on a sample site to provide information regarding the source characteristics.[350] Some multivariate RMs analyze the correlations between measured concentrations of chemical species, assuming that highly correlated compounds come from the same source. One multivariate RM is principal component analysis (PCA), which has been applied to identify PM sources.[350,351] However, PCA is rather inconvenient in quantifying the source contributions, compared to the specific methods such as PMF.

CMB is widely used for source apportionment: the mass balance is reconstructed by assuming that a specific chemical constituent in a given ambient sample is a linear combination of the relative chemical compositions of the contributing sources. The concentration of chemical constituent i in sample k (C_{ik}) is expressed as[350]

$$C_{ik} = \sum_{j=1}^{m} a_{ij} S_{jk} \tag{5.3}$$

where S_{jk} is the mass concentration of sample k originating from source j and a_{ij} is the mass fraction of chemical constituent i from source j. CMB is sensitive to and depends on the quality of localized source profiles. There exist several major uncertainties in the CMB modeling methodology. All sources are assumed to be independent, but potential collinearities between source compositions may exist. Occasionally, CMB yields inconsistent or unrealistic results because the receptor models do not include the information on the strength and location of the source emissions. Also, many physical processes, such as complex meteorology, are simplified. Since the mass of secondary components varies in the atmosphere due to chemical transformation, CMB does not apportion the secondary PM sources, but simply considers that the unapportioned mass mainly arises from the secondary formation.

PMF is another multivariate factor analysis tool that decomposes a matrix of speciated sample data into two matrices (factor contributions and factor profiles):[350]

$$X_{ij} = \sum_{k=1}^{p} g_{ik} f_{kj} + e_{ij} \tag{5.4}$$

DOI: 10.1021/acs.chemrev.5b00067
Chem. Rev. 2015, 115, 3803−3855

Table 2. Summary of Air Pollutant Characteristics in Houston, Los Angeles, Mexico City, and Beijing

	Houston, TX	Los Angeles, CA	Mexico City, Mexico	Beijing, China
population	6.2 million	18 million	21.2 million	21.2 million
city (metropolitan) area (km^2)	1625 (10062)	1302 (87940)	2072 (3540)	3820 (16801)
number of vehicles	3.3 million	6.1 million	3.5 million	5.4 million
primary pollutants	NO_x, VOCs (light olefins)	NO_x, VOCs (aromatics)	NO_x, VOCs (alkanes, aromatics)	NO_x, SO_2, VOCs (aromatics)
secondary pollutants	ozone	ozone, PM	ozone, PM	PM
av annual SO_2 concn (ppb)	0.35	0.37	2.50	7.8
av annual $PM_{2.5}$ concn ($\mu g\ m^{-3}$)	12	18	27	102
av measd particle concn (cm^{-3})	10700	20000	21000	72900
highest measd PM concn (cm^{-3})	40000	50000	40000	250000
dominant PM composition	organics (35%) and sulfate (30%)	organics (44%) and nitrate (24%)	organics (66%) and sulfate (14%)	organics (44%) and nitrate (22%)
refs	Jimenez et al.;[359] Levy et al.;[360] EPA AirData;[361] U.S. Census Bureau, Population Division[362]	Hayes et al.;[363] Moore et al.;[364] EPA AirData; U.S. Census Bureau, Population Division[362]	Molina and Molina;[365] Stephens et al.;[366] Kalafut-Pettibone et al.;[367] Calidad del Aire en la Ciudad de México—Informe;[368] Mexico City air data[369]	Guo et al.;[6] Lui et al.;[370] Beijing Traffic Management Bureau[83]

where g_{ik} is the amount of mass contributed by each factor to each individual sample, f_{kj} is the species profile of each source, and e_{ij} is the residual for each sample/species.[352] PMF assumes that receptors are impacted by the linear combinations of source emissions, which correspond to the factors derived by the model. The advantage of the PMF model is that it does not require the source profiles, but compiles its own source profiles by statistics.

Particulate water-soluble organic compounds (WSOCs) are typically considered from two major sources, i.e., biomass burning and secondary formation. WSOCs from secondary formation can be derived by subtracting WSOCs from biomass burning from the total WSOCs. WSOCs from biomass burning can be calculated from biomass burning OC and the WSOC/OC ratio of biomass burning particles. OC from biomass burning is readily obtained by the CMB model using the WSOC/OC ratio. However, this approach does not yield an accurate estimation for SOA. The EC tracer method is widely used for secondary organic carbon (SOC) estimation.[353] This method hypothesizes that primary organic carbon (POC) and EC are predominately formed through the combustion emission, and thus, EC is a good tracer for POC. Ambient SOC is calculated as

$$\mathrm{SOC} = \mathrm{OC} - \left[\mathrm{EC}\left(\frac{\mathrm{OC}}{\mathrm{EC}}\right)_{\mathrm{pri}} + N\right] \tag{5.5}$$

where $(\mathrm{OC/EC})_{\mathrm{pri}}$ is the primary OC/EC ratio and N is the contribution of POC from the noncombustion sources, which is negligible in urban environments. Millet et al.[354] developed a statistic approach to determine the primary OC/EC ratio. A series of primary OC/EC ratios are selected to estimate SOC (usually from 1 to 15 with a step of 0.01). The primary OC/EC ratio varies with time, so a fixed primary OC/EC ratio results in large uncertainties. In addition, SOC may contribute to ambient particles during the selected POC-dominated periods.

Primary organic tracers have been applied to primary PM source apportionment. The United States Environmental Protection Agency (U.S. EPA) has recently identified several SOA tracers from the oxidation of specific precursors, including isoprene, α-pinene, β-caryophyllene, and toluene, from environmental chamber experiments. A secondary organic tracer yield method has been developed to assess the SOA concentration derived from specific precursors.[326] This method obtains the tracer-to-SOA mass fractions ($f_{\mathrm{SOA,hc}}$) from chamber experiments. The tracer-to-SOA mass fraction is defined as

$$f_{\mathrm{SOA,hc}} = \frac{\sum[\mathrm{tr}_i]}{[\mathrm{SOA}]} \tag{5.6}$$

where $[\mathrm{tr}_i]$ is the mass concentration of tracer i and $[\mathrm{SOA}]$ is the total particle mass concentration in the chamber experiments. Using the mass fractions and the measured ambient SOA tracer concentrations, the atmospheric SOA mass contributions can be estimated. The uncertainty for this estimation is primarily due to the selection of the tracer compounds and the simplification using the single-valued tracer mass fractions. For the analyses of SOA in U.S. urban locations, this approach yields source contributions of 70−130% for isoprene, 50−220% for α-pinene, 70−120% for β-caryophyllene, and 60−160% for toluene;[326,355] the standard deviations of the tracer-to-SOC ratios are suitable as a source profile uncertainty.

Because of the limitation in its theoretical principle, the CMB model cannot be employed to apportion the secondary source contribution. PMF is also incapable of apportioning SOA contribution. However, with the development of organic tracer techniques, the detection of secondary organic tracers makes it feasible to apply PMF to apportion SOA derived from specific precursors.[356]

The recently developed HR-ToF-AMS system has the ability to provide composition information on the bulk OA. By analyzing the high-mass-resolution AMS spectra with a factor analysis technique (e.g., PMF), OA measured by AMS is often apportioned to several components, including hydrocarbon-like organic aerosol (HOA), regarded as a surrogate of POA, and oxygenated organic aerosol (OOA), typically a surrogate for SOA.[357] OOA is further distinguished into two factors due to the different oxidation states, which are low-volatility OOA (LV-OOA), typically representing aged SOA, and semivolatile oxygenated organic aerosol (SV-OOA), representing freshly formed SOA.[358] The development of AMS−PMF considerably advances the SOA apportionment, because this approach not only provides fast variation of ambient SOA concentrations, but also allows for the analysis of the SOA formation from a different aspect, in which organic aerosols are measured and classified by their oxidation state and volatility.

DOI: 10.1021/acs.chemrev.5b00067
Chem. Rev. 2015, 115, 3803−3855

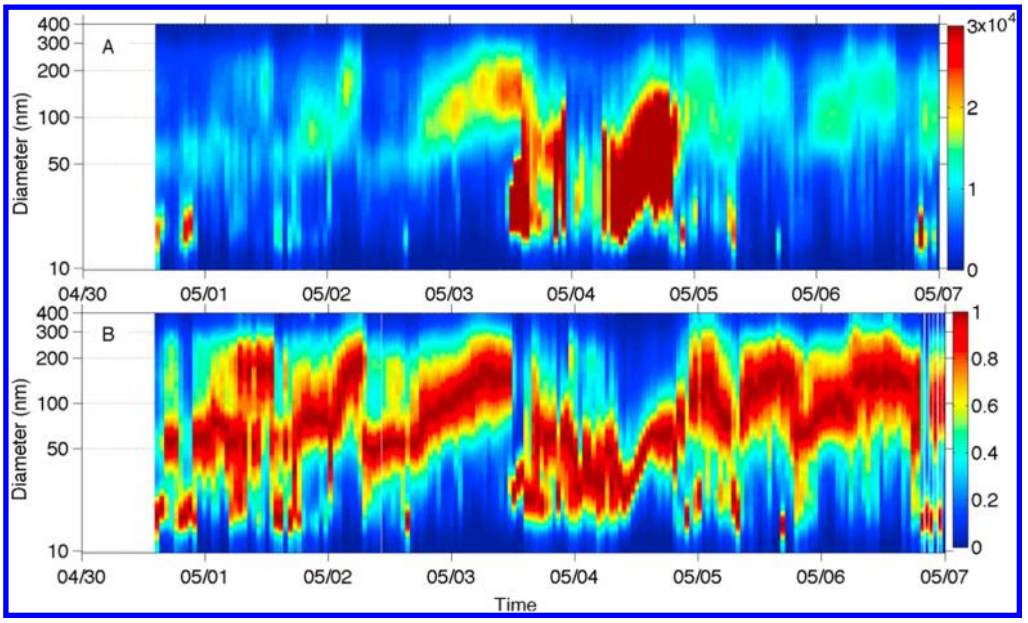

Figure 16. Aerosol mobility size distributions: (A) absolute number concentration for 10−400 nm diameter particles during the period of April 30 to May 7, 2009. The dates marked correspond to midnight of the local time (CST). (B) Normalized number concentration. The normalized plot is derived by dividing each observation (consisting of approximately 150 points between 20 and 400 nm) by the maximum concentration in each observation. Reprinted with permission from ref 360. Copyright 2013 American Geophysical Union.

5.3. Spatial and Temporal Characteristics of the Number Concentration, Size, Chemical Composition, and Other Properties of Urban Fine PM

Atmospheric PM measurements have been focused on quantifying the various particle properties, including the particle number, size, and composition, because these properties mostly determine the impacts of urban fine PM on human health, the climate, and cloud microphysics. In this section, we focus on four cities that are noticeable for their pollution problems: Houston, TX, and Los Angeles, CA, are known for their photochemical smog and associated gas-phase pollutants such as NO_x, VOCs, and ozone, whereas the pollution events in Mexico City, Mexico, and Beijing, China, are more noticeable for PM. A summary of the pollutant characteristics of the four cities is provided in Table 2.[6,52,83,359−371]

5.3.1. Houston, TX. Houston is the fourth largest city in the United States and one of the most rapidly expanding regions in the country. Between 2000 and 2005, the city exceeded the 8 h O_3 standard of 75 ppb on 219 occasions.[372−374] This region is typically humid because of its proximity to the Gulf of Mexico and the frequent influx of marine air, characterized by the diurnal sea-breeze circulation. Stagnation in Houston may develop with wind direction reversal in the late afternoon and nighttime hours, which circulates aged pollutant plumes back to the region.[360] NPF events in Houston have been occasionally measured during several campaigns.[360,375,376] Figure 16 shows the particle size distributions during the period of April 30 to May 7, 2009; an NPF event occurred shortly after a frontal passage on May 4.[360] The particle size distribution exhibits a sudden increase in the concentrations of nanoparticles and their subsequent growth, both characteristic of aerosol nucleation. For example, NPF on this day occurred at 9−10 a.m., when the concentration of 20−40 nm particles reached 4×10^4 cm^{-3}. The particle surface area was about 5 μm^2 cm^{-3} during the NPF episode, indicating a lower condensation sink for condensable gases and freshly nucleated particles. The SO_2 concentration was about 0.2−0.3 ppb between 9 and 10 a.m. and increased to over 3 ppb in the late afternoon. During the Texas Air Quality Study (TexAQS) 2000 field project, Brock et al.[375] also found that NPF is only observed with elevated SO_2 levels in Houston. Primary emissions are also evident by the high concentrations of particles during the rush hour periods.

The diurnal trends of the average aerosol diameter and concentration observed in Houston are shown in Figure 17.[360] The averaged particle size increases during the morning hours, decreases during the afternoon hours, and remains nearly constant during the night. The highest particle concentration occurs prior to sunrise, decreases during the daytime, and increases after 4:00 p.m. Particle growth is discernible, because the highest concentration of particles is located between 50 and 100 nm in the early morning (due to the high concentration of particles emitted during rush hour) and between 150 and 250 nm in the early afternoon, likely reflecting the photochemical production. Interestingly, a daily ozone peak of about 100 ppb occurred in the afternoon of May 4 (Figure 18), when the peaks of NO_x, SO_2, VOCs (toluene) were less than 10, 5, and 2 ppb, respectively.

PM in Houston is dominantly composed of organic aerosols (35%) and sulfates (30%), followed by ammonium (21%), nitrates (8%), and chloride (6%), as depicted in Figure 19.[6,359−361,377] The organic constituent is attributable to vehicle emissions and the abundant industrial source sites,[378] and the sulfate is likely due to the burning of sulfur-containing fuels in the Houston Ship Channel and from regional power plants.[379] The diurnal patterns of $PM_{2.5}$ mass concentrations throughout the region show a consistent morning peak and a weaker and slightly less consistent peak in the late afternoon to early evening.[378]

Similarly to other urban locations,[380] fine PM in Houston is often internally mixed, with one peak in the effective density distribution near 1.55 g cm^{-3}, consistent with PM comprised largely of sulfates and organics.[360] Periodically, a second mode below 1.0 g cm^{-3} is observed in the effective density distributions, reflecting the presence of freshly emitted BC particles.[360] The measured effective density also demonstrates a clear diurnal cycle

DOI: 10.1021/acs.chemrev.5b00067
Chem. Rev. 2015, 115, 3803−3855

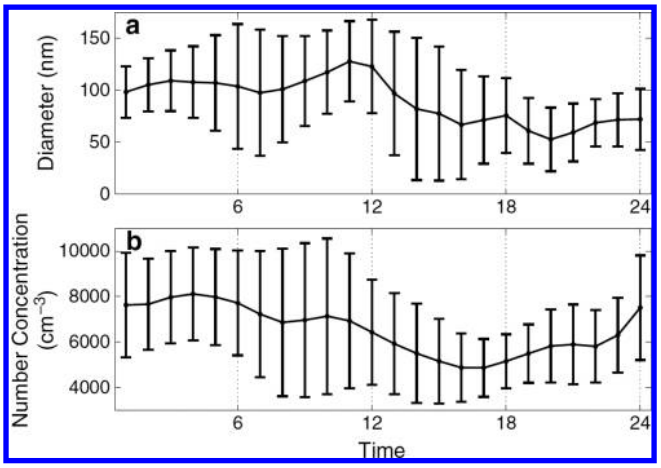

Figure 17. Diurnal trend of the (a) average aerosol diameter (nm) and (b) average aerosol concentration (cm^{-3}) observed between April 30 and May 7, 2009. Reprinted with permission from ref 360. Copyright 2013 American Geophysical Union.

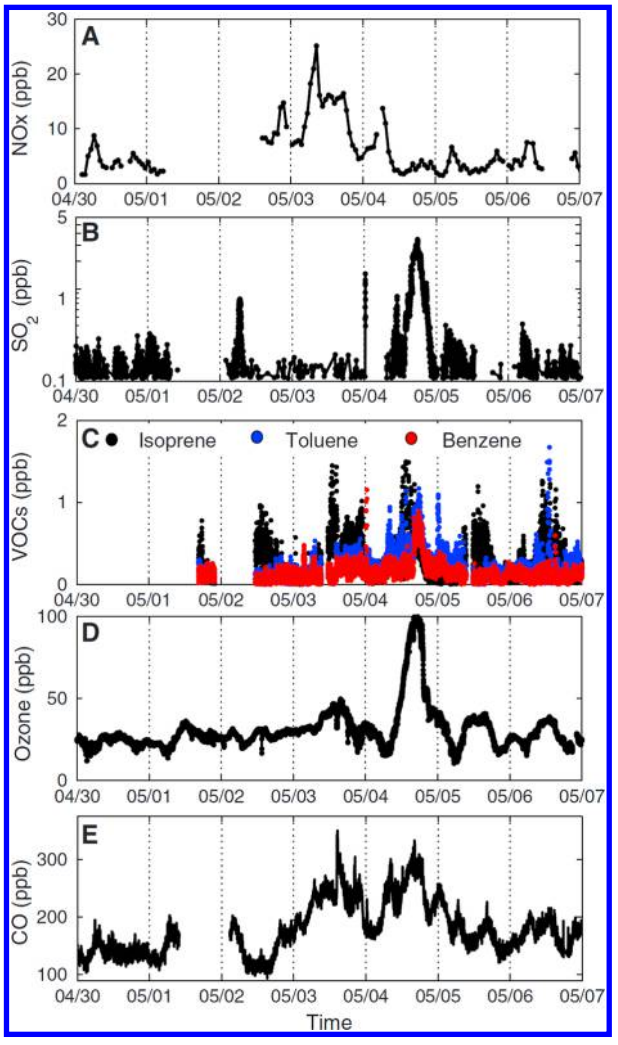

Figure 18. Mixing ratios (ppb) of ambient trace gases during the period of April 30 to May 7, 2009. The vertical lines correspond to midnight of the local time (CST). Reprinted with permission from ref 360. Copyright 2013 American Geophysical Union.

associated with primary emissions from transportation and photochemical aging, with a minimum during the morning rush

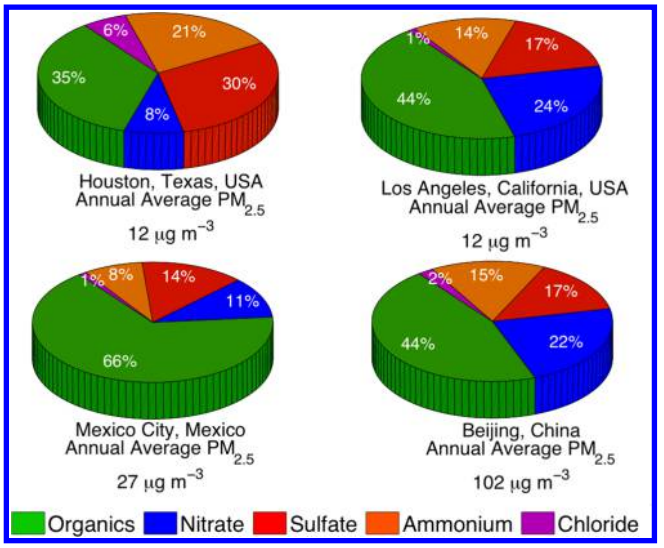

Figure 19. Nonrefractive compositions of particulate matter determined by an aerosol mass spectrometer in Houston, Los Angeles, Mexico City, and Beijing. The data are taken from refs 6, 360, 361, 377, and 391.

hour.[360] The measured average particle SSA is 0.94 ± 0.04, indicating the presence of light-absorbing particles (i.e., BC). When elevated BC concentrations are observed, typically during the morning rush hours, SSA decreases (Figure 20), with a smallest measured value of about 0.7. The largest extinction, scattering, and absorption are observed near 8 a.m. (Figure 20). Hygroscopicity measurements indicate that larger particles (e.g., 400 nm) are more hygroscopic than smaller particles (e.g., 100 nm), indicating a higher concentration of sulfates in larger particles.[360]

Hence, the PM properties, including particle number, size, mass concentration, density, and SSA, in Houston exhibit clear diurnal variations, jointly attributable to primary emissions, NPF, photochemical production, and the variation of the planetary boundary layer (PBL) height, which regulates the vertical mixing.

5.3.2. Los Angeles, CA. The Los Angeles region had over 18 million people as of 2010, making it the second-largest city in the United States. The Los Angeles basin is favorable for pollutant accumulation, because of the interaction from a complex terrain and daily sea breeze. NPF events are rarely measured in Los Angeles.[381] One plausible explanation is that the heavy accumulation of pre-existing particles and a lower level of SO_2 lead to unfavorable conditions for aerosol nucleation in the Los Angeles basin.[382] Several NPF events during the 2010 California Research at the Nexus of Air Quality and Climate Change (CalNex) field campaign have been inferred from measurements using nano aerosol mass spectrometry (NAMS) (Figure 21).[383] Sharp increases in the nanoparticle number concentration in the afternoon on sunny days coincide with a change in the wind direction. Higher levels of sulfur and silicon are identified after the nanoparticle occurrence, and the O/C ratios of the carbonaceous matter change from a distribution dominated by primary vehicle emissions to one dominated by secondary organic aerosol. Photochemical processing is suggested to be responsible for the change in the composition of pre-existing particles and NPF.[383]

The number concentration of PM measured in Los Angeles between 2008 and 2009 is shown in Figure 22.[384] The variations in PM concentrations indicate that the vehicle emissions are a strong contributor to the PM concentration, since the peak

DOI: 10.1021/acs.chemrev.5b00067
Chem. Rev. 2015, 115, 3803−3855

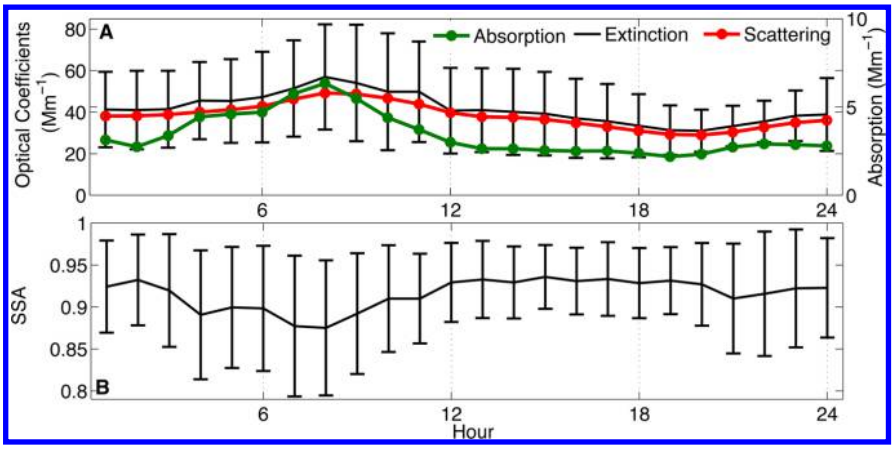

Figure 20. Diurnal cycles of (A) extinction, scattering, and absorption coefficients and the (B) single scattering albedo measured between April 30 and May 7, 2009. The optical properties are provided at a wavelength of 532 nm. Reprinted with permission from ref 360. Copyright 2013 American Geophysical Union.

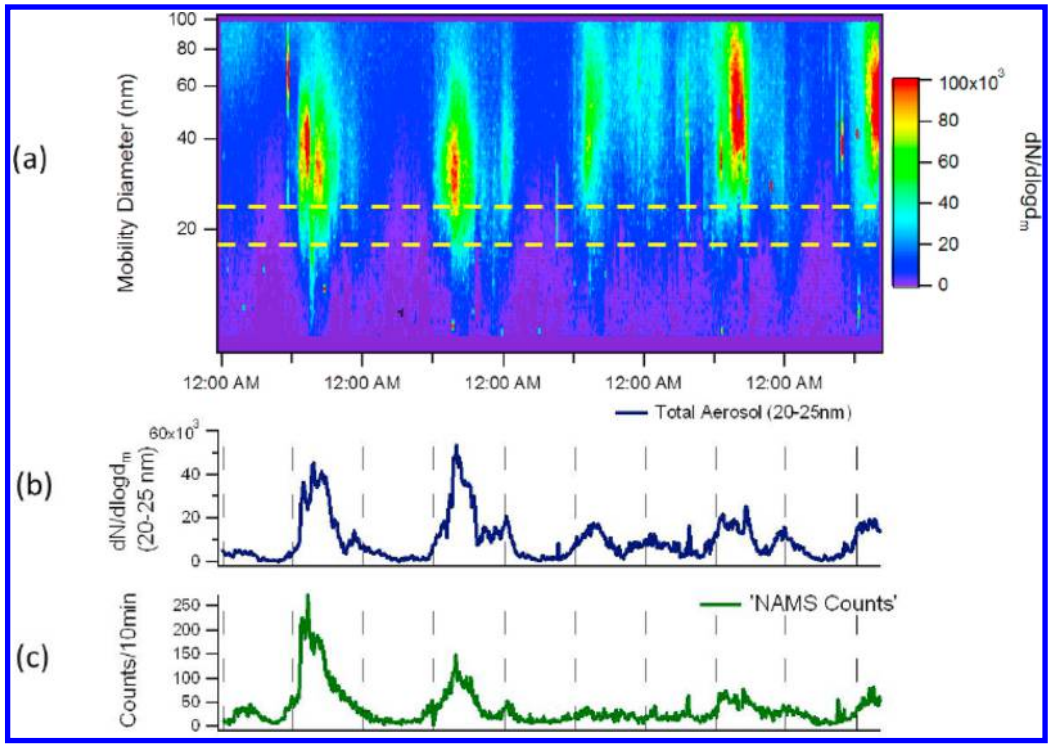

Figure 21. (a) Particle size distribution over a 5 day period during the CalNex campaign. Yellow lines indicate the approximate size range analyzed by NAMS. (b) Aerosol concentration in the approximate size range analyzed by NAMS. (c) NAMS hit rate (particles analyzed per 10 min period). Reprinted with permission from ref 383. Copyright 2012 American Geophysical Union.

values are observed near 7 a.m., when commuter traffic reaches a peak, but the number concentration dramatically drops during the late afternoon. The highest peak values are observed in the late fall and winter months, ranging between 40 000 and 50 000 cm^{-3}; the concentrations are lower overall in the warmer months, with peak concentrations of near 20 000 cm^{-3}.[384] During the late spring and summer months, a small, but significant peak occurs near noon, which is identified as PM produced by secondary particle formation processes.

PM in Los Angeles is dominantly composed of organic aerosols (44%), followed by nitrate (24%), sulfate (17%), ammonium (14%), and chloride (<1%), also shown in Figure 19.[363] The source apportionment determined by the PMF receptor model indicates that the largest sources of winter PM are vehicular emissions and secondary nitrates, both accounting for nearly 70% of the total PM; the remaining 30% is attributed to secondary sulfate, sea salt, soil emissions, biomass burning, and other sources.[88] During the summertime, secondary sulfate becomes one of the dominant components, indicating enhanced photochemical activity.

Fresh SOC consistently exhibits a brown color in Los Angeles, indicating the presence of absorbing organic aerosols.[385] Radiocarbon measurements of filter samples reveal that SOA is mainly from fossil fuel burning. Two modes are typically distinguishable in the hygroscopic distributions: a nonhygroscopic mode (growth factor of <1.15 at 92% RH) and a hygroscopic mode (growth factor of >1.15). The nonhygroscopic mode is typically identified during morning sampling

DOI: 10.1021/acs.chemrev.5b00067
Chem. Rev. 2015, 115, 3803−3855

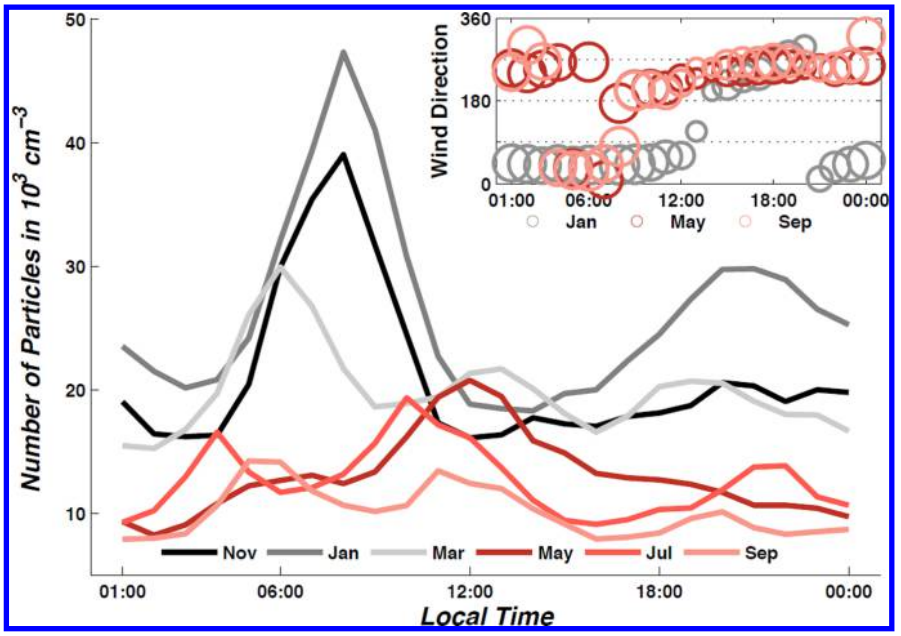

Figure 22. Hourly average particle number concentration at the University of Southern California (USC) plotted for hours of the day in local time. The relative standard error for the hourly averages reported above was less than 2%. The inset is a plot of the vector-averaged wind direction (WD) with the bubble area weighted to wind speed plotted for hours of the day in local time. Reprinted with permission from ref 384. Copyright 2010 Copernicus Publications.

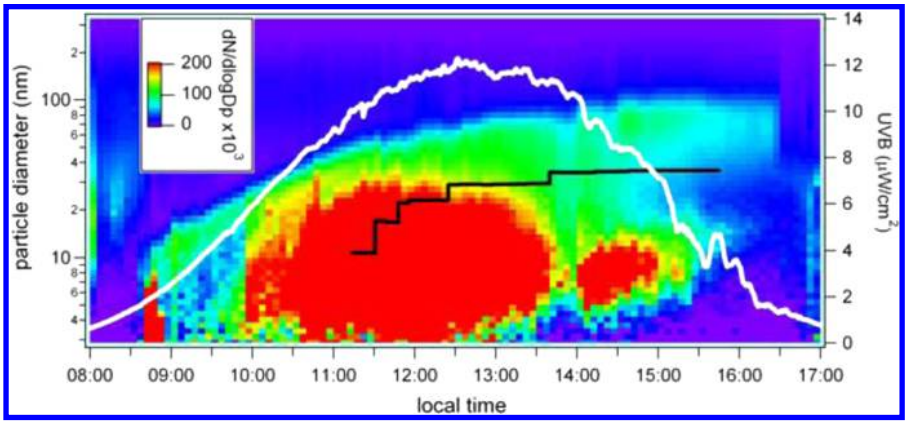

Figure 23. Contour plot of particle size distributions on March 16, showing the new particle formation event that is the focus of the current study. The white line is UVB, and the black line marks the particle size that is analyzed by TD-CIMS. Reprinted with permission from ref 390. Copyright 2008 American Geophysical Union.

(≤30% of aerosols) and decreases in the afternoon. Hence, aerosols sampled in the morning include a significant fraction of nonhygroscopic particles (i.e., BC), and the afternoon photochemistry and SOA production result in a more uniform, unimodal hygroscopicity distribution.[382] An average hygroscopicity parameter (κ) of 0.14 is calculated, indicating that the highly oxidized organic fraction of aerosols in Los Angeles is appreciably more hygroscopic than those measured in other urban centers.[382]

5.3.3. Mexico City, Mexico. The Mexico City Metropolitan Area (MCMA) is the largest megacity in North America with over 20 million residents. Air quality in Mexico City is influenced by the geography of the basin.[90,365,386] For example, the surrounding mountains contribute to spatial and temporal variability of pollutants, e.g., upslope and downslope winds transporting pollutants out and back during the day and at night, respectively. On the other hand, solar radiation is strong in Mexico City, because of its high elevation and subtropical location, which efficiently drives the daily PBL development and leads to significant ventilation of air pollutants into the free troposphere. The surface convergence and thermally driven flows decrease the probability of multiday accumulation for pollutants.

NPF events have frequently been observed during several field campaigns, such as the 2003 MCMA field study and the 2006 Megacity Initiative: Local and Global Research Observations (MILAGRO) campaign.[387−389] Kalafut et al.[367] showed the occurrence of three NPF events during a 10 day sampling period. Figure 23 shows the size distribution and composition of nucleation-mode particles: the growth of freshly nucleated particles is primarily attributed to secondary organics.[390] Iida et al.[98] derived the nucleation rates of 1 nm (J_1) ranging from 1900 to 3000 cm^{-3} s^{-1}, comparable to those of other megacities in the world.[4] Salcedo et al.[99] observed that NPF events were usually accompanied by a high level of sulfur dioxide during the 2003 MCMA campaign, indicating that the oxidation of SO_2

DOI: 10.1021/acs.chemrev.5b00067
Chem. Rev. 2015, 115, 3803−3855

contributes to the formation and growth of freshly nucleated particles. The polluted layer substantially ventilated from the Mexico City basin represents another potential factor driving NPF in the afternoon, which is characterized by the drops in the levels of NO_x, CO, and CO_2 and in the pre-existing particle concentrations preceding the NPF events.[367,387]

The PM number concentration measured during the MILAGRO field campaign in March 2006 is depicted in Figure 24.[367] The highest particle concentrations were typically observed in the morning between 7 and 8 a.m., with the peak concentration exceeding 40 000 particles cm^{-3}. The particle number decreased due to PBL ventilation between 9 and 11 a.m.,[367] and the lowest concentrations of about 10 000 cm^{-3} were typically observed overnight.

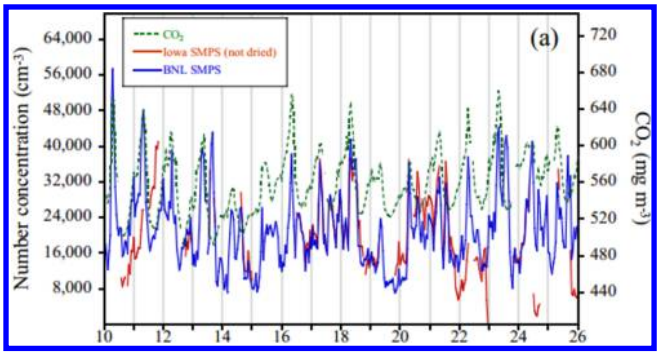

Figure 24. Time series measurements made at the T0 research site during March 2006. Particle number concentration (SMPS) and CO_2. Reprinted with permission from ref 367. Copyright 2011 Copernicus Publications.

The size-resolved PM composition measured in Mexico City is also shown in Figure 19. Fine PM in Mexico City is dominantly comprised of organic aerosols (66%), followed by sulfate (14%), nitrate (11%), ammonium (8%), and chloride (1%). PMF analysis indicates that the major components of organic aerosols originate from primary urban emissions, biomass burning/wood smoke, and secondary anthropogenic and biogenic sources. Paredes-Miranda et al.[391] showed that on average the secondary species accounts for about 75% of the fine PM mass. BC is also a major contributor to the overall fine PM (Figure 25).[90] For PM with a diameter of less than 100 nm, organic and BC aerosols are the two largest contributors, likely due to combustion emissions; however, as the particle size increases, the inorganic species becomes more dominant, because of photochemical growth. For particles with a diameter larger than 1 μm, soil dusts become a significant source of PM. The PM species exhibit a clear diurnal cycle (Figure 25), with the exception of soil dust.[90] The diurnal cycle of submicrometer nitrate is controlled by HNO_3 production from OH + NO_2 and gas-to-particle partitioning to form ammonium nitrate. Sulfate is shown to have a fraction similar to that of nitrate, yet with a much weaker diurnal cycle and a larger background, consistent with the regional presence of this species in Mexico City.

The diurnally averaged SSA at 532 nm varies from 0.60 at 7 a.m. to 0.85 at midday;[391] the maximum value is associated with strong photochemical generation of secondary aerosols, and the minimum value is associated with the morning rush hour emissions. A strong correlation of scattering at 532 nm and the total aerosol mass concentration is identified, and an average mass scattering efficiency factor of 3.8 m^2 g^{-1} is determined.[391] Fine PM in Mexico City exhibits a wide range of densities (1.1–3.4 g cm^{-3}), suggesting a dynamic, externally mixed aerosol population.[392]

5.3.4. Beijing, China. Beijing is one of the most populous cities in the world with a population of over 21 million in 2013. Similar to the Los Angeles basin, Beijing is prone to develop stagnant conditions, because of surrounding mountains to the

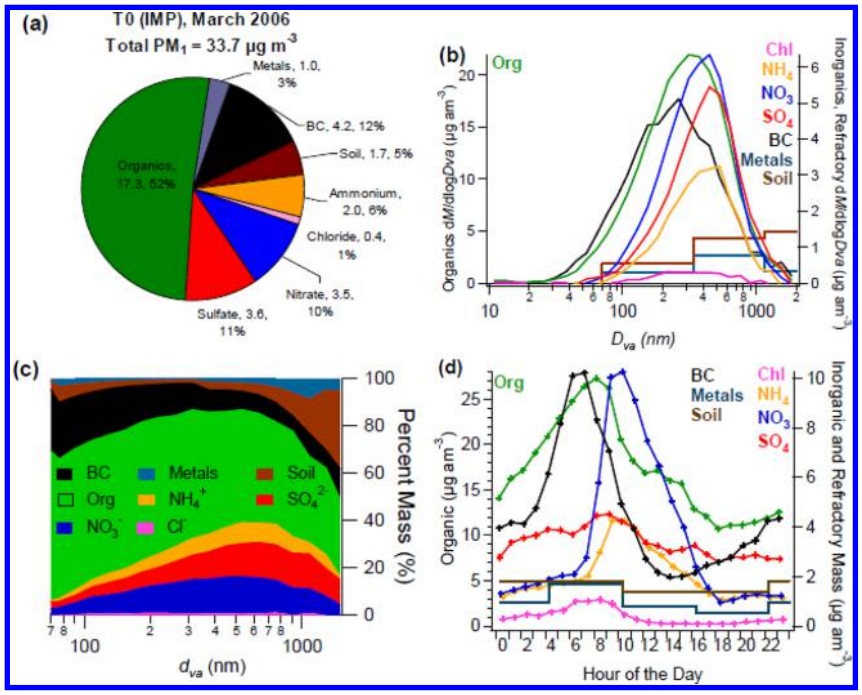

Figure 25. PM_1 aerosol mass concentrations, size distributions, and diurnal profiles. AMS species plus refractory species: (a) average mass concentrations, (b) size distributions, (c) NR-PM_1 (NR = nonrefractory) size distributions by percent mass, and (d) diurnal profiles. Reprinted with permission from ref 90. Copyright 2009 Copernicus Publications.

DOI: 10.1021/acs.chemrev.5b00067
Chem. Rev. 2015, 115, 3803–3855

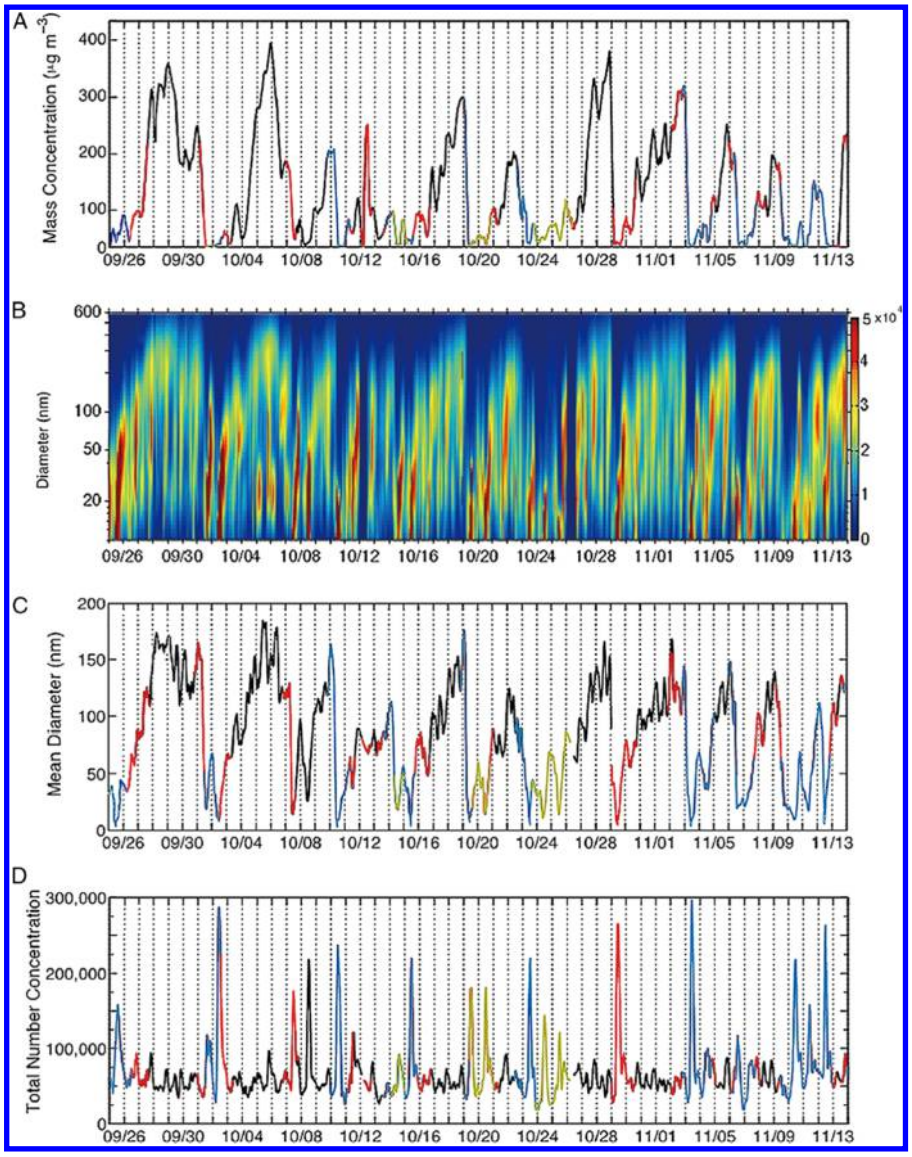

Figure 26. Periodic $PM_{2.5}$ cycles in Beijing. Temporal evolutions of $PM_{2.5}$ mass concentration (A), number size distribution (B), mean diameter (C), and total number concentration (D) during the $PM_{2.5}$ events from Sept 25 through Nov 14, 2013. The colors in (A), (C), and (D) represent the air mass originating from the south (black), northwest (blue and red), and northeast (yellow). The color contour in (B) denotes the particle number concentration, i.e., $dN/d \log D$ (cm^{-3}) on the right vertical axis (where N and D represent the particle number and size, respectively). Each $PM_{2.5}$ cycle includes a clean period in the beginning, a polluted period in the end, and their transition. The dates on the x axis (also the vertical lines) correspond to midnight local time. The mean particle diameter is computed using a log-normal function from each measured size distribution at a given time. Reprinted with permission from ref 6. Copyright 2014 National Academy of Science.

north of the city.[6] Recent severe haze events of unprecedentedly high PM levels in China have attracted significant public attention due to significantly reduced visibility and negative health effects. NPF events occur frequently in Beijing, according to several field campaigns, such as the Campaign of Atmospheric Research in Beijing and Surrounding Areas (CAREBejing) in the summer of 2008.[6,100,118,314,393] An annual statistics of NPF measurements from March 2004 to February 2005 shows that NPF events occur during all seasons in Beijing, with the frequency of 50%, 20%, 35%, and 45% for the spring, summer, fall, and winter, respectively.[393] The nucleation rates at 1.5 nm ($J_{1.5}$) and 3 nm (J_3) in NPF events observed in Beijing range from several to 100 particles cm^{-3} s^{-1},[100,118,314,393] comparable with the values observed in other cities.[394] Gaseous sulfuric acid is shown to play an important role in NPF in Beijing.[118,314] For instance, Yue et al.[314] showed that the average formation rates during the CAREBeijing-2008 campaign linearly correlate with the sulfuric acid concentration with a high correlation coefficient (R^2 = 0.85). In addition, Wang et al.[100] suggested that organic compounds participate in the nucleation process in Beijing, since the nucleation rate exhibits a good correlation with the concentrations of sulfuric acid and organic vapors.

The measured $PM_{2.5}$ properties in Beijing typically exhibit a periodic cycle of 4−7 days (Figure 26).[6] For example, the particle mass concentration is less than several tens of micrograms per cubic meter (clean) in the beginning of each cycle and reaches several hundred micrograms per cubic meter (polluted) within 2−4 days. A higher number concentration of smaller particles exists during the clean period, and a slightly lower particle number concentration of larger particles exists during the polluted period. During a pollution episode, an average daily particle mass growth of 50−110 $\mu g\ m^{-3}$ typically coincides with a

DOI: 10.1021/acs.chemrev.5b00067
Chem. Rev. 2015, 115, 3803−3855

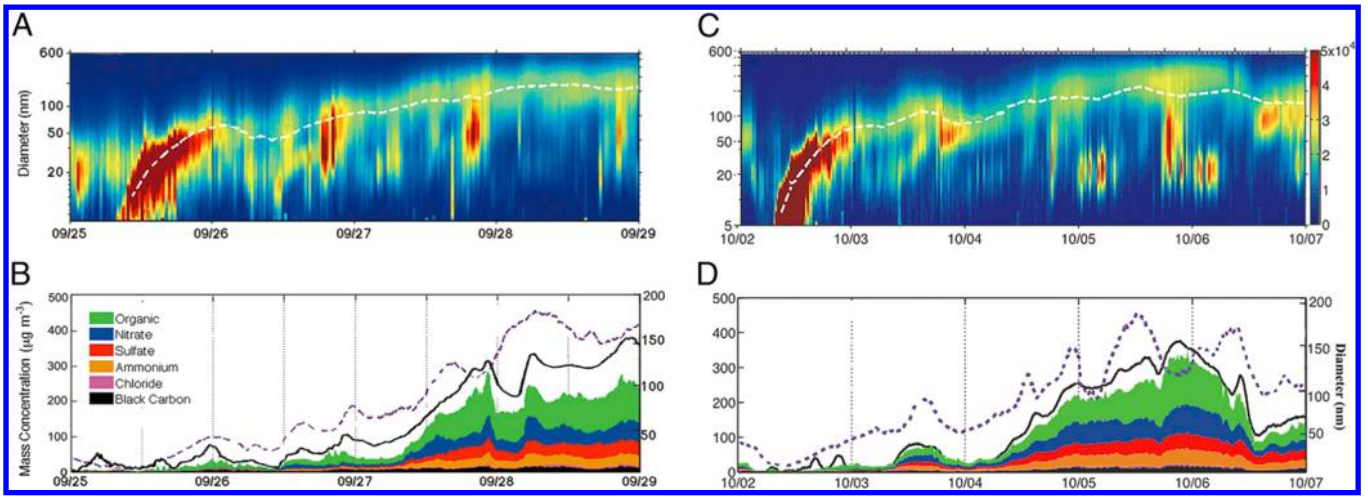

Figure 27. Aerosol nucleation and growth during the $PM_{2.5}$ episodes on Sept 25−29 and Oct 2−7. (A, C) Temporal evolutions of particle number size distribution and mean diameter (white dashed curve) on Sept 25−29 (A) and Oct 2−7 (C). (B, D) $PM_{2.5}$ mass concentration (black solid line), mean diameter (purple dashed line), and PM_1 (particulate matter smaller than 1.0 μm) chemical composition on Sept 25−29 (B) and Oct 2−7 (D). The shaded colors denote the mass concentrations of the aerosol constituents, i.e., green for organics, blue for nitrate, red for sulfate, yellow for ammonium, purple for chloride, and black for black carbon. Reprinted with permission from ref 6. Copyright 2014 National Academy of Science.

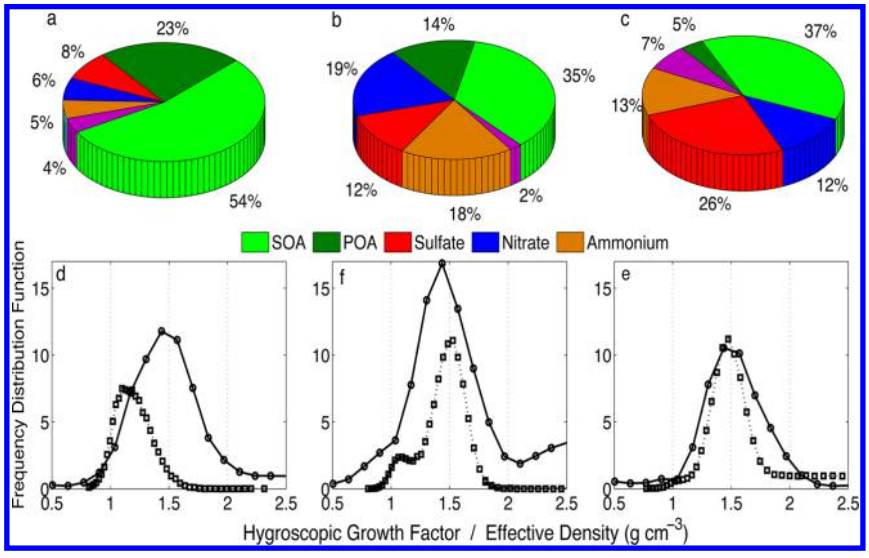

Figure 28. Particle chemical compositions during the clean, transition, and polluted periods for the Sept 25−29 and Oct 2−7 episodes. (a−c) Chemical compositions for 80 nm (a), 100 nm (b), and 240 nm (c) particles measured by AMS at 1500 h on Sept 25, 1200 h on Sept 27, and 1800 h on Sept 28, respectively. (d−f) Effective density (solid line, circles) and hygroscopicity (dashed line, squares) for 46 nm (d), 97 nm (e), and 240 nm (f) particles measured at 1500 h on Oct 2, 1200 h on Oct 4, and 1200 h on Oct 5, respectively. Reprinted with permission from ref 6. Copyright 2014 National Academy of Science.

daily increase of 40−65 nm in the mean diameter. The total particle number concentration is more than 200 000 cm^{-3} during the clean period, and decreases slightly and remains at about 50 000 cm^{-3} throughout the polluted period. The periodic cycles of severe haze episodes in Beijing are largely driven by meteorological conditions; stagnation typically develops with weak southerly wind from polluted industrial source regions.[6] The average particle mass concentrations of 35 and 114 $\mu g\ m^{-3}$ during the clean and polluted periods correspond closely to the northerly and southerly wind conditions, respectively.

The development of PM episodes in Beijing is characterized by two distinct aerosol formation processes, i.e., nucleation and growth (Figure 27).[6] Nucleation consistently occurs prior to a polluted period, producing a high number concentration of nanoparticles under clean conditions. The PM growth process is reflected by the particle mass concentration exceeding several hundred micrograms per cubic meter within 2−4 days, which is accompanied by a continuous size growth from the nucleation mode particles. Figure 27 shows very large particle mass increases of 270 $\mu g\ m^{-3}$ (on Sept 27, 2013) and 210 $\mu g\ m^{-3}$ (on Oct 4, 2013) during the daytime (6:00 a.m. to 6:00 p.m.), when the particle mean size increases by 60−70 nm. During the clean period, there exist high concentrations of ultrafine particles, but those particles contribute negligibly to the particle mass concentration; the severe pollution episodes in Beijing are attributable to the presence of numerous large particles with exceedingly high mass concentrations.

The PM chemical composition in Beijing consists dominantly of organics (44%) and nitrate (22%), followed by sulfate (17%), ammonium (15%), and chloride (2%) (Figure 19).[6] Measurements show continuously increasing mass concentrations of organics, sulfate, and nitrate during the transition and polluted

DOI: 10.1021/acs.chemrev.5b00067
Chem. Rev. 2015, 115, 3803−3855

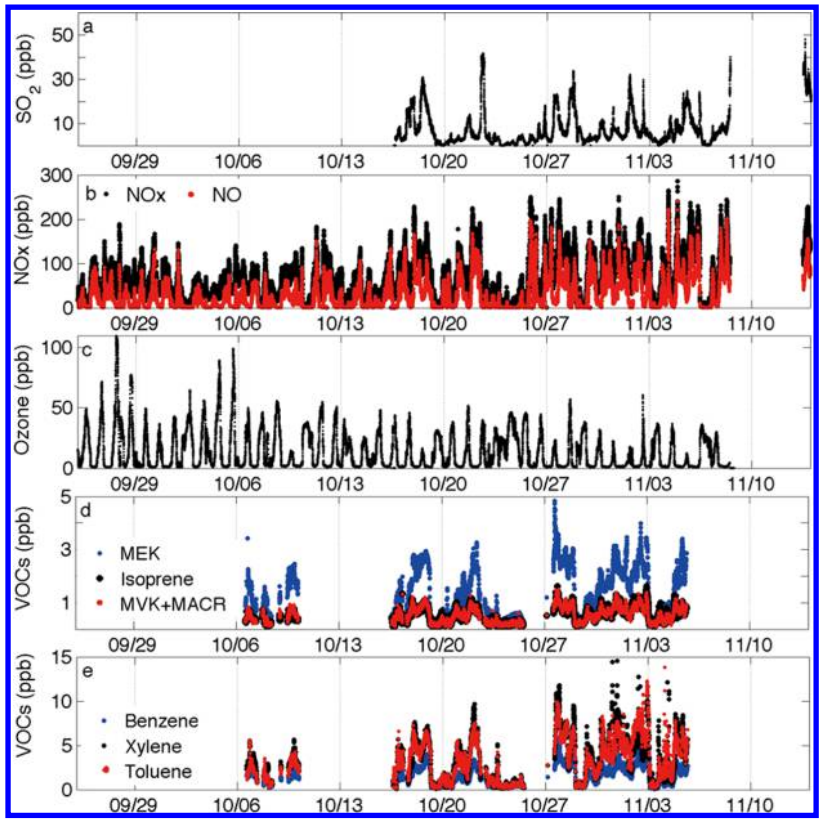

Figure 29. Measurements of gaseous species in Beijing. (a–c) Concentrations of SO_2 (a), NO_x (b), and O_3 (c) measured between Sept 25 and Nov 13. (d, e) Biogenic species, i.e., isoprene, methacrolein (MACR), methyl vinyl ketone (MVK), and methyl ethyl ketone (MEK) (d), and aromatic hydrocarbons, i.e., xylene, benzene, and toluene (e). The NO_x and SO_2 concentrations were the lowest with northwesterly and northeasterly winds (the clean period) but increased considerably with southerly winds (the transition and polluted periods). The high peak ozone concentrations that occurred on Sept 27 (110 ppb) and Oct 5 (99 ppb) clearly coincided closely with the largest particle mass growths during the two $PM_{2.5}$ events. Interestingly, the daily ozone peak on Oct 5 reached 100 ppb, when the $PM_{2.5}$ level was consistently about 300 $\mu g\ m^{-3}$, indicating sufficient photochemical activity during the polluted period. The peak isoprene concentration is typically around 1–2 ppb. Aromatic VOC concentrations are high throughout the pollution cycles. Reprinted with permission from ref 6. Copyright 2014 National Academy of Science.

periods, correlating closely with the evolutions of the $PM_{2.5}$ mass concentration and mean particle size (Figure 27). The organic mass fraction dominates in the clean period and decreases slightly from the clean to polluted periods (Figure 28). In contrast, the contributions of sulfate and nitrate to the particle mass concentration increase slightly during the pollution episodes. The primary organic aerosol mass fraction decreases during the episodes, indicating small contributions of primary particle emissions to the pollution development.[6]

The gaseous aerosol precursors (i.e., VOCs, NO_x, and SO_2) are high during the pollution episodes in Beijing (Figure 29). For example, the SO_2 and NO_x peak concentrations are over 40 and 200 ppb, respectively, and the aromatic hydrocarbons (xylenes and toluene) represent the most abundant types of VOCs, with a xylene peak concentration of more than 10 ppb. The photochemical oxidation and/or multiphase reactions of VOCs, SO_2, and NO_x lead to formation of less volatile or nonvolatile species,[145,239] contributing to the aerosol organic, sulfate, and nitrate constituents, respectively. On the other hand, the contributions from primary emissions and regional transport of particles to the formation of severe haze episodes in Beijing have been demonstrated to be small.

The density and hygroscopicity measurements also reveal an organic-dominant composition in Beijing. The peak effective density of 1.1 g cm^{-3} during the clean day (Figure 28d) is indicative of PM dominated by organics. The increased hygroscopicity and effective density from clean to polluted periods reveal the formation of an internal mixture of secondary organic and inorganic species, with increasing contributions from sulfate and nitrate.[6] The average SSA (at wavelengths of 470 and 500 nm) in Beijing is near 0.87, indicating the presence of moderately strong absorbing aerosol and being higher than those in the southern regions in China.[395] The differences in SSA in urban regions may cause totally opposite aerosol radiative effects and lead to distinct feedback processes on PM formation and removal.[41,396]

The efficient aerosol nucleation and growth in Beijing are clearly distinct from those in other urban cities. For example, the variations in the PM properties (i.e., particle number, size, and mass concentration) in Houston, Los Angeles, and Mexico City typically exhibit a clear diurnal characteristic. In contrast, the aerosol properties in Beijing exhibit continuous evolutions from the nucleation mode particles over an extended period of 2–4 days, yielding numerous large particles during the pollution episodes. The considerably more efficient aerosol nucleation and growth processes in Beijing are explained by much higher concentrations of aerosol precursor gases, i.e., anthropogenic VOCs (aromatics), NO_x, and SO_2, than those in the other three cities (i.e., Figures 3 and 18). On the other hand, the particle compositions in Beijing exhibit a general similarity to those commonly measured in many global urban areas, consistent with the chemical constituents that are dominated by secondary

DOI: 10.1021/acs.chemrev.5b00067
Chem. Rev. 2015, 115, 3803–3855

Table 3. List of Several Regional and Global Emission Inventories

inventory	resolution	spatial coverage	temporal coverage	VOC speciation	primary PM species	ref
TRACE-P	0.5 × 0.5	East, Southeast, and South Asia	2000	19 categories based on functional groups and reactivity	only BC and OC; no $PM_{2.5}$ and PM_{10}	Streets et al.[405]
INTEX-B	0.5 × 0.5	East, Southeast, and South Asia	2006	CB04, CB05, RADM2, SAPRC99, SAPRC07	BC, OC, $PM_{2.5}$, PM_{10}	Zhang et al.[406]
REAS	0.5 × 0.5	East, Southeast, and South Asia	1980−2020	not speciated	only BC and OC; no $PM_{2.5}$ and PM_{10}	Ohara et al.[407]
REAS2	0.25 × 0.25	Asia	2000−2008	19 categories based on functional groups and reactivity	BC, OC, $PM_{2.5}$, PM_{10}	Kurokawa et al.[408]
MEIC	multiresolution	China	2008, 2012	CB05, SAPRC99, RADM2	BC, OC, $PM_{2.5}$, PM_{10}	www.meicmodel.org
NEI	up to 4 km	North America	1999−2012	CB05	$PM_{2.5}$, PM_{10}; speciation profiles provided	www.epa.gov/ttn/chief/index.html
EMEP	0.1 × 0.1	Europe	1980−2012	14 species for EMEP air quality model	BC, OC, $PM_{2.5}$, PM_{10}	www.emep.int
EDGARv4.2	0.1 × 0.1	global	1970−2008	not speciated	PM_{10}	www.edgar.jrc.ec.europa.eu

aerosol formation (Figure 19). For example, the PM mass fractions of organic, sulfate, and nitrate of 44%, 17%, and 22% in Beijing are nearly identical to those of 44%, 17%, and 24% in Los Angeles, respectively, likely reflecting the chemical constituents dominantly from traffic emissions (i.e., VOCs and NO_x). For comparison, the mass fractions of organic, sulfate, and nitrate are 35%, 30%, and 8% in Houston and 66%, 14%, and 11% in Mexico City, respectively, indicating additional emission components from industry, biomass burning, and the regional biosphere (i.e., SO_2 for Houston and VOCs for Mexico City), in addition to those from urban traffic.[128,360,387−389]

6. ATMOSPHERIC MODELING

6.1. Primary PM and Gas Precursor Emissions

Since VOCs, NO_x, SO_2, and NH_3 represent the major precursors for secondary urban fine PM formation, an accurate representation of their emission sources is critical for air quality modeling.[397] For VOC emissions, major anthropogenic sources include gasoline and diesel vehicles, solvent utilization, and industries. For example, VOC emissions from the petrochemical industry in Houston are approximately 50% of the emissions from gasoline vehicles.[398] Vehicles and solvent utilization are the major sources of SOA based on a study[399] using a source-oriented community multiscale air quality (CMAQ) model. For NO_x emissions, diesel and gasoline vehicles and engines, industries, and coal combustion are the common sources in urban areas. Diesel vehicles have a much higher emission rate of NO_x per vehicle, but gasoline vehicles usually dominate the vehicle fleet. In Los Angeles and Houston, NO_x emissions from diesel vehicles and gasoline vehicles are approximately equal.[400,401] In the Houston area, another important source of NO_x is natural gas burning,[401] accounting for approximately 36% of the total anthropogenic NO_x emissions. In other urban areas such as Mexico City and Beijing, liquefied-petroleum-gas- or compressed-natural-gas-powered vehicles account for a noticeable fraction of the vehicle fleet and can be an important source of NO_x.[402] In Beijing, NO_x emission from power plants, industries, and motor vehicles is estimated to account for 40%, 20%, and 20% of the particle-phase nitrate.[403] Since there is little local emission of NO_x from power plants in Beijing, most of the NO_x is likely due to local transportation and regional transport from upwind source areas.[404] SO_2 in urban regions is mainly from fuel combustion. In Los Angeles, most of the SO_2 is emitted from commercial marine vessels, followed by aircraft and highway vehicles, based on National Emission Inventory (NEI) 2011. In Houston, most of the local SO_2 is emitted from chemical and petroleum industries based on NEI 2011. In Beijing, SO_2 from regional coal combustion dominates the emissions. In Mexico City, SO_2 emitted from a large thermoelectric power plant has a large impact on SO_2 concentrations in the city. NH_3 is mostly emitted from agricultural activities. In urban areas with heavy traffic, NH_3 emissions from catalyst-equipped motor vehicles can significantly contribute to NH_3 concentrations.[399,400]

Most of the primary PM in urban areas is emitted from combustion sources, such as highway vehicles, industries, residential fuel combustion, etc. Road dust, including paved road dust and construction dust, are also important in urban areas. In Beijing, residential fuel combustion dominates the local primary PM emissions.[8]

A number of regional and global emission inventories are available for modeling urban air pollution (Table 3). The most widely used inventories are NEI developed by the U.S. EPA. The NEI includes both criteria (CO, NO_x, SO_2, VOC, $PM_{2.5}$, and PM_{10}) and hazardous air pollutants and is updated every three years with a bottom-up approach using detailed reported emissions from industries, emission estimates, and emission model inputs from state, local, and tribal air pollution control agencies as well as data developed by the U.S. EPA.

For air quality modeling in Asia, the most widely used emission inventories are the Transport and Chemical Evolution over the Pacific (TRACE-P)[405] and the Intercontinental Chemical Transport Experiment B (INTEX-B) inventories.[406] In addition, the Regional Emission Inventory in Asia (REAS)[407] and its successor REAS2[408] have also been used in air quality modeling studies. Recently, detailed emission inventories for the entire country of China have been compiled and employed in a number of modeling studies.[409−411]

Emissions of VOCs and PM are speciated in air quality models. The SPECIATE database developed by the U.S. EPA (http://www.epa.gov/ttnchie1/software/speciate/) currently is the most comprehensive VOC and PM species profile database. Most of the fuel combustion profiles in SPECIATE, such as gasoline and diesel vehicles and engines[412,413] and wood burning,[414,415] are for U.S.-specific emitters.

Emissions from natural sources are also required for urban air quality modeling.[416] These emissions include gas and aerosol emissions from vegetation, soil, ocean, wildfire, sea spray, and lightning. For example, biogenic volatile organic compound (BVOC) emissions are typically estimated using the model of emissions of gases and aerosols from nature (MEGAN).[417,418]

DOI: 10.1021/acs.chemrev.5b00067
Chem. Rev. 2015, 115, 3803−3855

Emissions of primary aerosols from biogenic sources, such as pollen, can also be incorporated into the biogenic emission models because they depend on the vegetation types.[419] Emissions from soil include windblown dust, and NO_2 and CO from microbial processes. NO_x and CO emissions are estimated within MEGAN and biogenic emission inventory systems (BEISs) and are affected by soil moisture.[417] Windblown dust emissions from soil erosion can be estimated with a number of dust emission parametrizations.[420−422]

6.2. Gaseous and Multiphase Chemistry

6.2.1. Gas-Phase Photochemical Oxidation Mechanism. Reactions of inorganic species in different photochemical mechanisms are generally similar, and have been reviewed by Atkinson et al.[423] Reactions of NO_x and VOCs are extremely complex[424,425] and are represented differently in various photochemical mechanisms. The mechanisms used in current urban/regional chemical transport models include carbon bond 4 (CB04) and CB05,[426−428] regional acid deposition model 2 (RADM2),[429] regional atmospheric chemistry mechanism (RACM),[430] statewide air pollution research center 99 (SAPRC99) (S99),[431] S07,[432,433] and S11,[434] and master chemical mechanism (MCM).[435−437] These models represent primary organic molecules, intermediate reaction products, and radical reactions with different levels of complexity. The various models have generally been tuned to reproduce the ozone concentrations with similar capabilities, but lead to quite different predictions of oxidation products (e.g., HCHO), reservoir species (e.g., PAN), and radical (e.g., OH and HO_2) concentrations.[438−440] Another model for simulating aerosol interactions and chemistry (MOSAIC) has been increasingly used in regional models due to its computational efficiency.[441]

6.2.2. New Particle Formation. The particle size distribution is modeled either using an explicit multisize bin approach or using a modal approach with three modes representing the ultrafine, fine, and coarse mode aerosols. The nucleation process is typically modeled by binary nucleation involving water vapor and sulfuric acid or ternary NH_3−H_2SO_4−H_2O nucleation. On the basis of a study[442,443] that implemented and examined the different nucleation parametrizations in the CMAQ model and compared the predicted and observed PM number concentrations, the various nucleation parametrizations yield significantly different ultrafine particle number concentrations, but all underpredicted number concentrations (by up to a factor of 13.7). Fan et al.[103] implemented a nucleation scheme in CMAQ that considers the enhanced nucleation rate due to condensable secondary organic vapors[111] and shows a good model measurement intercomparison for the particle number size distribution in Houston, TX (Figure 30). On the other hand, the binary nucleation scheme underpredicts the concentrations of smaller particles (i.e., about 10 nm) by more than an order of magnitude.

6.2.3. Multiphase Processes. A review and an assessment of five inorganic thermodynamic modules have been presented by Zhang et al.[444] Earlier models, such as the aerosol inorganic model (AIM)[445] and ISORROPIA,[446] only treat the system H^+−NH_4^+−Na^+−SO_4^{2-}−NO_3^-−Cl^-−H_2O. Extension of these modules, such as ISORROPIA II,[447] includes crustal species such as K^+, Ca^{2+}, and Mg^{2+}, making them appropriate for sea salt and windblown dust particles. The detailed aerosol composition is determined either by using iterative algorithms to minimize the Gibbs free energy of the system (as used by the AIM model) or by iteratively solving the chemical and phase partitioning equilibrium equations using the estimated equilibrium constants (as used by the ISORROPIA model). Aerosol liquid water is typically calculated using the Zdanovskii−Stokes−Robinson (ZSR) method.[448]

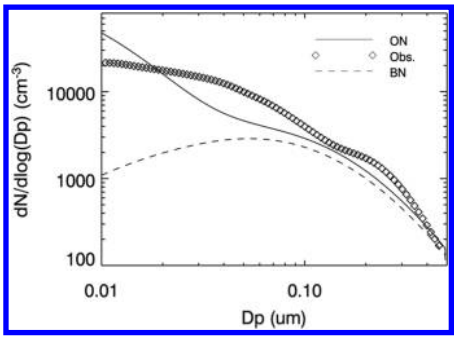

Figure 30. Comparison of aerosol simulations with the ground-level measurements at the Aldine site in Houston. The solid, dashed, and tilted square curves correspond to simulations using the organic nucleation (ON) and binary nucleation (BN) schemes and measurements, respectively. Both the modeled and measured number size distributions ($dN/d\log(D_p)$) were averaged over the daytime (8 a.m. to 6 p.m.) during the episode. Reprinted with permission from ref 103. Copyright 2006 American Geophysical Union.

In addition to gas-phase formation of HNO_3 and H_2SO_4 and their subsequent gas-to-particle partitioning, aqueous-phase reactions (in-cloud) are also important in sulfate formation. Oxidation of S(IV) (including dissolved SO_2, HSO_3^-, and SO_3^{2-}) by several common oxidants such as H_2O_2, O_3, and O_2 catalyzed by ferric iron (Fe^{3+}) and manganese ion (Mn^{2+}) is also included in several chemical transport models (CTMs). Zhang et al.[449] modeled sulfate formation in East Asia and determined that the gas- and aqueous-phase pathways are equally important. In summertime, the aqueous-phase pathways account for more than 70% of sulfate in the PRD region.[403] In polluted urban areas with high aerosol concentrations such as Beijing, the concentrations of Fe^{3+} and Mn^{2+} are also high, but most models currently do not accurately predict the Fe^{3+} and Mn^{2+} concentrations, leading to large uncertainties in predicting sulfate formation from this important pathway.

Nitrate formation from N_2O_5 on aqueous aerosols has been included in many CTMs.[400,450,451] A number of parametrizations have been used to estimate the uptake coefficient of N_2O_5 as a function of the aerosol sulfate, nitrate, ammonium, chloride, and water contents.[450,452−454] The importance of the N_2O_5 heterogeneous reaction varies between urban and rural areas and is more important in urban areas during wintertime due to the lower temperature, which favors nitrate partitioning to the aerosol phase and high concentrations of NO_2 to form N_2O_5. It has been shown that the N_2O_5 hydrolysis plays an important role in nighttime nitrate formation in Beijing.[270] The NO_2 heterogeneous reaction on a wet aerosol surface is also included in the CMAQ model, with the uptake coefficient of NO_2 based on that reported by Vogel et al.[455] Rapid nitrate and sulfate formations during a wintertime haze episode were observed in Beijing, but could not be explained by model simulations involving gaseous and aqueous reactions.[456] Recently, Zheng et al.[456] included a number of additional heterogeneous reactions for N_2O_5, NO_2, HNO_3, HO_2, NO_3, O_3, OH, and SO_2 on aerosol surfaces and suggested that inclusion of these reactions leads to significant improvements in nitrate and sulfate predictions under haze conditions in Beijing. The heterogeneous reactions have

DOI: 10.1021/acs.chemrev.5b00067
Chem. Rev. 2015, 115, 3803−3855

been originally proposed by Wang et al.[457] to occur on dust particle surfaces.

Li et al.[458] and Sarwar et al.[459] investigated the importance of CI reactions on regional sulfate and nitrate in the eastern United States and determined that CI reactions lead to a ~20% increase of sulfate in Southeast Texas near Houston, but a negligible increase in nitrate concentrations. The importance of the CI reactions is largely determined by competition from the reaction of H_2O with CI. Ying et al.[460] evaluated the formation of sulfate from CI and heterogeneous reaction of SO_2 in Mexico City and determined that CI reactions only lead to a slight increase in sulfate, while inclusion of the SO_2 heterogeneous reactions on aerosol surfaces significantly improves the sulfate predictions.

Traditionally, predictions of SOA in CTMs are mostly based on the equilibrium absorption partition theory of Pankow[154] with the aerosol yield and vapor pressure parameters derived from fitting of environmental chamber data for SOA yields using the two-product model of Odum et al.,[155] as discussed in section 4.1. Lumped or representative species have been used to represent many precursor VOCs and their oxidation products in CTMs.[461] The major precursors of traditional SOA include long-chain alkanes, aromatic compounds, monoterpenes, and sesquiterpenes. The SOA modeling approach has been implemented in widely used regional and global CTMs, such as CMAQ[462] and the Goddard Earth Observing System—3D chemical transport model (GEOS-Chem).[463] The condensed organics are assumed to form a single organic phase that does not mix with the inorganic aqueous phase. Thermodynamic models have also been proposed to allow for formation of multiple organic phases,[464,465] but have not been widely applied in regional SOA modeling.

Although the two-product equilibrium partitioning method can generally reproduce well-controlled laboratory measurements at relatively high SOA levels, simulated SOA concentrations in urban/regional models have been typically lower than field-measured concentrations,[141,147,466,467] partly because the two-product method cannot represent the photochemical aging of gas precursors and multigeneration formation of SOA products. The VBS approach addresses this problem by tracking the changes in the volatility distribution of the organic compounds due to photochemical aging.[468] Similar to the aerosol yields in the two-product model, the VBS approach does not model the detailed products, and additional parameters such as the rate of photochemical aging and volatility distribution of emissions and reaction products need to be estimated or determined from measurements for the SVOCs. In addition to the lumped photochemical mechanisms used in the two-product and VBS approaches, near-explicit photochemical mechanisms[142,435] that represent the multistep oxidations of a large number of primary emitted VOCs and their oxidation products have been used to simulate SOA formation.[458,469,470]

Recently, progress has been made in modeling SOA formation due to heterogeneous reactions of glyxoal/methylgloxal, IEPOX, and methacrylic acid epoxide. Near-explicit or lumped photochemical mechanisms are developed to include formation of these SOA precursors from parent species, such as aromatic compounds and isoprene. A simple approach to model SOA formation from these precursor species is to treat a surface-controlled uptake process.[45,471] A number of studies have modeled the detailed partitioning and subsequent aqueous-phase reactions of glyoxal/methylglyoxal and isoprene epoxides.[207,472,473] Formation of accretion products (oligomers) in the organic phase from condensed semivolatile compounds is also included in SOA models, assuming that it occurs by the reactions of semivolatile SOA following a uniform first-order rate constant of 0.8 day^{-1}.[462]

The importance of glyoxal and methylglyoxal in SOA formation has been shown in model simulations for Mexico City,[170] Houston,[471] and Los Angeles.[474] In urban areas, acetylene, ethylene, aromatic compounds, and direct emissions of glyoxal are important sources of glyoxal and methylglyoxal. In Beijing, high concentrations of anthropogenic VOCs and rapid increases of SOA have been measured in fall and winter.[6] SOA modeling including the surface uptake of glyoxal and methylglyoxal needs to be performed to evaluate if such a rapid formation rate can be reproduced. Primary emission of VOCs and gas-phase reaction mechanisms also need to be further examined. The importance of isoprene on SOA formation also needs to be further examined in urban areas, since isoprene is a significant source of glyoxal, methylglyoxal, and IEPOX. The contribution of IEPOX to SOA in Houston is estimated to be approximately 40%.[471]

6.3. Regional Transport and Removal Processes

Urban areas act as a source of PM to areas downwind and are also influenced by direct PM or its precursor emissions from upwind regions. Primary PM has a typical transport distance of approximately 20−30 km.[475] Atmospheric modeling using tagged reactive species to track emissions from different source regions reveals that secondary ammonium nitrate and sulfate particles may be formed from precursors emitted hundreds of kilometers downwind. For example, approximately 20% of the secondary ammonium nitrate and ammonium sulfate in Beijing and surrounding areas in northern China is estimated due to long-range transport of emissions from eastern China.[404] In Mexico City, SO_2 emissions from the Tula Industrial Complex, cement plants, and the Popo volcano greatly contribute to the sulfate concentration in the city.[460,476] In Houston, the majority of sulfate aerosols is from upwind SO_2 sources in the northeastern United States.[399] In the Los Angeles area, the highest ammonium nitrate concentrations always occur in areas north of Riverside, approximately 100 km downwind of downtown Los Angeles, where most of the NO_x is emitted.[400] The availability of NH_3 often determines the regional transport of secondary nitrate. In areas with large NH_3 emissions, HNO_3 formed from upwind sources readily combined with NH_3 to form secondary ammonium nitrate, while in low NH_3 regions NO_x cannot be converted to ammonium nitrate effectively.[400,475]

Dry deposition represents an important removal mechanism for air pollutants.[477] Dry deposition velocities of gaseous precursor species and PM in CTMs are commonly calculated using a resistance-in-series model, in which the deposition velocity is governed by the aerodynamic resistance, quasi-laminar layer resistance, and surface/canopy resistance.[5] A number of parametrizations of PM dry deposition velocities have been developed for use with the resistance-in-series approach in regional CTMs.[478,479] More detailed urban canopy models have been used in meteorological models to account for the influence of urban areas on heat and momentum transfer, but only a few developments and applications of the urban canopy model in dry deposition simulation have been reported.[480] Over the United States in summer, it has been found that dry deposition of condensable organic vapors is responsible for major reductions in SOA, decreasing the surface concentrations by about 50% for biogenic and 40% for short-chain anthropogenic precursors.[477]

DOI: 10.1021/acs.chemrev.5b00067
Chem. Rev. 2015, 115, 3803−3855

In general, two cloud removal processes are included in CTMs: in-cloud scavenging and below-cloud scavenging. For gaseous species, the scavenging coefficient is affected mostly by the Henry law constant, precipitation rate, droplet size distribution, and pH of the droplets, if dissolved gases participate in acid−base reactions. For PM, the scavenging coefficient is a function of the precipitation rate, particle and rain droplet size distributions, and particle−cloud collision efficiency. Details of the parametrizations of scavenging coefficients can be found elsewhere.[5] Similar to the cloud treatment in mesoscale meteorological models, for coarse-resolution domains, a subgrid cloud model is used to parametrize precipitation from subgrid convective and nonconvective clouds. A resolved cloud model is used to estimate precipitation from clouds for fine resolution grid cells (horizontal resolution less or equal to 4 km). The major uncertainty in wet-deposition modeling lies in the precipitation rate, as regional meteorological models are known to perform poorly on high-resolution precipitation rate calculations.

7. FUTURE DIRECTIONS AND CONCLUSIONS

It is clear that fine PM in different global urban areas exhibits distinct characteristics in particle properties, dependent on the emission sources, the formation mechanisms, removal, and the meteorological conditions. For example, while the four urban centers exhibit a noticeable secondary PM formation, the secondary PM formation in Beijing is most prominent, characterized by two aerosol formation mechanisms, i.e., nucleation and growth. Typically, there exist clear diurnal variations in the PM number, size, and mass concentration in Houston, Los Angeles, and Mexico City (i.e., Figures 17, 21, and 25), reflecting the interplay between primary emissions, new particle formation, photochemical growth, removal, and the PBL variation. In contrast, the fine PM properties in Beijing typically exhibit a periodic cycle of 4−7 days (Figure 26). Aerosol nucleation consistently precedes a polluted period in Beijing, producing a high number concentration of nanosized particles under clean conditions, and accumulation of the particle mass concentration exceeding several hundred micrograms per cubic meter is accompanied by a continuous size growth from the nucleation mode particles over multiple days to yield numerous large particles (Figure 27).

The efficient aerosol nucleation and growth in Beijing are attributable to highly elevated concentrations of gaseous aerosol precursors, most noticeably anthropogenic VOCs (aromatics), NO_x, and SO_2 emitted from local transportation and regional industrial activities (Figure 29). For example, during pollution episodes, the peak SO_2 and NO_x concentrations exceed 40 and 200 ppb, respectively, and the peak xylene and toluene concentrations exceed 10 ppb in Beijing.[6] These concentrations are significantly higher than those observed in the other three urban regions. For comparison, the typical peaks of NO_x and SO_2 were below 25 and 4 ppb and the aromatic hydrocarbon concentrations were typically less than 1−2 ppb in Houston, TX, during the 2009 Study of Houston Atmospheric Radical Precursors (SHARP) field campaign (Figure 18).[360] In Mexico City, the toluene concentrations can be elevated during the nighttime (10−20 ppb) because of industrial emissions but decrease to below 10 ppb during the daytime.[128] Interestingly, the levels of anthropogenic VOCs and NO_x in Beijing are comparable to those more than 50 years ago in Los Angeles, but much higher than the present values in Los Angeles (Figure 3).[79,81]

The combination of the enormously efficient aerosol nucleation and growth over an extended period leading to the severe $PM_{2.5}$ episodes in Beijing is uniquely different from those typically observed in the urban regions of developed countries (i.e., Houston and Los Angeles), Mexico City, and pristine environments worldwide. The efficient secondary formation in Beijing is also reflected by the much higher annual $PM_{2.5}$ mass concentration (102 $\mu g\ m^{-3}$) than those in Houston (12 $\mu g\ m^{-3}$), Los Angeles (12 $\mu g\ m^{-3}$), and Mexico City (27 $\mu g\ m^{-3}$). On the other hand, the PM chemical compositions measured in Beijing and Los Angeles are nearly identical, likely reflecting the secondary formation dominated from traffic emissions. Also, the secondary aerosol formation processes identified in Beijing may be characteristic of those in other urban cities of the developing world (such as India and other Asian developing countries), because of the rapidly growing economy and fast urbanization, leading to lower standards but higher rates for air pollutant emissions.

The currently available atmospheric chemical mechanisms in the gas and aqueous phases have yet to quantitatively account for the rapid accumulations of the PM chemical constituents under polluted conditions (i.e., Figure 27), particularly for the formations of secondary organic matter, sulfate, and nitrate.[237] It is plausible that there exist synergetic effects among the various organic and inorganic compounds (i.e., organics, sulfate, nitrate, basic species, etc.) to enhance the particle growth.[6] For example, the presence of basic species (i.e., ammonia and amines) may not only considerably enhance sulfate and nitrate formation, but also promote secondary organic matter production under polluted environments.[214] One such example is the acid−base reaction between organic acids and basic species to form more stable ammonium and aminium carboxylate salts, shifting the gas-particle equilibrium and increasing SOA formation.

The chemical mechanisms for the formation of secondary organic matter may also be distinct between developed and developing urban regions, leading to not only different PM production rates, but also different product types and aerosol properties. For example, while gas−particle partitioning of organic matter is linearly dependent on the gaseous reactant concentrations, oligomerization for hydration of small α-dicarbonyls and polymerization for aldol condensation of large aldehydes correspond to second- or higher-order reactions with respect to the organics to form high-molecular-weight species in the particle phase. The latter are expected to occur more efficiently with elevated gaseous concentrations under polluted conditions. Oligomerization of glyoxal and methyglyoxal may be especially important under urban environments, considering their large yields from the photochemical oxidation and the large abundance of aromatic hydrocarbons from traffic emissions.[6] In addition, while the gas-phase oxidation leading to formation of semivolatile and low-volatility organic compounds and subsequent gas−particle partitioning increase the particle hygroscopicity, oligomerization/polymerization generally leads to decreased hygroscopicity.[213] Furthermore, organic matter formed from oligomerization/polymerization may exhibit enhanced light absorption in the ultraviolet and visible ranges.[67] Presently, very few of the multiphase reactions have been incorporated into atmospheric models to assess their roles in the formation, growth, transformation, properties, and impacts of urban fine PM.

To improve the understanding of the formation of urban fine PM, future laboratory kinetic and mechanistic measurements of multiphase chemistry are critically needed, particularly for those

DOI: 10.1021/acs.chemrev.5b00067
Chem. Rev. 2015, 115, 3803−3855

leading to secondary organic matter, sulfate, and nitrate formations under atmospherically relevant conditions, i.e., RH, temperature, and reactant concentrations. The currently available yields of SOA formation for various VOC types using the environmental chamber method may not be representative of those under ambient conditions, since few studies have assessed the SOA formation potential from continuing VOC oxidation on a longer timescale, particle-phase reactions at variable RH and particle acidity, and cloud-processing. Laboratory experiments are also needed to quantify the different aerosol properties (i.e., hygroscopicity and optical properties) formed from the multiphase reactions involving organic and inorganic species. Those experimental results on atmospheric multiphase chemistry may assist in not only atmospheric modeling, but also interpretation and identification of urban fine PM in field measurements.

Further atmospheric measurements are needed to monitor simultaneously the gaseous aerosol precursors and a comprehensive set of aerosol properties (i.e., particle number, size, chemical composition, morphology, light scattering and absorption, hygroscopicity, etc.). Atmospheric field measurements are crucial to providing the information on the temporal and spatial distributions of gaseous concentrations and PM properties under diverse urban environments. To achieve the highest level of chemical speciation, the development of more advanced analytical techniques is required, including identification and quantification of the diverse gaseous aerosol precursors (i.e., carbonyls, sulfuric acid, nitric acid, organic acids, basic species, etc.) present in ambient air at parts per billion or lower levels and detailed chemical composition characterization of aerosols from the molecular cluster (<1 nm) to subnanometer and submicrometer size ranges. Simultaneous measurements of the particle density, hygroscopicity, volatility, and optical properties can further assist in identification of the particle chemical compositions, since those particle properties are distinct for different PM types.[6,329,360] Furthermore, improved physically based parametrizations of aerosol nucleation and growth developed on the basis of and validated against laboratory and field studies are required for incorporation into atmospheric models.

The human health effects of both high concentrations of ultrafine particles produced from NPF and high PM mass concentrations under urban environments need to be carefully evaluated. For example, the PM episodes in Beijing typically consist of clean and polluted periods, characterized by high concentrations of ultrafine particles ($>10^5$ particles cm^{-3} for particles smaller than 100 nm) with small mass concentrations and numerous large particles (about 5×10^4 for particles larger than 150 nm) with high mass concentrations, respectively. While many epidemiological studies have emphasized the correlations of the various health syndromes with the $PM_{2.5}$ mass concentrations,[2,15] little is known about the potential health outcomes of highly elevated concentrations of ultrafine particles produced from NPF under clean conditions.

The regional and climatic impacts of urban fine PM need to be further assessed to quantify their direct and indirect radiative forcing. A comparison of the aerosol optical depth over many megacities in the world reveals that the urban centers exhibit distinct levels of impacts on the global and regional climate.[481] Aerosols exhibit a much greater effect on direct radiative forcing in Beijing than in Los Angeles and Mexico City, and the annual reduction of net solar radiation at the surface in most tropical megacities exceeds 20 W m^{-2}, equivalent to reducing solar irradiance at the top of the atmosphere by more than 10%.[481] Also, in urban areas identified as PM hotspots, which include many megacities worldwide, solar heating by BC-containing particles has been shown to be comparable to warming caused by the greenhouse gases.[482]

In addition, model simulations have shown several-fold increases in the SOA mass for multiple days in the urban outflow from Mexico City, indicating that anthropogenic aerosol precursors influence the regional and global chemical and radiative characteristics of the atmosphere.[483] The ultimate fate of atmospheric organic carbon species is determined by their conversion to carbon dioxide (i.e., remaining in the gas phase), formation of secondary organic matter (leading to dry or wet deposition), or dry deposition of their certain gaseous forms.[4,5,27,477] For different VOC types, the distinct molecular functionalities and associated kinetic behaviors govern the yield, rate, and timescale of SOA formation from gas-phase oxidation (first- and multi-generations), particle-phase reactions, and cloud-processing, responsible for their atmospheric impacts. For example, it is plausible that reactive VOCs (such as aromatics, isoprene, and monoterpenes) dominate the local and regional PM production and subsequently contribute to the global tropospheric PM loading. On the other hand, even less reactive VOCs (including methane and smaller alkanes), which are unimportant locally to PM production, may need to be considered for their role in the global tropospheric PM loading, since oxidation of those species yields a large fraction of carbonyl products (such as formaldehyde and acetaldehyde) that engage in particle-phase reactions and cloud-processing to contribute to SOA formation.[46,194,484] Furthermore, gaseous anthropogenic organic and inorganic compounds transported from urban locations may interact with biogenic species, enhancing aerosol nucleation and growth on the regional and global scales.[113]

Considering the profound societal implications of urban fine PM on human health, the ecosystem, the weather, and the climate, it is imperative that sound science is employed to develop effective regulatory polices to mediate the local, regional, and global impacts of urban fine PM. The large urban centers/megacities may also represent the ideal locations to best achieve the cobenefits in simultaneously controlling air pollution and mitigating climate change.[485] Furthermore, it is essential that knowledge is transferred from well-researched to less researched urban areas and the experience in mitigating urban fine PM for developed countries (e.g., Los Angeles) is considered in guiding development of regulatory policies for developing countries.

AUTHOR INFORMATION

Corresponding Author

*E-mail: Renyi-zhang@tamu.edu.

Notes

The authors declare no competing financial interest.

DOI: 10.1021/acs.chemrev.5b00067
Chem. Rev. 2015, 115, 3803−3855

Biographies

Renyi Zhang received a B.S. in atmospheric physics from the Nanjing Institute of Meteorology, a M.S. in physics from the University of Nevada—Reno, and a Ph.D. in atmospheric chemistry from the Massachusetts Institute of Technology (MIT) (under the supervision of Mario J. Molina). After his postdoctoral research in the NASA Jet Propulsion Laboratory, California Institute of Technology, he was a Research Associate at MIT, before he became Assistant Professor (1997), Associate Professor (2002), and Professor (2005) in the Department of Atmospheric Sciences at Texas A&M University (TAMU). He is also a Professor in the Department of Chemistry (since 2007), the holder of the Harold J. Haynes Endowed Chair in Geosciences, and University Distinguished Professor at TAMU. He serves as Editor of the *Journal of Atmospheric Sciences* and Senior Editor of *Oxford Research Encyclopedias: Environmental Science*, Oxford University Press, and is a member of the International Commission on Atmospheric Chemistry and Global Pollution. He chaired the American Meteorological Society's Atmospheric Chemistry Committee (2010–2014), was Editor of the *Journal of Geophysical Research: Atmospheres* (2009–2013), and served as Director of the Center for Atmospheric Chemistry and the Environment (2007–2014) at TAMU.

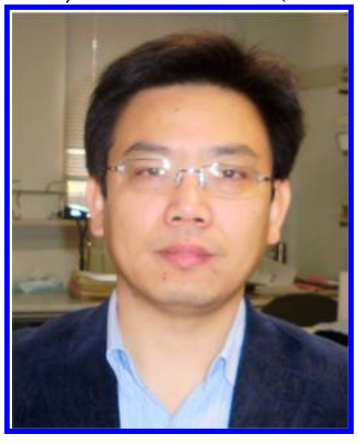

Gehui Wang is a Professor of the Institute of Earth Environment, Chinese Academy of Sciences (IEE-CAS). He received a Ph.D. in forestry chemistry and engineering from Nanjing University (2000). After two years of postdoctoral research in the School of the Environment, Nanjing University, and one year of postdoctoral research in the Chemistry Department of the University of California—Davis, he became an Associate Professor at Nanjing University until 2008. He conducted research work at Hokkaido University as a Japan Society for the Promotion of Science Fellow (2004–2006). He has been a Professor at IEE-CAS since 2008. He was a visiting scientist with Prof. Renyi Zhang at Texas A&M University (2014–2015). His research interests include analytical and atmospheric chemistry with focuses on the source and formation mechanism of atmospheric aerosols. He was awarded the Distinguished Young Scholar from the National Natural Science Foundation of China (2013).

Song Guo received a B.S. (2001) and a Ph.D. (2011) in environmental sciences from Peking University. He was a postdoctoral researcher (2012–2014) and is an Assistant Research Scientist working under Prof. Renyi Zhang at Texas A&M University. His main research area is in atmospheric chemistry, with a focus on secondary aerosol formation and aerosol nucleation in the atmosphere.

Misti L. Zamora received a B.S. in meteorology with a minor in mathematics (2010) and an M.S. in atmospheric sciences (2013) from Texas A&M University (TAMU). She is presently a Ph.D. candidate in the Department of Atmospheric Science at TAMU under Prof. Renyi Zhang. Her dissertation research seeks to elucidate the nucleation and growth mechanisms of atmospheric aerosols as well as the influence of air pollution on fetal development.

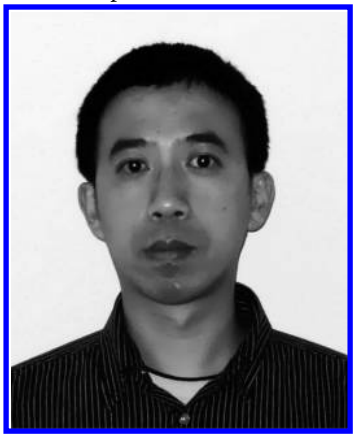

Qi Ying received his B.S. (2000) and Ph.D. (2004) degrees in environmental engineering from Tsinghua University and the

DOI: 10.1021/acs.chemrev.5b00067
Chem. Rev. 2015, 115, 3803–3855

University of California—Davis (UC Davis), respectively. He worked as an Air Resources Engineer in the California Air Resources Board (2005−2007) after completing one year of postdoctoral research at UC Davis. He became an Assistant Professor (2007) and was promoted to Associate Professor (2013) at Texas A&M University. His research interests include urban and regional air quality modeling, focusing on photochemical mechanisms and formation of secondary inorganic and organic aerosol, and source apportionment of air pollution, focusing on developing methods for regional source apportionment of both gaseous and particulate air pollutants.

Yun Lin received a B.S. (2006) and an M.S. (2009) in environmental sciences at Peking University. He is presently a Ph.D. candidate in the Department of Atmospheric Science at Texas A&M University under Prof. Renyi Zhang. His research seeks to elucidate aerosol−cloud−climate interactions using cloud-resolving models and the aerosol nucleation mechanism using quantum chemical methods.

Weigang Wang received a B.S. in chemistry (2003) from Qufu Normal University, China, and a Ph.D. in chemistry (2008) from the Institute of Chemistry, Chinese Academy of Science (ICCAS). He was as Assistant Research Fellow (2008−2011) and was promoted to Associate Research Fellow at ICCAS (2011). He has been a visiting scientist with Prof. Renyi Zhang at Texas A&M University since 2014. His research areas cover fundamental physical chemistry and atmospheric chemistry, focusing on new particle formation, multiphase reactions, and the influence of photooxidation of organic compounds on the hygroscopicity and optical properties of secondary aerosols.

Min Hu is a Professor and the Director of the State Key Joint Laboratory of Environmental Simulation and Pollution Control, College of Environmental Sciences and Engineering, at Peking University. She received her B.S. in applied chemistry (1987) and M.S. (1990) and Ph.D. (1993) in environmental chemistry from Peking University. She worked as a Lecturer and an Associate Professor and was promoted to Professor in the Center for Environmental Sciences (2001−2007) and College of Environmental Sciences and Engineering (June 2007 to present) at Peking University. Her research interests span from the characteristics of aerosol and its impacts to biogenic sulfur emissions from the sea—dimethyl sulfide. Her recent research focuses on aerosol chemical and physical characteristics, source identification, and formation of secondary aerosol and its impact on air quality, local visibility degradation, and health. She was awarded the Distinguished Young Scholar by the National Natural Science Foundation of China (2010) and Cheung-Kong Distinguished Scholar Award by the Ministry of Education of China (2013). She is a member of the Editorial Advisory Board of *Atmospheric Environment*.

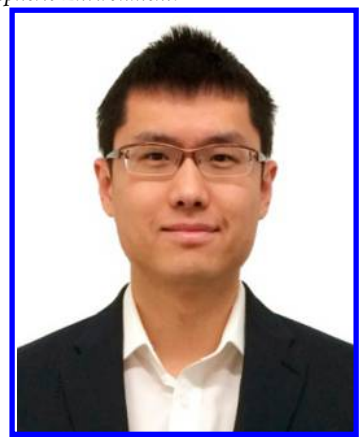

Yuan Wang received a B.S. in computer science from Fudan University (2007) and a Ph.D. (2013) in atmospheric sciences from Texas A&M University (under the supervision of Renyi Zhang). He is presently a Postdoctoral Research Fellow at the Jet Propulsion Laboratory, California Institute of Technology. His research areas include aerosol physics and chemistry, aerosol−cloud interactions and their climate implications, and mesoscale and global climate modeling.

ACKNOWLEDGMENTS

This work was supported by the Robert A. Welch Foundation (Grant A-1417), the Ministry of Science and Technology of China (Grant 2013CB955800), a collaborative research program by Texas A&M University and the National Natural Science Foundation of China, and a Texas A&M University−Weizmann Collaborative Program. G.W. acknowledged the National

DOI: 10.1021/acs.chemrev.5b00067
Chem. Rev. 2015, 115, 3803−3855

Natural Science Foundation of China and the Strategic Priority Research Program of the Chinese Academy of Sciences for financial support (Grants 41325014, XDA05100103, and XDB05020401). W.W. acknowledged financial support for the Visiting Scholar Program by the Chinese Academy of Science and the National Natural Science Foundation of China (Grant 41227805). M.H. was supported by the National Basic Research Program, China Ministry of Science and Technology (Grant 2013CB228503), and National Natural Science Foundation of China (21190052). Y.W. was supported by the NASA ROSES10-COUND program. We were grateful to Professor A. R. Ravishankara of Colorado State University, Professor of Robert D. Kuchta of University of Colorado at Boulder, and Dr. Sasha Madronich of NCAR for helpful suggestions and discussions.

GLOSSARY OF ACRONYMS

ACSM	aerosol chemical speciation monitor
AIOMFAC	aerosol inorganic−organic mixture functional group activity coefficient
AIM	aerosol inorganic model
AIS	air ion spectrometry
AMS	aerosol mass spectrometry
AMS−PMF	aerosol mass spectrometry−positive matrix factorization
APM	aerosol particle mass analyzer
BC	black carbon
BEIS	biogenic emission inventory system
BVOCs	biogenic volatile organic compounds
CAA	Clean Air Act
CAREBeijing	Campaign of Atmospheric Research in Beijing and Surrounding Areas
CB04	carbon bond 4
CB05	carbon bond 5
CCN	cloud condensation nuclei
CE	capillary electrophoresis
CI	Criegee intermediate
CIMS	chemical ionization mass spectrometry
CLOUD	Cosmics Leaving Outdoor Droplets
CMAQ	community multiscale air quality
CMB	chemical mass balance
CMB-OMM	chemical mass balance of organic molecular markers
CPCs	condensation particle counters
CRDS	cavity ring down spectrometry
CTMs	chemical transport models
DEG	diethylene glycol
DMA	differential mobility analyzer
DMPS	differential mobility particle sizer
1D-VBS	one-dimensional volatility basis set
2D-VBS	two-dimensional volatility basis set
EC	elemental carbon
ECD	electron capture detection
ED-XRF	energy-dispersive X-ray fluorescence
ERH	efflorescence relative humidity
FID	flame ionization detection
FTIR	Fourier transform infrared spectroscopy
GC	gas chromatography
GDP	gross domestic product
GEOS-Chem	Goddard Earth Observing System—3D chemical transport model
GC−MS/FID	gas chromatography−mass spectrometry/flame ionization detection
HOA	hydrocarbon-like organic aerosol
HR-ToF-AMS	high-resolution time-of-flight aerosol mass spectrometry
ICP-MS	inductively coupled plasma mass spectrometry
ICs	ion chromatographs
ID-CIMS	ion drift chemical ionization mass spectrometry
IEPOX	isoprene epoxydiol
IMPROVE	Interagency Monitoring of Protected Visual Environments
IN	ice nuclei
INTEX-B	International Chemical Transport Experiment B
IPCC	Intergovernmental Panel on Climate Change
LC−MS	liquid chromatography−mass spectrometry
LDI-MS	laser desorption/ionization mass spectrometry
LV-OOA	low-volatility oxygenated organic aerosol
MAAP	multiangle absorption photometer
MARGA	monitor for aerosols and gases in ambient air
MEGAN	model of emission of gases and aerosol from nature
MCM	master chemical mechanism
MCMA	Mexico City Metropolitan Area
MILAGRO	Megacity Initiative: Local and Global Research Observations
MOVI−CIMS	micro-orifice volatilization impact coupled to chemical ionization mass spectrometry
MOUDIs	micro-orifice uniform deposit impactors
MS	mass spectrometry
NAMS	nano aerosol mass spectrometry
NAIS	neutral cluster and air ion spectrometry
NEI	National Emission Inventory
NIOSH	National Institute of Occupational Safety and Health
NO_x	nitrogen oxides
NPF	new particle formation
OC	organic carbon
OOA	oxygenated organic aerosol
PAHs	polycyclic aromatic hydrocarbons
PAN	peroxyacyl nitrate
PASS-3	photoacoustic soot spectrometry, three wavelengths
PAX	photoacoustic extinctiometry
PBL	planetary boundary layer
PCA	principal component analysis
PCBs	polychlorinated biphenyls
PID	photoionization detection
PILS	particle-into-liquid sampler
PM	particulate matter
$PM_{2.5}$	particles with the aerodynamic diameter smaller than 2.5 μm
PM_{10}	particles with the aerodynamic diameter smaller than 10 μm
PMF	positive matrix factorization
POC	primary organic carbon
POM	particulate organic matter
ppb	parts per billion
ppm	parts per million
ppt	parts per trillion

DOI: 10.1021/acs.chemrev.5b00067
Chem. Rev. 2015, 115, 3803−3855

PRD	Pearl River Delta
PSAP	particle soot absorption photometer
PTR-MS	proton-transfer-reaction mass spectrometry
RACM	regional atmospheric chemistry mechanism
RADM2	regional acid deposition model 2
REAS	Regional Emission Inventory in Asia
RH	relative humidity
SAPRC99	statewide air pollution research center 99
SHARP	Study of Houston Atmospheric Radical Precursors
SJAC	steam-jet aerosol collector
SMPS	scanning mobility particle sizer
SOC	secondary organic carbon
SOA	secondary organic aerosol
SP2	single-particle soot photometer
SSA	single scattering albedo
SVOCs	semivolatile organic compounds
SV-OOA	semivolatile oxygenated organic aerosol
TAG GC−MS/FID	thermal desorption aerosol GC−MS/FID
TD-EI-MS	thermal desorption electron impact ionization mass spectrometry
TD-CIMS	thermal desorption chemical ionization mass spectrometry
TD-ID-CIMS	thermal desorption ion drift chemical ionization mass spectrometry
n-TDMA	nano tandem differential mobility analyzer
TDMA−TD	tandem differential mobility analyzer−thermodenuder
TexAQS	Texas Air Quality Study
TOR	thermal−optical reflectance
TOT	thermal−optical transmittance
TRACE-P	Transport and Chemical Evolution over the Pacific
TSPs	total suspended particles
U.S. EPA	United States Environmental Protection Agency
VBS	volatility basis set
VOCs	volatile organic compounds
WSOC	water-soluble organic carbon
ZSR	Zdanovskii−Stokes−Robinson

REFERENCES

(1) Intergovernmental Panel on Climate Change (IPCC). *Climate Change 2013: The Physical Science Basis. Contribution of Working Group I to the Fifth Assessment Report of the Intergovernmental Panel on Climate Change*; Cambridge University Press: Cambridge, U.K. and New York, U.S.A., 2013. http://www.ipcc.ch/report/ar5/wg1/ (accessed Jan 2, 2015).

(2) National Research Council (NRC). *Research Priorities for Airborne Particulate Matter, IV. Continuing Research Progress*; National Academy Press: Washington, DC, 2004.

(3) *World Urbanization Prospects: The 2014 Revision*; United Nations (UN): New York, 2014. http://esa.un.org/unpd/wup/Highlights/WUP2014-Highlights.pdf (accessed Jan 2, 2015).

(4) Zhang, R.; Khalizov, A.; Wang, L.; Hu, M.; Xu, W. Nucleation and Growth of Nanoparticles in the Atmosphere. *Chem. Rev.* **2012**, *112*, 1957−2011.

(5) Seinfeld, J. H.; Pandis, S. N. *Atmospheric Chemistry and Physics—From Air Pollution to Climate Change*, 2nd ed.; John Wiley & Sons: Hoboken, NJ, 2006.

(6) Guo, S.; Hu, M.; Zamora, M. L.; Peng, J.; Shang, D.; Zheng, J.; Du, Z.; Wu, Z.; Shao, M.; Zeng, L.; Molina, M. J.; Zhang, R. Elucidating Severe Urban Haze Formation in China. *Proc. Natl. Acad. Sci. U.S.A.* **2014**, *111*, 17373−17378.

(7) Zhang, R.; Jing, J.; Tao, J.; Hsu, S. C.; Wang, G.; Cao, J.; Lee, C. S. L.; Zhu, L.; Chen, Z.; Zhao, Y.; Shen, Z. Chemical Characterization and Source Apportionment of $PM_{2.5}$ in Beijing: Seasonal Perspective. *Atmos. Chem. Phys.* **2013**, *13*, 7053−7074.

(8) Huang, R. J.; Zhang, Y. L.; Bozzetti, C.; Ho, K. F.; Cao, J. J.; Han, Y. M.; Daellenbach, K. R.; Slowik, J. G.; Platt, S. M.; Canonaco, F.; Zotter, P.; Wolf, R.; Pieber, S. M.; Bruns, E. A.; Crippa, M.; Ciarelli, G.; Piazzalunga, A.; Schwikowski, M.; Abbaszade, G.; Schnelle-Kreis, J.; Zimmermann, R.; An, Z. S.; Szidat, S.; Baltensperger, U.; El Haddad, I.; Prevot, A. S. H. High Secondary Aerosol Contribution to Particulate Pollution during Haze Events in China. *Nature* **2014**, *514*, 218−222.

(9) Kanakidou, M.; Seinfeld, J. H.; Pandis, S. N.; Barnes, I.; Dentener, F. J.; Facchini, M. C.; Van Dingenen, R.; Ervens, B.; Nenes, A.; Nielsen, C. J.; Swietlicki, E.; Putaud, J. P.; Balkanski, Y.; Fuzzi, S.; Horth, J.; Moortgat, G. K.; Winterhalter, R.; Myhre, C. E. L.; Tsigaridis, K.; Vignati, E.; Stephanou, E. G.; Wilson, J. Organic Aerosol and Global Climate Modelling: A Review. *Atmos. Chem. Phys.* **2005**, *5*, 1053−1123.

(10) Hallquist, M.; Wenger, J. C.; Baltensperger, U.; Rudich, Y.; Simpson, D.; Claeys, M.; Dommen, J.; Donahue, N. M.; George, C.; Goldstein, A. H.; Hamilton, J. F.; Herrmann, H.; Hoffmann, T.; Iinuma, Y.; Jang, M.; Jenkin, M. E.; Jimenez, J. L.; Kiendler-Scharr, A.; Maenhaut, W.; McFiggans, G.; Mentel, T. F.; Monod, A.; Prevot, A. S. H.; Seinfeld, J. H.; Surratt, J. D.; Szmigielski, R.; Wildt, J. The Formation, Properties and Impact of Secondary Organic Aerosol: Current and Emerging Issues. *Atmos. Chem. Phys.* **2009**, *9*, 5155−5236.

(11) Zhang, Q.; Jimenez, J. L.; Canagaratna, M. R.; Ulbrich, I. M.; Ng, N. L.; Worsnop, D. R.; Sun, Y. L. Understanding Atmospheric Organic Aerosols via Factor Analysis of Aerosol Mass Spectrometry: A Review. *Anal. Bioanal. Chem.* **2011**, *401*, 3045−3067.

(12) Zhang, H. F.; Ye, X. N.; Cheng, T. T.; Chen, J. M.; Yang, X.; Wang, L.; Zhang, R. Y. A Laboratory Study of Agricultural Crop Residue Combustion in China: Emission Factors and Emission Inventory. *Atmos. Environ.* **2008**, *42*, 8432−8441.

(13) Gauderman, W. J.; Avol, E.; Gilliland, F.; Vora, H.; Thomas, D.; Berhane, K.; McConnell, R.; Kuenzli, N.; Lurmann, F.; Rappaport, E.; Margolis, H.; Bates, D.; Peters, J. The Effect of Air Pollution on Lung Development from 10 to 18 Years of Age. *N. Engl. J. Med.* **2004**, *351*, 1057−1067.

(14) Kunzli, N.; Jerrett, M.; Mack, W. J.; Beckerman, B.; LaBree, L.; Gilliland, F.; Thomas, D.; Peters, J.; Hodis, H. N. Ambient Air Pollution and Atherosclerosis in Los Angeles. *Environ. Health Perspect.* **2005**, *113*, 201−206.

(15) Pope, C. A.; Dockery, D. W. Health Effects of Fine Particulate Air Pollution: Lines That Connect. *J. Air Waste Manage. Assoc.* **2006**, *56*, 709−742.

(16) Correia, A. W.; Pope, C. A.; Dockery, D. W.; Wang, Y.; Ezzati, M.; Dominici, F. Effect of Air Pollution Control on Life Expectancy in the United States: An Analysis of 545 US Counties for the Period from 2000 to 2007. *Epidemiology* **2013**, *24*, 23−31.

(17) Matus, K.; Nam, K. M.; Selin, N. E.; Lamsal, L. N.; Reilly, J. M.; Paltsev, S. Health Damages from Air Pollution in China. *Global Environ. Change* **2012**, *22*, 55−66.

(18) Schlesinger, R. B.; Kunzli, N.; Hidy, G. M.; Gotschi, T.; Jerrett, M. The Health Relevance of Ambient Particulate Matter Characteristics: Coherence of Toxicological and Epidemiological Inferences. *Inhalation Toxicol.* **2006**, *18*, 95−125.

(19) Oberdörster, G.; Sharp, Z.; Atudorei, V.; Elder, A.; Gelein, R.; Kreyling, W.; Cox, C. Translocation of Inhaled Ultrafine Particles to the Brain. *Inhalation Toxicol.* **2004**, *16*, 437−445.

(20) Kreyling, W. G.; Semmler, M.; M?ller, W. Dosimetry and Toxicology of Ultrafine Particles. *J. Aerosol Med.* **2004**, *17*, 140−152.

(21) Araujo, J. A.; Barajas, B.; Kleinman, M.; Wang, X.; Bennett, B. J.; Gong, K. W.; Navab, M.; Harkema, J.; Sioutas, C.; Lusis, A. J.; Nel, A. E. Ambient Particulate Pollutants in the Ultrafine Range Promote Early Atherosclerosis and Systemic Oxidative Stress. *Circ. Res.* **2008**, *102*, 589−596.

DOI: 10.1021/acs.chemrev.5b00067
Chem. Rev. 2015, 115, 3803−3855

(22) Nikula, K. J.; Snipes, M. B.; Barr, E. B.; Griffith, W. C.; Henderson, R. F.; Mauderly, J. L. Comparative Pulmonary Toxicities and Carcinogenicities of Chronically Inhaled Diesel Exhaust and Carbon Black in F344 Rats. *Fundam. Appl. Toxicol.* **1995**, *25*, 80−94.
(23) Zanobetti, A.; Schwartz, J. Air Pollution and Emergency Admissions in Boston, MA. *J. Epidemiol. Community Health* **2006**, *60*, 890−895.
(24) Bell, M. L.; Ebisu, K.; Peng, R. D.; Samet, J. M.; Dominici, F. Hospital Admissions and Chemical Composition of Fine Particle Air Pollution. *Am. J. Respir. Crit. Care Med.* **2009**, *179*, 1115−1120.
(25) Delfino, R. J.; Staimer, N.; Tjoa, T.; Gillen, D. L.; Polidori, A.; Arhami, M.; Kleinman, M. T.; Vaziri, N. D.; Longhurst, J.; Sioutas, C. Air Pollution Exposures and Circulating Biomarkers of Effect in a Susceptible Population: Clues to Potential Causal Component Mixtures and Mechanisms. *Environ. Health Perspect.* **2009**, *117*, 1232−1238.
(26) Peng, R. D.; Bell, M. L.; Geyh, A. S.; McDermott, A.; Zeger, S. L.; Samet, J. M.; Dominici, F. Emergency Admissions for Cardiovascular and Respiratory Diseases and the Chemical Composition of Fine Particle Air Pollution. *Environ. Health Perspect.* **2009**, *117*, 957−963.
(27) Dockery, D. W.; Pope, C. A.; Xu, X.; Spengler, J. D.; Ware, J. H.; Fay, M. E.; Ferris, B. G.; Speizer, F. E. An Association between Air Pollution and Mortality in Six U.S. Cities. *N. Engl. J. Med.* **1993**, *329*, 1753−1759.
(28) Dockery, D. W.; Pope, C. A. Acute Respiratory Effects of Particulate Air-Pollution. *Annu. Rev. Public Health* **1994**, *15*, 107−132.
(29) Chen, Y. Y.; Ebenstein, A.; Greenstone, M.; Li, H. B. Evidence on the Impact of Sustained Exposure to Air Pollution on Life Expectancy from China's Huai River Policy. *Proc. Natl. Acad. Sci. U.S.A.* **2013**, *110*, 12936−12941.
(30) Committee on the Medical Effects of Air Pollutants (COMEAP). *Cardiovascular Disease and Air Pollution*; Department of Health: London, 2006. https://www.gov.uk/government/uploads/system/uploads/attachment_data/file/304668/COMEAP_cardiovascular_disease_and_air_pollution.pdf (accessed Jan 2, 2015).
(31) Millman, A.; Tang, D. L.; Perera, F. P. Air Pollution Threatens the Health of Children in China. *Pediatrics* **2008**, *122*, 620−628.
(32) *Air Quality Guidelines for Particulate Matter, Ozone, Nitrogen Dioxide and Sulfur Dioxide*; World Health Organization (WHO): Geneva, Switzerland, 2006. http://whqlibdoc.who.int/hq/2006/WHO_SDE_PHE_OEH_06.02_eng.pdf (accessed Jan 2, 2015).
(33) Organization for Economic Cooperation and Development (OECD). *Environmental Outlook to 2050: The Consequences of Inaction: Key Findings on Health and Environment*; Paris, 2012. http://www.oecd.org/environment/outlookto2050 (accessed Jan 2, 2015).
(34) Lim, S. S.; Vos, T.; Flaxman, A. D.; Danaei, G.; Shibuya, K.; Adair-Rohani, H.; Amann, M.; Anderson, H. R.; Andrews, K. G.; Aryee, M.; Atkinson, C.; Bacchus, L. J.; Bahalim, A. N.; Balakrishnan, K.; Balmes, J.; Barker-Collo, S.; Baxter, A.; Bell, M. L.; Blore, J. D.; Blyth, F.; Bonner, C.; Borges, G.; Bourne, R.; Boussinesq, M.; Brauer, M.; Brooks, P.; Bruce, N. G.; Brunekreef, B.; Bryan-Hancock, C.; Bucello, C.; Buchbinder, R.; Bull, F.; Burnett, R. T.; Byers, T. E.; Calabria, B.; Carapetis, J.; Carnahan, E.; Chafe, Z.; Charlson, F.; Chen, H. L.; Chen, J. S.; Cheng, A. T. A.; Child, J. C.; Cohen, A.; Colson, K. E.; Cowie, B. C.; Darby, S.; Darling, S.; Davis, A.; Degenhardt, L.; Dentener, F.; Des Jarlais, D. C.; Devries, K.; Dherani, M.; Ding, E. L.; Dorsey, E. R.; Driscoll, T.; Edmond, K.; Ali, S. E.; Engell, R. E.; Erwin, P. J.; Fahimi, S.; Falder, G.; Farzadfar, F.; Ferrari, A.; Finucane, M. M.; Flaxman, S.; Fowkes, F. G. R.; Freedman, G.; Freeman, M. K.; Gakidou, E.; Ghosh, S.; Giovannucci, E.; Gmel, G.; Graham, K.; Grainger, R.; Grant, B.; Gunnell, D.; Gutierrez, H. R.; Hall, W.; Hoek, H. W.; Hogan, A.; Hosgood, H. D.; Hoy, D.; Hu, H.; Hubbell, B. J.; Hutchings, S. J.; Ibeanusi, S. E.; Jacklyn, G. L.; Jasrasaria, R.; Jonas, J. B.; Kan, H. D.; Kanis, J. A.; Kassebaum, N.; Kawakami, N.; Khang, Y. H.; Khatibzadeh, S.; Khoo, J. P.; Kok, C.; Laden, F. A Comparative Risk Assessment of Burden of Disease and Injury Attributable to 67 Risk Factors and Risk Factor Clusters in 21 Regions, 1990−2010: A Systematic Analysis for the Global Burden of Disease Study 2010. *Lancet* **2012**, *380*, 2224−2260.
(35) Fan, J. W.; Zhang, R. Y.; Li, G. H.; Tao, W. K.; Li, X. W. Simulations of Cumulus Clouds Using a Spectral Microphysics Cloud-Resolving Model. *J. Geophys. Res.* **2007**, *112*, DOI: 10.1029/2006jd007688, D04201.
(36) Fan, J. W.; Zhang, R. Y.; Tao, W. K.; Mohr, K. I. Effects of Aerosol Optical Properties on Deep Convective Clouds and Radiative Forcing. *J. Geophys. Res.* **2008**, *113*, DOI: 10.1029/2007jd009257, D08209.
(37) Wang, Y.; Wan, Q.; Meng, W.; Liao, F.; Tan, H.; Zhang, R. Long-Term Impacts of Aerosols on Precipitation and Lightning over the Pearl River Delta Megacity Area in China. *Atmos. Chem. Phys.* **2011**, *11*, 12421−12436.
(38) Li, Z. Q.; Niu, F.; Fan, J. W.; Liu, Y. G.; Rosenfeld, D.; Ding, Y. N. Long-Term Impacts of Aerosols on the Vertical Development of Clouds and Precipitation. *Nat. Geosci.* **2011**, *4*, 888−894.
(39) Orville, R. E.; Huffines, G.; Nielsen-Gammon, J.; Zhang, R. Y.; Ely, B.; Steiger, S.; Phillips, S.; Allen, S.; Read, W. Enhancement of Cloud-to-Ground Lightning over Houston, Texas. *Geophys. Res. Lett.* **2001**, *28*, 2597−2600.
(40) Williams, E. R.; Zhang, R.; Rydock, J. Mixed-Phase Microphysics and Cloud Electrification. *J. Atmos. Sci.* **1991**, *48*, 2195−2203.
(41) Yang, X.; Li, Z. Increases in Thunderstorm Activity and Relationships with Air Pollution in Southeast China. *J. Geophys. Res.* **2014**, *119*, 1835−1844.
(42) Li, G. H.; Zhang, R. Y.; Fan, J. W.; Tie, X. X. Impacts of Black Carbon Aerosol on Photolysis and Ozone. *J. Geophys. Res.* **2005**, *110*, DOI: 10.1029/2005jd005898, D23206.
(43) Tie, X. X.; Madronich, S.; Walters, S.; Edwards, D. P.; Ginoux, P.; Mahowald, N.; Zhang, R. Y.; Lou, C.; Brasseur, G. Assessment of the Global Impact of Aerosols on Tropospheric Oxidants. *J. Geophys. Res.* **2005**, *110*, DOI: 10.1029/2004jd005359, D03204.
(44) Tie, X. X.; Madronich, S.; Walters, S.; Zhang, R. Y.; Rasch, P.; Collins, W. Effect of Clouds on Photolysis and Oxidants in the Troposphere. *J. Geophys. Res.* **2003**, *108*, DOI: 10.1029/2003jd003659, 4642.
(45) Fu, T. M.; Jacob, D. J.; Wittrock, F.; Burrows, J. P.; Vrekoussis, M.; Henze, D. K. Global Budgets of Atmospheric Glyoxal and Methylglyoxal, and Implications for Formation of Secondary Organic Aerosols. *J. Geophys. Res.* **2008**, *113*, DOI: 10.1029/2007jd009505, L09802.
(46) Zhao, J.; Levitt, N. P.; Zhang, R. Y. Heterogeneous Chemistry of Octanal and 2,4-Hexadienal with Sulfuric Acid. *Geophys. Res. Lett.* **2005**, *32*, DOI: 10.1029/2004gl022200, L09802.
(47) Xu, W. Nucleation and growth of atmospheric nanoparticles at molecular scale. *Ph.D. Dissertation*, Texas A&M University, College Station, TX, 2014.
(48) Lin, J. T.; Pan, D.; Davis, S. J.; Zhang, Q.; He, K. B.; Wang, C.; Streets, D. G.; Wuebbles, D. J.; Guan, D. B. China's International Trade and Air Pollution in the United States. *Proc. Natl. Acad. Sci. U.S.A.* **2014**, *111*, 1736−1741.
(49) Li, Z.; Lee, K.-H.; Wang, Y.; Xin, J.; Hao, W.-M. First Observation-Based Estimates of Cloud-Free Aerosol Radiative Forcing Across China. *J. Geophys. Res.* **2010**, *115*, DOI: 10.1029/2009JD013306.
(50) Li, G. H.; Wang, Y.; Zhang, R. Y. Implementation of a Two-Moment Bulk Microphysics Scheme to the WRF Model to Investigate Aerosol-Cloud Interaction. *J. Geophys. Res.* **2008**, *113*, DOI: 10.1029/2007jd009361, D15211.
(51) Li, G. H.; Wang, Y.; Lee, K. H.; Diao, Y. W.; Zhang, R. Y. Impacts of Aerosols on the Development and Precipitation of a Mesoscale Squall Line. *J. Geophys. Res.* **2009**, *114*, DOI: 10.1029/2008jd011581, D17205.
(52) Li, Z. Q.; Li, C.; Chen, H.; Tsay, S. C.; Holben, B.; Huang, J.; Li, B.; Maring, H.; Qian, Y.; Shi, G.; Xia, X.; Yin, Y.; Zheng, Y.; Zhuang, G. East Asian Studies of Tropospheric Aerosols and Their Impact on Regional Climate (EAST-AIRC): An Overview. *J. Geophys. Res.* **2011**, *116*, DOI: 10.1029/2010JD015257.
(53) Rosenfeld, D.; Lohmann, U.; Raga, G. B.; O'Dowd, C. D.; Kulmala, M.; Fuzzi, S.; Reissell, A.; Andreae, M. O. Flood or Drought: How Do Aerosols Affect Precipitation? *Science* **2008**, *321*, 1309−1313.

DOI: 10.1021/acs.chemrev.5b00067
Chem. Rev. 2015, 115, 3803−3855

(54) Tao, W. K.; Chen, J. P.; Li, Z. Q.; Wang, C.; Zhang, C. D. Impact of Aerosols on Convective Clouds and Precipitation. *Rev. Geophys.* **2012**, *50*, DOI: 10.1029/2011rg000369.
(55) Wang, Y.; Fan, J. W.; Zhang, R. Y.; Leung, L. R.; Franklin, C. Improving Bulk Microphysics Parameterizations in Simulations of Aerosol Effects. *J. Geophys. Res.* **2013**, *118*, 5361−5379.
(56) Koren, I.; Kaufman, Y. J.; Rosenfeld, D.; Remer, L. A.; Rudich, Y. Aerosol Invigoration and Restructuring of Atlantic Convective Clouds. *Geophys. Res. Lett.* **2005**, *32*, DOI: 10.1029/2005gl023187.
(57) Fan, J. W.; Zhang, R. Y.; Li, G. H.; Tao, W. K. Effects of Aerosols and Relative Humidity on Cumulus Clouds. *J. Geophys. Res.* **2007**, *112*, DOI: 10.1029/2006jd008136, D14204.
(58) Yuan, T. L.; Li, Z. Q.; Zhang, R. Y.; Fan, J. W. Increase of Cloud Droplet Size with Aerosol Optical Depth: An Observation and Modeling Study. *J. Geophys. Res.* **2008**, *113*, DOI: 10.1029/2007jd008632, D04201.
(59) Li, G. H.; Wang, Y.; Lee, K. H.; Diao, Y. W.; Zhang, R. Y. Increased Winter Precipitation over the North Pacific from 1984−1994 to 1995−2005 Inferred from the Global Precipitation Climatology Project. *Geophys. Res. Lett.* **2008**, *35*, DOI: 10.1029/2008gl034668, L13821.
(60) Zhang, R. Y.; Li, G. H.; Fan, J. W.; Wu, D. L.; Molina, M. J. Intensification of Pacific Storm Track Linked to Asian Pollution. *Proc. Natl. Acad. Sci. U.S.A.* **2007**, *104*, 5295−5299.
(61) Wang, Y.; Zhang, R. Y.; Saravanan, R. Asian Pollution Climatically Modulates Mid-Latitude Cyclones Following Hierarchical Modelling and Observational Analysis. *Nat. Commun.* **2014**, *5*, 3098.
(62) Wang, Y.; Lee, K. H.; Lin, Y.; Levy, M.; Zhang, R. Y. Distinct Effects of Anthropogenic Aerosols on Tropical Cyclones. *Nat. Clim. Change* **2014**, *4*, 368−373.
(63) Petters, M. D.; Kreidenweis, S. M. A Single Parameter Representation of Hygroscopic Growth and Cloud Condensation Nucleus Activity. *Atmos. Chem. Phys.* **2007**, *7*, 1961−1971.
(64) Ma, Y.; Brooks, S. D.; Vidaurre, G.; Khalizov, A. F.; Wang, L.; Zhang, R. Y. Rapid Modification of Cloud-Nucleating Ability of Aerosols by Biogenic Emissions. *Geophys. Res. Lett.* **2013**, *40*, 6293−6297.
(65) Zhang, F.; Li, Y.; Li, Z.; Sun, L.; Li, R.; Zhao, C.; Wang, P.; Sun, Y.; Liu, X.; Li, J.; Li, P.; Ren, G.; Fan, T. Aerosol Hygroscopicity and Cloud Condensation Nuclei Activity during the AC3Exp Campaign: Implications for Cloud Condensation Nuclei Parameterization. *Atmos. Chem. Phys.* **2014**, *14*, 13423−13437.
(66) Zhang, R.; Khalizov, A. F.; Pagels, J.; Zhang, D.; Xue, H.; McMurry, P. H. Variability in Morphology, Hygroscopicity, and Optical Properties of Soot Aerosols during Atmospheric Processing. *Proc. Natl. Acad. Sci. U.S.A.* **2008**, *105*, 10291−10296.
(67) Wang, Y.; Khalizov, A.; Levy, M.; Zhang, R. Y. New Directions: Light Absorbing Aerosols and Their Atmospheric Impacts. *Atmos. Environ.* **2013**, *81*, 713−715.
(68) Laskin, A.; Laskin, J.; Nizkorodov, S. A. Chemistry of Atmospheric Brown Carbon. *Chem. Rev.* **2015**, DOI: 10.1021/cr5006167.
(69) Barbaro, E.; de Arellano, J. V. G.; Krol, M. C.; Holtslag, A. A. M. Impacts of Aerosol Shortwave Radiation Absorption on the Dynamics of an Idealized Convective Atmospheric Boundary Layer. *Boundary-Layer Meteorol.* **2013**, *148*, 31−49.
(70) Poschl, U. Atmospheric Aerosols: Composition, Transformation, Climate and Health Effects. *Angew. Chem., Int. Ed.* **2005**, *44*, 7520−7540.
(71) Rudich, Y.; Donahue, N. M.; Mentel, T. F. Aging of Organic Aerosol: Bridging the Gap between Laboratory and Field Studies. *Annu. Rev. Phys. Chem.* **2007**, *58*, 321−352.
(72) Stone, R. Counting the Cost of London's Killer Smog. *Science* **2002**, *298*, 2106−2107.
(73) Bonacina, L. C. W. An Estimation of the Great London Fog of 5−8 December 1952. *Weather* **2012**, *67*, 326−326.
(74) Brimblecombe, P. The Clean Air Act after 50 Years. *Weather* **2006**, *61*, 311−314.
(75) Bell, M. L.; Davis, D. L. Reassessment of the Lethal London Fog of 1952: Novel Indicators of Acute and Chronic Consequences of Acute Exposure to Air Pollution. *Environ. Health Perspect.* **2001**, *109* (Suppl. 3), 389−394.
(76) Revuelta, M. A.; Harrison, R. M.; Nunez, L.; Gomez-Moreno, F. J.; Pujadas, M.; Artinano, B. Comparison of Temporal Features of Sulphate and Nitrate at Urban and Rural Sites in Spain and the UK. *Atmos. Environ.* **2012**, *60*, 383−391.
(77) Harrison, R. M.; Dall'Osto, M.; Beddows, D. C. S.; Thorpe, A. J.; Bloss, W. J.; Allan, J. D.; Coe, H.; Dorsey, J. R.; Gallagher, M.; Martin, C.; Whitehead, J.; Williams, P. I.; Jones, R. L.; Langridge, J. M.; Benton, A. K.; Ball, S. M.; Langford, B.; Hewitt, C. N.; Davison, B.; Martin, D.; Petersson, K. F.; Henshaw, S. J.; White, I. R.; Shallcross, D. E.; Barlow, J. F.; Dunbar, T.; Davies, F.; Nemitz, E.; Phillips, G. J.; Helfter, C.; Di Marco, C. F.; Smith, S. Atmospheric Chemistry and Physics in the Atmosphere of a Developed Megacity (London): An Overview of the REPARTEE Experiment and Its Conclusions. *Atmos. Chem. Phys.* **2012**, *12*, 3065−3114.
(78) Parrish, D. D.; Singh, H. B.; Molina, L.; Madronich, S. Air Quality Progress in North American Megacities: A Review. *Atmos. Environ.* **2011**, *45*, 7015−7025.
(79) Parrish, D. D. *Synthesis of Policy Relevant Findings from the CalNex 2010 Field Study*; Final Report to the Research Division of the California Air Resources Board; National Oceanic and Atmospheric Administration (NOAA) Earth System Research Laboratory: Boulder, CO, 2014. http://www.esrl.noaa.gov/csd/projects/calnex/synthesisreport.pdf (accessed Jan 2, 2015).
(80) Pollack, I. B.; Ryerson, T. B.; Trainer, M.; Neuman, J. A.; Roberts, J. M.; Parrish, D. D. Trends in Ozone, Its Precursors, and Related Secondary Oxidation Products in Los Angeles, California: A Synthesis of Measurements from 1960 to 2010. *J. Geophys. Res.* **2013**, *118*, 5893−5911.
(81) Warneke, C.; de Gouw, J. A.; Holloway, J. S.; Peischl, J.; Ryerson, T. B.; Atlas, E.; Blake, D.; Trainer, M.; Parrish, D. D. Multiyear Trends in Volatile Organic Compounds in Los Angeles, California: Five Decades of Decreasing Emissions. *J. Geophys. Res.* **2012**, *117*, DOI: 10.1029/2012jd017899.
(82) Hasheminassab, S.; Daher, N.; Saffari, A.; Wang, D.; Ostro, B. D.; Sioutas, C. Spatial and Temporal Variability of Sources of Ambient Fine Particulate Matter ($PM_{2.5}$) in California. *Atmos. Chem. Phys.* **2014**, *14*, 12085−12097.
(83) Beijing Car Ownership Exceeds 5 mln, 2012. Xinhuanet. http://news.xinhuanet.com/english/china/2012-02/16/c_122713279.htm (accessed Jan 2, 2015).
(84) Sun, Y. L.; Jiang, Q.; Wang, Z. F.; Fu, P. Q.; Li, J.; Yang, T.; Yin, Y. Investigation of the Sources and Evolution Processes of Severe Haze Pollution in Beijing in January 2013. *J. Geophys. Res.* **2014**, *119*, 4380−4398.
(85) Wang, Y. S.; Yao, L.; Wang, L. L.; Liu, Z. R.; Ji, D. S.; Tang, G. Q.; Zhang, J. K.; Sun, Y.; Hu, B.; Xin, J. Y. Mechanism for the Formation of the January 2013 Heavy Haze Pollution Episode over Central and Eastern China. *Sci. China: Earth Sci.* **2014**, *57*, 14−25.
(86) Cass, G. R. Organic Molecular Tracers for Particulate Air Pollution Sources. *Trends Anal. Chem.* **1998**, *17*, 356−366.
(87) Schauer, J. J.; Rogge, W. F.; Hildemann, L. M.; Mazurek, M. A.; Cass, G. R. Source Apportionment of Airborne Particulate Matter Using Organic Compounds as Tracers. *Atmos. Environ.* **1996**, *30*, 3837−3855.
(88) Hasheminassab, S.; Daher, N.; Ostro, B. D.; Sioutas, C. Long-Term Source Apportionment of Ambient Fine Particulate Matter ($PM_{2.5}$) in the Los Angeles Basin: A Focus on Emissions Reduction from Vehicular Sources. *Environ. Pollut.* **2014**, *193*, 54−64.
(89) Fraser, M. P.; Yue, Z. W.; Buzcu, B. Source Apportionment of Fine Particulate Matter in Houston, TX, Using Organic Molecular Markers. *Atmos. Environ.* **2003**, *37*, 2117−2123.
(90) Aiken, A. C.; Salcedo, D.; Cubison, M. J.; Huffman, J. A.; DeCarlo, P. F.; Ulbrich, I. M.; Docherty, K. S.; Sueper, D.; Kimmel, J. R.; Worsnop, D. R.; Trimborn, A.; Northway, M.; Stone, E. A.; Schauer, J. J.; Volkamer, R. M.; Fortner, E.; de Foy, B.; Wang, J.; Laskin, A.; Shutthanandan, V.; Zheng, J.; Zhang, R.; Gaffney, J.; Marley, N. A.; Paredes-Miranda, G.; Arnott, W. P.; Molina, L. T.; Sosa, G.; Jimenez, J. L. Mexico City Aerosol Analysis During MILAGRO Using High Resolution Aerosol Mass Spectrometry at the Urban Supersite (T0)—

DOI: 10.1021/acs.chemrev.5b00067
Chem. Rev. 2015, 115, 3803−3855

Part 1: Fine Particle Composition and Organic Source Apportionment. *Atmos. Chem. Phys.* **2009**, *9*, 6633−6653.
(91) Johnson, K. S.; de Foy, B.; Zuberi, B.; Molina, L. T.; Molina, M. J.; Xie, Y.; Laskin, A.; Shutthanandan, V. Aerosol Composition and Source Apportionment in the Mexico City Metropolitan Area with PIXE/PESA/STIM and Multivariate Analysis. *Atmos. Chem. Phys.* **2006**, *6*, 4591−4600.
(92) Guo, S.; Hu, M.; Guo, Q.; Zhang, X.; Schauer, J. J.; Zhang, R. Quantitative Evaluation of Emission Controls on Primary and Secondary Organic Aerosol Sources during Beijing 2008 Olympics. *Atmos. Chem. Phys.* **2013**, *13*, 8303−8314.
(93) Wang, Q.; Shao, M.; Zhang, Y.; Wei, Y.; Hu, M.; Guo, S. Source Apportionment of Fine Organic Aerosols in Beijing. *Atmos. Chem. Phys.* **2009**, *9*, 8573−8585.
(94) Belis, C. A.; Karagulian, F.; Larsen, B. R.; Hopke, P. K. Critical Review and Meta-Analysis of Ambient Particulate Matter Source Apportionment Using Receptor Models in Europe. *Atmos. Environ.* **2013**, *69*, 94−108.
(95) Chowdhury, Z.; Zheng, M.; Schauer, J. J.; Sheesley, R. J.; Salmon, L. G.; Cass, G. R.; Russell, A. G. Speciation of Ambient Fine Organic Carbon Particles and Source Apportionment of $PM_{2.5}$ in Indian Cities. *J. Geophys. Res.* **2007**, *112*, DOI: 10.1029/2007jd008386.
(96) Heo, J. B.; Dulger, M.; Olson, M. R.; McGinnis, J. E.; Shelton, B. R.; Matsunaga, A.; Sioutas, C.; Schauer, J. J. Source Apportionments of $PM_{2.5}$ Organic Carbon Using Molecular Marker Positive Matrix Factorization and Comparison of Results from Different Receptor Models. *Atmos. Environ.* **2013**, *73*, 51−61.
(97) Zhang, R. Atmospheric Science. Getting to the Critical Nucleus of Aerosol Formation. *Science* **2010**, *328*, 1366−1367.
(98) Iida, K.; Stolzenburg, M. R.; McMurry, P. H.; Smith, J. N. Estimating Nanoparticle Growth Rates from Size-Dependent Charged Fractions: Analysis of New Particle Formation Events in Mexico City. *J. Geophys. Res.* **2008**, *113*, DOI: 10.1029/2007jd009260.
(99) Salcedo, D.; Onasch, T. B.; Dzepina, K.; Canagaratna, M. R.; Zhang, Q.; Huffman, J. A.; DeCarlo, P. F.; Jayne, J. T.; Mortimer, P.; Worsnop, D. R.; Kolb, C. E.; Johnson, K. S.; Zuberi, B.; Marr, L. C.; Volkamer, R.; Molina, L. T.; Molina, M. J.; Cardenas, B.; Bernabé, R. M.; Márquez, C.; Gaffney, J. S.; Marley, N. A.; Laskin, A.; Shutthanandan, V.; Xie, Y.; Brune, W.; Lesher, R.; Shirley, T.; Jimenez, J. L. Characterization of Ambient Aerosols in Mexico City During the MCMA-2003 Campaign with Aerosol Mass Spectrometry: Results from the CENICA Supersite. *Atmos. Chem. Phys.* **2006**, *6*, 925−946.
(100) Wang, Z. B.; Hu, M.; Pei, X. Y.; Zhang, R. Y.; Paasonen, P.; Zheng, J.; Yue, D. L.; Wu, Z. J.; Boy, M.; Wiedensohler, A. Connection of Organics to Atmospheric New Particle Formation and Growth at an Urban Site of Beijing. *Atmos. Environ.* **2015**, *103*, 7−17.
(101) Kulmala, M.; Pirjola, U.; Makela, J. M. Stable Sulphate Clusters as a Source of New Atmospheric Particles. *Nature* **2000**, *404*, 66−69.
(102) McGraw, R.; Zhang, R. Y. Multivariate Analysis of Homogeneous Nucleation Rate Measurements. Nucleation in the *p*-Toluic Acid/Sulfuric Acid/Water System. *J. Chem. Phys.* **2008**, *128*, DOI: 10.1063/1061.2830030, 064508.
(103) Fan, J. W.; Zhang, R. Y.; Collins, D.; Li, G. H. Contribution of Secondary Condensable Organics to New Particle Formation: A Case Study in Houston, Texas. *Geophys. Res. Lett.* **2006**, *33*, DOI: 10.1029/2006gl026295, L15802.
(104) Stolzenburg, M. R.; McMurry, P. H.; Sakurai, H.; Smith, J. N.; Mauldin, R. L.; Eisele, F. L.; Clement, C. F. Growth Rates of Freshly Nucleated Atmospheric Particles in Atlanta. *J. Geophys. Res.* **2005**, *110*, DOI: 10.1029/2005jd005935.
(105) Nieminen, T.; Manninen, H. E.; Sihto, S. L.; Yli-Juuti, T.; Mauldin, R. L., III; Petaja, T.; Riipinen, I.; Kerminen, V. M.; Kulmala, M. Connection of Sulfuric Acid to Atmospheric Nucleation in Boreal Forest. *Environ. Sci. Technol.* **2009**, *43*, 4715−4721.
(106) McMurry, P. H.; Fink, M.; Sakurai, H.; Stolzenburg, M. R.; Mauldin, R. L.; Smith, J.; Eisele, F.; Moore, K.; Sjostedt, S.; Tanner, D.; Huey, L. G.; Nowak, J. B.; Edgerton, E.; Voisin, D. A Criterion for New Particle Formation in the Sulfur-Rich Atlanta Atmosphere. *J. Geophys. Res.* **2005**, *110*, DOI: 10.1029/2005jd005901.
(107) Lee, S. H.; Reeves, J. M.; Wilson, J. C.; Hunton, D. E.; Viggiano, A. A.; Miller, T. M.; Ballenthin, J. O.; Lait, L. R. Particle Formation by Ion Nucleation in the Upper Troposphere and Lower Stratosphere. *Science* **2003**, *301*, 1886−1889.
(108) Erupe, M. E.; Viggiano, A. A.; Lee, S. H. The Effect of Trimethylamine on Atmospheric Nucleation Involving H_2SO_4. *Atmos. Chem. Phys.* **2011**, *11*, 4767−4775.
(109) Zollner, J. H.; Glasoe, W. A.; Panta, B.; Carlson, K. K.; McMurry, P. H.; Hanson, D. R. Sulfuric Acid Nucleation: Power Dependencies, Variation with Relative Humidity, and Effect of Bases. *Atmos. Chem. Phys.* **2012**, *12*, 4399−4411.
(110) Yu, H.; McGraw, R.; Lee, S.-H. Effects of Amines on Formation of Sub-3 nm Particles and Their Subsequent Growth. *Geophys. Res. Lett.* **2012**, *39*, DOI: 10.1029/2011GL050099.
(111) Zhang, R. Y.; Suh, I.; Zhao, J.; Zhang, D.; Fortner, E. C.; Tie, X. X.; Molina, L. T.; Molina, M. J. Atmospheric New Particle Formation Enhanced by Organic Acids. *Science* **2004**, *304*, 1487−1490.
(112) Chebbi, A.; Carlier, P. Carboxylic Acids in the Troposphere, Occurrence, Sources, and Sinks: A Review. *Atmos. Environ.* **1996**, *30*, 4233−4249.
(113) Zhang, R.; Wang, L.; Khalizov, A. F.; Zhao, J.; Zheng, J.; McGraw, R. L.; Molina, L. T. Formation of Nanoparticles of Blue Haze Enhanced by Anthropogenic Pollution. *Proc. Natl. Acad. Sci. U.S.A.* **2009**, *106*, 17650−17654.
(114) Zhao, J.; Khalizov, A.; Zhang, R. Y.; McGraw, R. Hydrogen-Bonding Interaction in Molecular Complexes and Clusters of Aerosol Nucleation Precursors. *J. Phys. Chem. A* **2009**, *113*, 680−689.
(115) Nadykto, A. B.; Yu, F. Q. Strong Hydrogen Bonding between Atmospheric Nucleation Precursors and Common Organics. *Chem. Phys. Lett.* **2007**, *435*, 14−18.
(116) Riccobono, F.; Schobesberger, S.; Scott, C. E.; Dommen, J.; Ortega, I. K.; Rondo, L.; Almeida, J.; Amorim, A.; Bianchi, F.; Breitenlechner, M.; David, A.; Downard, A.; Dunne, E. M.; Duplissy, J.; Ehrhart, S.; Flagan, R. C.; Franchin, A.; Hansel, A.; Junninen, H.; Kajos, M.; Keskinen, H.; Kupc, A.; Kurten, A.; Kvashin, A. N.; Laaksonen, A.; Lehtipalo, K.; Makhmutov, V.; Mathot, S.; Nieminen, T.; Onnela, A.; Petaja, T.; Praplan, A. P.; Santos, F. D.; Schallhart, S.; Seinfeld, J. H.; Sipila, M.; Spracklen, D. V.; Stozhkov, Y.; Stratmann, F.; Tome, A.; Tsagkogeorgas, G.; Vaattovaara, P.; Viisanen, Y.; Vrtala, A.; Wagner, P. E.; Weingartner, E.; Wex, H.; Wimmer, D.; Carslaw, K. S.; Curtius, J.; Donahue, N. M.; Kirkby, J.; Kulmala, M.; Worsnop, D. R.; Baltensperger, U. Oxidation Products of Biogenic Emissions Contribute to Nucleation of Atmospheric Particles. *Science* **2014**, *344*, 717−721.
(117) Aalto, P.; Hameri, K.; Becker, E.; Weber, R.; Salm, J.; Makela, J. M.; Hoell, C.; O'Dowd, C. D.; Karlsson, H.; Hansson, H. C.; Vakeva, M.; Koponen, I. K.; Buzorius, G.; Kulmala, M. Physical Characterization of Aerosol Particles During Nucleation Events. *Tellus, Ser. B: Chem. Phys. Meteorol.* **2001**, *53*, 344−358.
(118) Wang, Z. B.; Hu, M.; Yue, D. L.; Zheng, J.; Zhang, R. Y.; Wiedensohler, A.; Wu, Z. J.; Nieminen, T.; Boy, M. Evaluation on the Role of Sulfuric Acid in the Mechanisms of New Particle Formation for Beijing Case. *Atmos. Chem. Phys.* **2011**, *11*, 12663−12671.
(119) Peng, J. F.; Hu, M.; Wang, Z. B.; Huang, X. F.; Kumar, P.; Wu, Z. J.; Guo, S.; Yue, D. L.; Shang, D. J.; Zheng, Z.; He, L. Y. Submicron Aerosols at Thirteen Diversified Sites in China: Size Distribution, New Particle Formation and Corresponding Contribution to Cloud Condensation Nuclei Production. *Atmos. Chem. Phys.* **2014**, *14*, 10249−10265.
(120) Lei, W. F.; Zhang, R. Y.; McGivern, W. S.; Derecskei-Kovacs, A.; North, S. W. Theoretical Study of Isomeric Branching in the Isoprene-OH Reaction: Implications to Final Product Yields in Isoprene Oxidation. *Chem. Phys. Lett.* **2000**, *326*, 109−114.
(121) Lei, W. F.; Derecskei-Kovacs, A.; Zhang, R. Y. Ab Initio Study of OH Addition Reaction to Isoprene. *J. Chem. Phys.* **2000**, *113*, 5354−5360.
(122) Lei, W.; Zhang, R.; McGivern, W. S.; Derecskei-Kovacs, A.; North, S. W. Theoretical Study of OH−O_2−Isoprene Peroxy Radicals. *J. Phys. Chem. A* **2001**, *105*, 471−477.

DOI: 10.1021/acs.chemrev.5b00067
Chem. Rev. 2015, 115, 3803−3855

(123) Lei, W.; Zhang, R. Theoretical Study of Hydroxyisoprene Alkoxy Radicals and Their Decomposition Pathways. *J. Phys. Chem. A* **2001**, *105*, 3808−3815.
(124) Suh, I.; Lei, W. F.; Zhang, R. Y. Experimental and Theoretical Studies of Isoprene Reaction with NO_3. *J. Phys. Chem. A* **2001**, *105*, 6471−6478.
(125) Zhang, D.; Zhang, R.; Park, J.; North, S. W. Hydroxy Peroxy Nitrites and Nitrates from OH Initiated Reactions of Isoprene. *J. Am. Chem. Soc.* **2002**, *124*, 9600−9605.
(126) McGivern, W. S.; Suh, I.; Clinkenbeard, A. D.; Zhang, R. Y.; North, S. W. Experimental and Computational Study of the OH-Isoprene Reaction: Isomeric Branching and Low-Pressure Behavior. *J. Phys. Chem. A* **2000**, *104*, 6609−6616.
(127) Fan, J. W.; Zhang, R. Y. Atmospheric Oxidation Mechanism of Isoprene. *Environ. Chem.* **2004**, *1*, 140−149.
(128) Fortner, E. C.; Zheng, J.; Zhang, R.; Knighton, W. B.; Volkamer, R. M.; Sheehy, P.; Molina, L.; Andre, M. Measurements of Volatile Organic Compounds Using Proton Transfer Reaction−Mass Spectrometry during the MILAGRO 2006 Campaign. *Atmos. Chem. Phys.* **2009**, *9*, 467−481.
(129) Wang, M.; Zhu, T.; Zheng, J.; Zhang, R. Y.; Zhang, S. Q.; Xie, X. X.; Han, Y. Q.; Li, Y. Use of a Mobile Laboratory to Evaluate Changes in On-Road Air Pollutants during the Beijing 2008 Summer Olympics. *Atmos. Chem. Phys.* **2009**, *9*, 8247−8263.
(130) Zhang, R. Y.; Suh, I.; Lei, W.; Clinkenbeard, A. D.; North, S. W. Kinetic Studies of OH-Initiated Reactions of Isoprene. *J. Geophys. Res.* **2000**, *105*, 24627−24635.
(131) Molina, M. J.; Zhang, R.; Broekhuizen, K.; Lei, W.; Navarro, R.; Molina, L. T. Experimental Study of Intermediates from OH-Initiated Reactions of Toluene. *J. Am. Chem. Soc.* **1999**, *121*, 10225−10226.
(132) Suh, I.; Zhang, D.; Zhang, R. Y.; Molina, L. T.; Molina, M. J. Theoretical Study of OH Addition Reaction to Toluene. *Chem. Phys. Lett.* **2002**, *364*, 454−462.
(133) Suh, I.; Zhang, R. Y.; Molina, L. T.; Molina, M. J. Oxidation Mechanism of Aromatic Peroxy and Bicyclic Radicals from OH−Toluene Reactions. *J. Am. Chem. Soc.* **2003**, *125*, 12655−12665.
(134) Zhao, J.; Zhang, R. Y.; Misawa, K.; Shibuya, K. Experimental Product Study of the OH-Initiated Oxidation of *m*-Xylene. *J. Photochem. Photobiol., A* **2005**, *176*, 199−207.
(135) Suh, I.; Zhao, J.; Zhang, R. Unimolecular Decomposition of Aromatic Bicyclic Alkoxy Radicals and Their Acyclic Radicals. *Chem. Phys. Lett.* **2006**, *432*, 313−320.
(136) Fan, J. W.; Zhang, R. Y. Density Functional Theory Study on OH-Initiated Atmospheric Oxidation of *m*-Xylene. *J. Phys. Chem. A* **2008**, *112*, 4314−4323.
(137) Ng, N. L.; Kroll, J. H.; Chan, A. W. H.; Chhabra, P. S.; Flagan, R. C.; Seinfeld, J. H. Secondary Organic Aerosol Formation from *m*-Xylene, Toluene, and Benzene. *Atmos. Chem. Phys.* **2007**, *7*, 3909−3922.
(138) Qiu, C.; Khalizov, A. F.; Zhang, R. Y. Soot Aging from OH-Initiated Oxidation of Toluene. *Environ. Sci. Technol.* **2012**, *46*, 9464−9472.
(139) Odum, J. R.; Jungkamp, T. P. W.; Griffin, R. J.; Flagan, R. C.; Seinfeld, J. H. The Atmospheric Aerosol-Forming Potential of Whole Gasoline Vapor. *Science* **1997**, *276*, 96−99.
(140) Donahue, N. M.; Robinson, A. L.; Stanier, C. O.; Pandis, S. N. Coupled Partitioning, Dilution, and Chemical Aging of Semivolatile Organics. *Environ. Sci. Technol.* **2006**, *40*, 2635−2643.
(141) Heald, C. L.; Jacob, D. J.; Park, R. J.; Russell, L. M.; Huebert, B. J.; Seinfeld, J. H.; Liao, H.; Weber, R. J. A Large Organic Aerosol Source in the Free Troposphere Missing from Current Models. *Geophys. Res. Lett.* **2005**, *32*, DOI: 10.1029/2005gl023831.
(142) Camredon, M.; Aumont, B.; Lee-Taylor, J.; Madronich, S. The $SOA/VOC/NO_x$ System: An Explicit Model of Secondary Organic Aerosol Formation. *Atmos. Chem. Phys.* **2007**, *7*, 5599−5610.
(143) Jang, M.; Czoschke, N. M.; Lee, S.; Kamens, R. M. Heterogeneous Atmospheric Aerosol Production by Acid-Catalyzed Particle-Phase Reactions. *Science* **2002**, *298*, 814−817.
(144) Kalberer, M.; Paulsen, D.; Sax, M.; Steinbacher, M.; Dommen, J.; Prevot, A. S. H.; Fisseha, R.; Weingartner, E.; Frankevich, V.; Zenobi, R.; Baltensperger, U. Identification of Polymers as Major Components of Atmospheric Organic Aerosols. *Science* **2004**, *303*, 1659−1662.
(145) Zhao, J.; Levitt, N. P.; Zhang, R. Y.; Chen, J. M. Heterogeneous Reactions of Methylglyoxal in Acidic Media: Implications for Secondary Organic Aerosol Formation. *Environ. Sci. Technol.* **2006**, *40*, 7682−7687.
(146) Gomez, M. E.; Lin, Y.; Guo, S.; Zhang, R. Heterogeneous Chemistry of Glyoxal on Acidic Solutions. An Oligomerization Pathway for Secondary Organic Aerosol Formation. *J. Phys. Chem. A* **2015**, DOI: 10.1021/jp509916r.
(147) Volkamer, R.; Jimenez, J. L.; San Martini, F.; Dzepina, K.; Zhang, Q.; Salcedo, D.; Molina, L. T.; Worsnop, D. R.; Molina, M. J. Secondary Organic Aerosol Formation from Anthropogenic Air Pollution: Rapid and Higher Than Expected. *Geophys. Res. Lett.* **2006**, *33*, DOI: 10.1029/2006gl026899.
(148) Lee, A. K. Y.; Li, Y. J.; Lau, A. P. S.; Chan, C. K. A Re-Evaluation on the Atmospheric Significance of Octanal Vapor Uptake by Acidic Particles: Roles of Particle Acidity and Gas-Phase Octanal Concentration. *Aerosol Sci. Technol.* **2008**, *42*, 992−1000.
(149) Liggio, J.; Li, S. M.; Mclaren, R. Heterogeneous Reactions of Glyoxal on Particulate Matter: Identification of Acetals and Sulfate Esters. *Environ. Sci. Technol.* **2005**, *39*, 1532−1541.
(150) Xu, W.; Guo, S.; Gomez-Hernandez, M.; Zamora, M. L.; Secrest, J.; Marrero-Ortiz, W.; Zhang, A. L.; Collins, D. R.; Zhang, R. Cloud Forming Potential of Oligomers Relevant to Secondary Organic Aerosols. *Geophys. Res. Lett.* **2014**, *41*, 6538−6545.
(151) Zhang, R.; Leu, M.-T.; Keyser, L. F. Heterogeneous Chemistry of HONO on Liquid Sulfuric Acid: A New Mechanism of Chlorine Activation on Stratospheric Sulfate Aerosols. *J. Phys. Chem.* **1996**, *100*, 339−345.
(152) Zhang, R.; Jayne, J. T.; Molina, M. J. Heterogeneous Reactions of $ClONO_2$ and HCl on Sulfuric Acid Tetrahydrate: Implications for the Stratosphere. *J. Phys. Chem.* **1994**, *98*, 867−874.
(153) Pankow, J. F. An Absorption-Model of Gas-Particle Partitioning of Organic-Compounds in the Atmosphere. *Atmos. Environ.* **1994**, *28*, 185−188.
(154) Pankow, J. F. An Absorption-Model of the Gas Aerosol Partitioning Involved in the Formation of Secondary Organic Aerosol. *Atmos. Environ.* **1994**, *28*, 189−193.
(155) Odum, J. R.; Hoffmann, T.; Bowman, F.; Collins, D.; Flagan, R. C.; Seinfeld, J. H. Gas/Particle Partitioning and Secondary Organic Aerosol Yields. *Environ. Sci. Technol.* **1996**, *30*, 2580−2585.
(156) Donahue, N. M.; Epstein, S. A.; Pandis, S. N.; Robinson, A. L. A Two-Dimensional Volatility Basis Set: 1. Organic-Aerosol Mixing Thermodynamics. *Atmos. Chem. Phys.* **2011**, *11*, 3303−3318.
(157) Donahue, N. M.; Kroll, J. H.; Pandis, S. N.; Robinson, A. L. A Two-Dimensional Volatility Basis Set—Part 2: Diagnostics of Organic-Aerosol Evolution. *Atmos. Chem. Phys.* **2012**, *12*, 615−634.
(158) Kroll, J. H.; Donahue, N. M.; Jimenez, J. L.; Kessler, S. H.; Canagaratna, M. R.; Wilson, K. R.; Altieri, K. E.; Mazzoleni, L. R.; Wozniak, A. S.; Bluhm, H.; Mysak, E. R.; Smith, J. D.; Kolb, C. E.; Worsnop, D. R. Carbon Oxidation State as a Metric for Describing the Chemistry of Atmospheric Organic Aerosol. *Nat. Chem.* **2011**, *3*, 133−139.
(159) Aiken, A. C.; Decarlo, P. F.; Kroll, J. H.; Worsnop, D. R.; Huffman, J. A.; Docherty, K. S.; Ulbrich, I. M.; Mohr, C.; Kimmel, J. R.; Sueper, D.; Sun, Y.; Zhang, Q.; Trimborn, A.; Northway, M.; Ziemann, P. J.; Canagaratna, M. R.; Onasch, T. B.; Alfarra, M. R.; Prevot, A. S.; Dommen, J.; Duplissy, J.; Metzger, A.; Baltensperger, U.; Jimenez, J. L. O/C and OM/OC Ratios of Primary, Secondary, and Ambient Organic Aerosols with High-Resolution Time-of-Flight Aerosol Mass Spectrometry. *Environ. Sci. Technol.* **2008**, *42*, 4478−4485.
(160) Pankow, J. F.; Barsanti, K. C. The Carbon Number-Polarity Grid: A Means To Manage the Complexity of the Mix of Organic Compounds When Modeling Atmospheric Organic Particulate Matter. *Atmos. Environ.* **2009**, *43*, 2829−2835.
(161) Cappa, C. D.; Wilson, K. R. Multi-Generation Gas-Phase Oxidation, Equilibrium Partitioning, and the Formation and Evolution of Secondary Organic Aerosol. *Atmos. Chem. Phys.* **2012**, *12*, 9505−9528.

DOI: 10.1021/acs.chemrev.5b00067
Chem. Rev. 2015, 115, 3803−3855

(162) Shiraiwa, M.; Zuend, A.; Bertram, A. K.; Seinfeld, J. H. Gas-Particle Partitioning of Atmospheric Aerosols: Interplay of Physical State, Non-Ideal Mixing and Morphology. *Phys. Chem. Chem. Phys.* **2013**, *15*, 11441−11453.
(163) Zuend, A.; Marcolli, C.; Peter, T.; Seinfeld, J. H. Computation of Liquid-Liquid Equilibria and Phase Stabilities: Implications for RH-Dependent Gas/Particle Partitioning of Organic-Inorganic Aerosols. *Atmos. Chem. Phys.* **2010**, *10*, 7795−7820.
(164) Zuend, A.; Marcolli, C.; Luo, B. P.; Peter, T. A Thermodynamic Model of Mixed Organic-Inorganic Aerosols to Predict Activity Coefficients. *Atmos. Chem. Phys.* **2008**, *8*, 4559−4593.
(165) Volkamer, R.; Platt, U.; Wirtz, K. Primary and Secondary Glyoxal Formation from Aromatics: Experimental Evidence for the Bicycloalkyl−Radical Pathway from Benzene, Toluene, and *p*-Xylene. *J. Phys. Chem. A* **2001**, *105*, 7865−7874.
(166) Grosjean, E.; Grosjean, D.; Fraser, M. P.; Cass, G. R. Air Quality Model Evaluation Data for Organics. 2. C_1−C_{14} Carbonyls in Los Angeles Air. *Environ. Sci. Technol.* **1996**, *30*, 2687−2703.
(167) Munger, J. W.; Jacob, D. J.; Daube, B. C.; Horowitz, L. W.; Keene, W. C.; Heikes, B. G. Formaldehyde, Glyoxal, and Methylglyoxal in Air and Cloudwater at a Rural Mountain Site in Central Virginia. *J. Geophys. Res.* **1995**, *100*, 9325−9333.
(168) Volkamer, R.; Molina, L. T.; Molina, M. J.; Shirley, T.; Brune, W. H. DOAS Measurement of Glyoxal as an Indicator for Fast VOC Chemistry in Urban Air. *Geophys. Res. Lett.* **2005**, *32*, DOI: 10.1029/2005gl022616.
(169) Ho, S. S. H.; Yu, J. Z. Feasibility of Collection and Analysis of Airborne Carbonyls by On-Sorbent Derivatization and Thermal Desorption. *Anal. Chem.* **2002**, *74*, 1232−1240.
(170) Volkamer, R.; Martini, F. S.; Molina, L. T.; Salcedo, D.; Jimenez, J. L.; Molina, M. J. A Missing Sink for Gas-Phase Glyoxal in Mexico City: Formation of Secondary Organic Aerosol. *Geophys. Res. Lett.* **2007**, *34*, DOI: 10.1029/2007gl030752.
(171) Nemet, I.; Vikic-Topic, D.; Varga-Defterdarovic, L. Spectroscopic Studies of Methylglyoxal in Water and Dimethylsulfoxide. *Bioorg. Chem.* **2004**, *32*, 560−570.
(172) Ip, H. S. S.; Huang, X. H. H.; Yu, J. Z. Effective Henry's Law Constants of Glyoxal, Glyoxylic Acid, and Glycolic Acid. *Geophys. Res. Lett.* **2009**, *36*, DOI: 10.1029/2008gl036212.
(173) Kampf, C. J.; Waxman, E. M.; Slowik, J. G.; Dommen, J.; Pfaffenberger, L.; Praplan, A. P.; Prevot, A. S. H.; Baltensperger, U.; Hoffmann, T.; Volkamer, R. Effective Henry's Law Partitioning and the Salting Constant of Glyoxal in Aerosols Containing Sulfate. *Environ. Sci. Technol.* **2013**, *47*, 4236−4244.
(174) De Haan, D. O.; Corrigan, A. L.; Smith, K. W.; Stroik, D. R.; Turley, J. J.; Lee, F. E.; Tolbert, M. A.; Jimenez, J. L.; Cordova, K. E.; Ferrell, G. R. Secondary Organic Aerosol-Forming Reactions of Glyoxal with Amino Acids. *Environ. Sci. Technol.* **2009**, *43*, 2818−2824.
(175) Carlton, A. G.; Turpin, B. J.; Altieri, K. E.; Seitzinger, S.; Reff, A.; Lim, H. J.; Ervens, B. Atmospheric Oxalic Acid and SOA Production from Glyoxal: Results of Aqueous Photooxidation Experiments. *Atmos. Environ.* **2007**, *41*, 7588−7602.
(176) Corrigan, A. L.; Hanley, S. W.; Haan, D. O. Uptake of Glyoxal by Organic and Inorganic Aerosol. *Environ. Sci. Technol.* **2008**, *42*, 4428−4433.
(177) Schwier, A. N.; Sareen, N.; Mitroo, D.; Shapiro, E. L.; McNeill, V. F. Glyoxal-Methylglyoxal Cross-Reactions in Secondary Organic Aerosol Formation. *Environ. Sci. Technol.* **2010**, *44*, 6174−6182.
(178) Zhou, S.; Gonzalez, L.; Leithead, A.; Finewax, Z.; Thalman, R.; Vlasenko, A.; Vagle, S.; Miller, L. A.; Li, S. M.; Bureekul, S.; Furutani, H.; Uematsu, M.; Volkamer, R.; Abbatt, J. Formation of Gas-Phase Carbonyls from Heterogeneous Oxidation of Polyunsaturated Fatty Acids at the Air-Water Interface and of the Sea Surface Microlayer. *Atmos. Chem. Phys.* **2014**, *14*, 1371−1384.
(179) Liggio, J.; Li, S. M.; Mclaren, R. Reactive Uptake of Glyoxal by Particulate Matter. *J. Geophys. Res.* **2005**, *110*, DOI: 10.1029/2004jd005113.
(180) Schweitzer, F.; Magi, L.; Mirabel, P.; George, C. Uptake Rate Measurements of Methanesulfonic Acid and Glyoxal by Aqueous Droplets. *J. Phys. Chem. A* **1998**, *102*, 593−600.
(181) Wang, L.; Khalizov, A. F.; Zheng, J.; Xu, W.; Ma, Y.; Lal, V.; Zhang, R. Y. Atmospheric Nanoparticles Formed from Heterogeneous Reactions of Organics. *Nat. Geosci.* **2010**, *3*, 238−242.
(182) Wang, L.; Xu, W.; Khalizov, A. F.; Zheng, J.; Qiu, C.; Zhang, R. Y. Laboratory Investigation on the Role of Organics in Atmospheric Nanoparticle Growth. *J. Phys. Chem. A* **2011**, *115*, 8940−8947.
(183) Barton, D.; Ollis, W. D. *Comprehensive Organic Chemistry: The Synthesis and Reactions of Organic Compounds*, 1st ed.; Pergamon Press: Oxford, U.K., New York, 1979.
(184) Carey, F. A.; Sundberg, R. J. *Advanced Organic Chemistry*, 4th ed.; Kluwer Academic/Plenum Publishers: New York, 2000.
(185) Jayne, J. T.; Worsnop, D. R.; Kolb, C. E.; Swartz, E.; Davidovits, P. Uptake of Gas-Phase Formaldehyde by Aqueous Acid Surfaces. *J. Phys. Chem.* **1996**, *100*, 8015−8022.
(186) Jang, M.; Kamens, R. M. Atmospheric Secondary Aerosol Formation by Heterogeneous Reactions of Aldehydes in the Presence of a Sulfuric Acid Aerosol Catalyst. *Environ. Sci. Technol.* **2001**, *35*, 4758−4766.
(187) Jang, M.; Carroll, B.; Chandramouli, B.; Kamens, R. M. Particle Growth by Acid-Catalyzed Heterogeneous Reactions of Organic Carbonyls on Preexisting Aerosols. *Environ. Sci. Technol.* **2003**, *37*, 3828−3837.
(188) Jang, M.; Lee, S.; Kamens, R. M. Organic Aerosol Growth by Acid-Catalyzed Heterogeneous Reactions of Octanal in a Flow Reactor. *Atmos. Environ.* **2003**, *37*, 2125−2138.
(189) Jang, M. S.; Czoschke, N. M.; Northcross, A. L. Semiempirical Model for Organic Aerosol Growth by Acid-Catalyzed Heterogeneous Reactions of Organic Carbonyls. *Environ. Sci. Technol.* **2005**, *39*, 164−174.
(190) Kroll, J. H.; Ng, N. L.; Murphy, S. M.; Varutbangkul, V.; Flagan, R. C.; Seinfeld, J. H. Chamber Studies of Secondary Organic Aerosol Growth by Reactive Uptake of Simple Carbonyl Compounds. *J. Geophys. Res.* **2005**, *110*, DOI: 10.1029/2005JD006004.
(191) Garland, R. M.; Elrod, M. J.; Kincaid, K.; Beaver, M. R.; Jimenez, J. L.; Tolbert, M. A. Acid-Catalyzed Reactions of Hexanal on Sulfuric Acid Particles: Identification of Reaction Products. *Atmos. Environ.* **2006**, *40*, 6863−6878.
(192) Kane, S. M.; Leu, M.-T. Uptake of Methanol Vapor in Sulfuric Acid Solutions. *J. Phys. Chem. A* **2001**, *105*, 1411−1415.
(193) Iraci, L. T.; Essin, A. M.; Golden, D. M. Solubility of Methanol in Low-Temperature Aqueous Sulfuric Acid and Implications for Atmospheric Particle Composition. *J. Phys. Chem. A* **2002**, *106*, 4054−4060.
(194) Levitt, N. P.; Zhao, J.; Zhang, R. Heterogeneous Chemistry of Butanol and Decanol with Sulfuric Acid: Implications for Secondary Organic Aerosol Formation. *J. Phys. Chem. A* **2006**, *110*, 13215−13220.
(195) Timonen, R. S.; Leu, M.-T. Interaction of Ethyl Alcohol Vapor with Sulfuric Acid Solutions. *J. Phys. Chem. A* **2006**, *110*, 6660−6666.
(196) Michelsen, R. R.; Staton, S. J. R.; Iraci, L. T. Uptake and Dissolution of Gaseous Ethanol in Sulfuric Acid. *J. Phys. Chem. A* **2006**, *110*, 6711−6717.
(197) Iinuma, Y.; Boge, O.; Kahnt, A.; Herrmann, H. Laboratory Chamber Studies on the Formation of Organosulfates from Reactive Uptake of Monoterpene Oxides. *Phys. Chem. Chem. Phys.* **2009**, *11*, 7985−7997.
(198) Surratt, J. D.; Chan, A. W. H.; Eddingsaas, N. C.; Chan, M. N.; Loza, C. L.; Kwan, A. J.; Hersey, S. P.; Flagan, R. C.; Wennberg, P. O.; Seinfeld, J. H. Reactive Intermediates Revealed in Secondary Organic Aerosol Formation from Isoprene. *Proc. Natl. Acad. Sci. U.S.A.* **2010**, *107*, 6640−6645.
(199) Paulot, F.; Crounse, J. D.; Kjaergaard, H. G.; Kurten, A.; Clair, J. M., St; Seinfeld, J. H.; Wennberg, P. O. Unexpected Epoxide Formation in the Gas-Phase Photooxidation of Isoprene. *Science* **2009**, *325*, 730−733.
(200) Lin, Y. H.; Zhang, Z. F.; Docherty, K. S.; Zhang, H. F.; Budisulistiorini, S. H.; Rubitschun, C. L.; Shaw, S. L.; Knipping, E. M.;

DOI: 10.1021/acs.chemrev.5b00067
Chem. Rev. 2015, 115, 3803−3855

Edgerton, E. S.; Kleindienst, T. E.; Gold, A.; Surratt, J. D. Isoprene Epoxydiols as Precursors to Secondary Organic Aerosol Formation: Acid-Catalyzed Reactive Uptake Studies with Authentic Compounds. *Environ. Sci. Technol.* **2012**, *46*, 250−258.
(201) Minerath, E. C.; Elrod, M. J. Assessing the Potential for Diol and Hydroxy Sulfate Ester Formation from the Reaction of Epoxides in Tropospheric Aerosols. *Environ. Sci. Technol.* **2009**, *43*, 1386−1392.
(202) Cole-Filipiak, N. C.; O'Connor, A. E.; Elrod, M. J. Kinetics of the Hydrolysis of Atmospherically Relevant Isoprene-Derived Hydroxy Epoxides. *Environ. Sci. Technol.* **2010**, *44*, 6718−6723.
(203) Darer, A. I.; Cole-Filipiak, N. C.; O'Connor, A. E.; Elrod, M. J. Formation and Stability of Atmospherically Relevant Isoprene-Derived Organosulfates and Organonitrates. *Environ. Sci. Technol.* **2011**, *45*, 1895−1902.
(204) Lal, V.; Khalizov, A. F.; Lin, Y.; Galvan, M. D.; Connell, B. T.; Zhang, R. Y. Heterogeneous Reactions of Epoxides in Acidic Media. *J. Phys. Chem. A* **2012**, *116*, 6078−6090.
(205) Wang, T. H.; Liu, Z.; Wang, W. G.; Ge, M. F. Uptake Kinetics of Three Epoxides into Sulfuric Acid Solution. *Atmos. Environ.* **2012**, *56*, 58−64.
(206) Bleier, D. B.; Elrod, M. J. Kinetics and Thermodynamics of Atmospherically Relevant Aqueous Phase Reactions of α-Pinene Oxide. *J. Phys. Chem. A* **2013**, *117*, 4223−4232.
(207) Lin, Y. H.; Zhang, H. F.; Pye, H. O. T.; Zhang, Z. F.; Marth, W. J.; Park, S.; Arashiro, M.; Cui, T. Q.; Budisulistiorini, H.; Sexton, K. G.; Vizuete, W.; Xie, Y.; Luecken, D. J.; Piletic, I. R.; Edney, E. O.; Bartolotti, L. J.; Gold, A.; Surratt, J. D. Epoxide as a Precursor to Secondary Organic Aerosol Formation from Isoprene Photooxidation in the Presence of Nitrogen Oxides. *Proc. Natl. Acad. Sci. U.S.A.* **2013**, *110*, 6718−6723.
(208) Lin, Y. H.; Knipping, E. M.; Edgerton, E. S.; Shaw, S. L.; Surratt, J. D. Investigating the Influences of SO_2 and NH_3 Levels on Isoprene-Derived Secondary Organic Aerosol Formation Using Conditional Sampling Approaches. *Atmos. Chem. Phys.* **2013**, *13*, 8457−8470.
(209) Zhang, H. F.; Worton, D. R.; Lewandowski, M.; Ortega, J.; Rubitschun, C. L.; Park, J. H.; Kristensen, K.; Campuzano-Jost, P.; Day, D. A.; Jimenez, J. L.; Jaoui, M.; Offenberg, J. H.; Kleindienst, T. E.; Gilman, J.; Kuster, W. C.; de Gouw, J.; Park, C.; Schade, G. W.; Frossard, A. A.; Russell, L.; Kaser, L.; Jud, W.; Hansel, A.; Cappellin, L.; Karl, T.; Glasius, M.; Guenther, A.; Goldstein, A. H.; Seinfeld, J. H.; Gold, A.; Kamens, R. M.; Surratt, J. D. Organosulfates as Tracers for Secondary Organic Aerosol (SOA) Formation from 2-Methyl-3-buten-2-ol (MBO) in the Atmosphere. *Environ. Sci. Technol.* **2012**, *46*, 9437−9446.
(210) Zhang, H.; Zhang, Z.; Cui, T.; Lin, Y.-H.; Bhathela, N. A.; Ortega, J.; Worton, D. R.; Goldstein, A. H.; Guenther, A.; Jimenez, J. L.; Gold, A.; Surratt, J. D. Secondary Organic Aerosol Formation via 2-Methyl-3-buten-2-ol Photooxidation: Evidence of Acid-Catalyzed Reactive Uptake of Epoxides. *Environ. Sci. Technol. Lett.* **2014**, *1*, 242−247.
(211) Drozd, G. T.; Woo, J. L.; McNeill, V. F. Self-Limited Uptake of α-Pinene Oxide to Acidic Aerosol: The Effects of Liquid-Liquid Phase Separation and Implications for the Formation of Secondary Organic Aerosol and Organosulfates from Epoxides. *Atmos. Chem. Phys.* **2013**, *13*, 8255−8263.
(212) Gaston, C. J.; Riedel, T. P.; Zhang, Z.; Gold, A.; Surratt, J. D.; Thornton, J. A. Reactive Uptake of an Isoprene-Derived Epoxydiol to Submicron Aerosol Particles. *Environ. Sci. Technol.* **2014**, *48*, 11178−11186.
(213) Xu, W.; Gomez-Hernandez, M.; Guo, S.; Secrest, J.; Marrero-Ortiz, W.; Zhang, A. L.; Zhang, R. Y. Acid-Catalyzed Reactions of Epoxides for Atmospheric Nanoparticle Growth. *J. Am. Chem. Soc.* **2014**, *136*, 15477−15480.
(214) Qiu, C.; Zhang, R. Y. Multiphase Chemistry of Atmospheric Amines. *Phys. Chem. Chem. Phys.* **2013**, *15*, 5738−5752.
(215) Xu, W.; Zhang, R. Y. Theoretical Investigation of Interaction of Dicarboxylic Acids with Common Aerosol Nucleation Precursors. *J. Phys. Chem. A* **2012**, *116*, 4539−4550.
(216) Xu, W.; Zhang, R. Y. A Theoretical Study of Hydrated Molecular Clusters of Amines and Dicarboxylic Acids. *J. Chem. Phys.* **2013**, *139*.
(217) Dawson, M. L.; Varner, M. E.; Perraud, V.; Ezell, M. J.; Gerber, R. B.; Finlayson-Pitts, B. J. Simplified Mechanism for New Particle Formation from Methanesulfonic Acid, Amines, and Water via Experiments and ab Initio Calculations. *Proc. Natl. Acad. Sci. U.S.A.* **2012**, *109*, 18719−18724.
(218) Barsanti, K. C.; McMurry, P. H.; Smith, J. N. The Potential Contribution of Organic Salts to New Particle Growth. *Atmos. Chem. Phys.* **2009**, *9*, 2949−2957.
(219) Paciga, A. L.; Riipinen, I.; Pandis, S. N. Effect of Ammonia on the Volatility of Organic Diacids. *Environ. Sci. Technol.* **2014**, *48*, 13769−13775.
(220) Na, K.; Song, C.; Switzer, C.; Cocker, D. R. Effect of Ammonia on Secondary Organic Aerosol Formation from α-Pinene Ozonolysis in Dry and Humid Conditions. *Environ. Sci. Technol.* **2007**, *41*, 6096−6102.
(221) Liu, Y.; Ma, Q.; He, H. Heterogeneous Uptake of Amines by Citric Acid and Humic Acid. *Environ. Sci. Technol.* **2012**, *46*, 11112−11118.
(222) Barsanti, K. C.; Pankow, J. F. Thermodynamics of the Formation of Atmospheric Organic Particulate Matter by Accretion Reactions—Part 3: Carboxylic and Dicarboxylic Acids. *Atmos. Environ.* **2006**, *40*, 6676−6686.
(223) Lavi, A.; Segre, E.; Gomez-Hernandez, M.; Zhang, R.; Rudich, Y. Volatility of Atmospherically Relevant Alkylaminium Carboxylate Salts. *J. Phys. Chem. A* **2015**, DOI: 10.1021/jp507320v.
(224) De Haan, D. O.; Tolbert, M. A.; Jimenez, J. L. Atmospheric Condensed-Phase Reactions of Glyoxal with Methylamine. *Geophys. Res. Lett.* **2009**, *36*, DOI: 10.1029/2009GL037441.
(225) Galloway, M. M.; Chhabra, P. S.; Chan, A. W. H.; Surratt, J. D.; Flagan, R. C.; Seinfeld, J. H.; Keutsch, F. N. Glyoxal Uptake on Ammonium Sulphate Seed Aerosol: Reaction Products and Reversibility of Uptake under Dark and Irradiated Conditions. *Atmos. Chem. Phys.* **2009**, *9*, 3331−3345.
(226) Trainic, M.; Abo Riziq, A.; Lavi, A.; Flores, J. M.; Rudich, Y. The Optical, Physical and Chemical Properties of the Products of Glyoxal Uptake on Ammonium Sulfate Seed Aerosols. *Atmos. Chem. Phys.* **2011**, *11*, 9697−9707.
(227) Trainic, M.; Abo Riziq, A.; Lavi, A.; Rudich, Y. Role of Interfacial Water in the Heterogeneous Uptake of Glyoxal by Mixed Glycine and Ammonium Sulfate Aerosols. *J. Phys. Chem. A* **2012**, *116*, 5948−5957.
(228) Wang, X.; Gao, S.; Yang, X.; Chen, H.; Chen, J.; Zhuang, G.; Surratt, J. D.; Chan, M. N.; Seinfeld, J. H. Evidence for High Molecular Weight Nitrogen-Containing Organic Salts in Urban Aerosols. *Environ. Sci. Technol.* **2010**, *44*, 4441−4446.
(229) Zahardis, J.; Geddes, S.; Petrucci, G. A. The Ozonolysis of Primary Aliphatic Amines in Fine Particles. *Atmos. Chem. Phys.* **2008**, *8*, 1181−1194.
(230) Shiraiwa, M.; Ammann, M.; Koop, T.; Pöschl, U. Gas Uptake and Chemical Aging of Semisolid Organic Aerosol Particles. *Proc. Natl. Acad. Sci. U.S.A.* **2011**, *108*, 11003−11008.
(231) Rodhe, H.; Crutzen, P.; Vanderpol, A. Formation of Sulfuric and Nitric-Acid in the Atmosphere during Long-Range Transport. *Tellus* **1981**, *33*, 132−141.
(232) Sun, Y. L.; Wang, Z. F.; Fu, P. Q.; Yang, T.; Jiang, Q.; Dong, H. B.; Li, J.; Jia, J. J. Aerosol Composition, Sources and Processes during Wintertime in Beijing, China. *Atmos. Chem. Phys.* **2013**, *13*, 4577−4592.
(233) Wang, Y. X.; Zhang, Q. Q.; Jiang, J. K.; Zhou, W.; Wang, B. Y.; He, K. B.; Duan, F. K.; Zhang, Q.; Philip, S.; Xie, Y. Y. Enhanced Sulfate Formation during China's Severe Winter Haze Episode in January 2013 Missing from Current Models. *J. Geophys. Res.* **2014**, *119*, 10425−10440.
(234) Lee, Y. N.; Schwartz, S. E. In *Precipitation Scavenging, Dry Deposition and Resuspension*; Pruppacher, H. R.; Semonin, R. G., Slinn, W. G. N., Eds.; Elsevier: New York, 1983; Vol. *1*.
(235) Behra, P.; Sigg, L.; Werner, S. Dominating Influence of NH_3 on the Oxidation of Aqueous SO_2: The Coupling of NH_3 and SO_2 in Atmospheric Water. *Atmos. Environ. (1967−1989)* **1989**, *23*, 2691−2707.
(236) Harris, E.; Sinha, B.; van Pinxteren, D.; Tilgner, A.; Fomba, K. W.; Schneider, J.; Roth, A.; Gnauk, T.; Fahlbusch, B.; Mertes, S.; Lee, T.; Collett, J.; Foley, S.; Borrmann, S.; Hoppe, P.; Herrmann, H. Enhanced

DOI: 10.1021/acs.chemrev.5b00067
Chem. Rev. 2015, 115, 3803−3855

Role of Transition Metal Ion Catalysis during In-Cloud Oxidation of SO_2. *Science* **2013**, *340*, 727−730.
(237) Wang, G. H.; Zhou, B. H.; Cheng, C. L.; Cao, J. J.; Li, J. J.; Meng, J. J.; Tao, J.; Zhang, R. J.; Fu, P. Q. Impact of Gobi Desert Dust on Aerosol Chemistry of Xi'an, Inland China during Spring 2009: Differences in Composition and Size Distribution between the Urban Ground Surface and the Mountain Atmosphere. *Atmos. Chem. Phys.* **2013**, *13*, 819−835.
(238) Zhuang, G.; Guo, J.; Yuan, H.; Zhang, X. Coupling and Feedback between Iron and Sulphur in Air-Sea Exchange. *Chin. Sci. Bull.* **2003**, *48*, 1080−1086.
(239) He, H.; Wang, Y.; Ma, Q.; Ma, J.; Chu, B.; Ji, D.; Tang, G.; Liu, C.; Zhang, H.; Hao, J. Mineral Dust and NOx Promote the Conversion of SO_2 to Sulfate in Heavy Pollution Days. *Sci. Rep.* **2014**, *4*, DOI: 10.1038/srep04172.
(240) Fan, J. W.; Zhao, J.; Zhang, R. Y. Theoretical Study of OH Addition to α-Pinene and β-Pinene. *Chem. Phys. Lett.* **2005**, *411*, 1−7.
(241) Zhang, D.; Zhang, R. Ozonolysis of α-Pinene and β-Pinene: Kinetics and Mechanism. *J. Chem. Phys.* **2005**, *122*, DOI: 10.1063/1061.1862616, 114308.
(242) Zhang, D.; Zhang, R. Y. Mechanism of OH Formation from Ozonolysis of Isoprene: A Quantum-Chemical Study. *J. Am. Chem. Soc.* **2002**, *124*, 2692−2703.
(243) Zhang, D.; Lei, W. F.; Zhang, R. Y. Mechanism of OH Formation from Ozonolysis of Isoprene: Kinetics and Product Yields. *Chem. Phys. Lett.* **2002**, *358*, 171−179.
(244) Welz, O.; Savee, J. D.; Osborn, D. L.; Vasu, S. S.; Percival, C. J.; Shallcross, D. E.; Taatjes, C. A. Direct Kinetic Measurements of Criegee Intermediate (CH_2OO) Formed by Reaction of CH_2I with O_2. *Science* **2012**, *335*, 204−207.
(245) Mauldin, R. L.; Berndt, T.; Sipila, M.; Paasonen, P.; Petaja, T.; Kim, S.; Kurten, T.; Stratmann, F.; Kerminen, V. M.; Kulmala, M. A New Atmospherically Relevant Oxidant of Sulphur Dioxide. *Nature* **2012**, *488*, 193−196.
(246) Shi, Q.; Davidovits, P.; Jayne, J. T.; Worsnop, D. R.; Kolb, C. E. Uptake of Gas-Phase Ammonia. 1. Uptake by Aqueous Surfaces as a Function of pH. *J. Phys. Chem. A* **1999**, *103*, 8812−8823.
(247) Swartz, E.; Shi, Q.; Davidovits, P.; Jayne, J. T.; Worsnop, D. R.; Kolb, C. E. Uptake of Gas-Phase Ammonia. 2. Uptake by Sulfuric Acid Surfaces. *J. Phys. Chem. A* **1999**, *103*, 8824−8833.
(248) Bzdek, B. R.; Ridge, D. P.; Johnston, M. V. Amine Exchange into Ammonium Bisulfate and Ammonium Nitrate Nuclei. *Atmos. Chem. Phys.* **2010**, *10*, 3495−3503.
(249) Bzdek, B. R.; Ridge, D. P.; Johnston, M. V. Size-Dependent Reactions of Ammonium Bisulfate Clusters with Dimethylamine. *J. Phys. Chem. A* **2010**, *114*, 11638−11644.
(250) Murphy, S. M.; Sorooshian, A.; Kroll, J. H.; Ng, N. L.; Chhabra, P.; Tong, C.; Surratt, J. D.; Knipping, E.; Flagan, R. C.; Seinfeld, J. H. Secondary Aerosol Formation from Atmospheric Reactions of Aliphatic Amines. *Atmos. Chem. Phys.* **2007**, *7*, 2313−2337.
(251) Lloyd, J. A.; Heaton, K. J.; Johnston, M. V. Reactive Uptake of Trimethylamine into Ammonium Nitrate Particles. *J. Phys. Chem. A* **2009**, *113*, 4840−4843.
(252) Qiu, C.; Wang, L.; Lal, V.; Khalizov, A. F.; Zhang, R. Heterogeneous Reactions of Alkylamines with Ammonium Sulfate and Ammonium Bisulfate. *Environ. Sci. Technol.* **2011**, *45*, 4748−4755.
(253) Wang, L.; Lal, V.; Khalizov, A. F.; Zhang, R. Y. Heterogeneous Chemistry of Alkylamines with Sulfuric Acid: Implications for Atmospheric Formation of Alkylaminium Sulfates. *Environ. Sci. Technol.* **2010**, *44*, 2461−2465.
(254) Qiu, C.; Zhang, R. Physiochemical Properties of Alkylaminium Sulfates: Hygroscopicity, Thermostability, and Density. *Environ. Sci. Technol.* **2012**, *46*, 4474−4480.
(255) Clegg, S. L.; Qiu, C.; Zhang, R. The Deliquescence Behaviour, Solubilities, and Densities of Aqueous Solutions of Five Methyl- and Ethyl-Aminium Sulphate Salts. *Atmos. Environ.* **2013**, *73*, 145−158.
(256) Finlayson-Pitts, B. J.; Wingen, L. M.; Sumner, A. L.; Syomin, D.; Ramazan, K. A. The Heterogeneous Hydrolysis of NO_2 in Laboratory Systems and in Outdoor and Indoor Atmospheres: An Integrated Mechanism. *Phys. Chem. Chem. Phys.* **2003**, *5*, 223−242.
(257) Zhang, R.; Wooldridge, P. J.; Molina, M. J. Vapor Pressure Measurements for the $H_2SO_4/HNO_3/H_2O$ and $H_2SO_4/HCl/H_2O$ Systems: Incorporation of Stratospheric Acids into Background Sulfate Aerosols. *J. Phys. Chem.* **1993**, *97*, 8541−8548.
(258) Molina, M. J.; Zhang, R.; Wooldridge, P. J.; McMahon, J. R.; Kim, J. E.; Chang, H. Y.; Beyer, K. D. Physical Chemistry of the $H_2SO_4/HNO_3/H_2O$ System: Implications for Polar Stratospheric Clouds. *Science* **1993**, *261*, 1418−1423.
(259) Wooldridge, P. J.; Zhang, R.; Molina, M. J. Phase Equilibria of H_2SO_4, HNO_3, and HCl Hydrates and the Composition of Polar Stratospheric Clouds. *J. Geophys. Res.* **1995**, *100*, 1389−1396.
(260) Zheng, J.; Zhang, R.; Fortner, E. C.; Volkamer, R. M.; Molina, L.; Aiken, A. C.; Jimenez, J. L.; Gaeggeler, K.; Dommen, J.; Dusanter, S.; Stevens, P. S.; Tie, X. Measurements of HNO_3 and N_2O_5 Using Ion Drift-Chemical Ionization Mass Spectrometry during the MILAGRO/MCMA-2006 Campaign. *Atmos. Chem. Phys.* **2008**, *8*, 6823−6838.
(261) Salo, K.; Westerlund, J.; Andersson, P. U.; Nielsen, C.; D'Anna, B.; Hallquist, M. Thermal Characterization of Aminium Nitrate Nanoparticles. *J. Phys. Chem. A* **2011**, *115*, 11671−11677.
(262) Pratt, K. A.; Hatch, L. E.; Prather, K. A. Seasonal Volatility Dependence of Ambient Particle Phase Amines. *Environ. Sci. Technol.* **2009**, *43*, 5276−5281.
(263) Pathak, R. K.; Wu, W. S.; Wang, T. Summertime $PM_{2.5}$ Ionic Species in Four Major Cities of China: Nitrate Formation in an Ammonia-Deficient Atmosphere. *Atmos. Chem. Phys.* **2009**, *9*, 1711−1722.
(264) Wahner, A.; Mentel, T. F.; Sohn, M. Gas-Phase Reaction of N_2O_5 with Water Vapor: Importance of Heterogeneous Hydrolysis of N_2O_5 and Surface Desorption of HNO_3 in a Large Teflon Chamber. *Geophys. Res. Lett.* **1998**, *25*, 2169−2172.
(265) Zhang, R.; Leu, M.-T.; Keyser, L. F. Hydrolysis of N_2O_5 and $ClONO_2$ on the $H_2SO_4/HNO_3/H_2O$ Ternary Solutions under Stratospheric Conditions. *Geophys. Res. Lett.* **1995**, *22*, 1493−1496.
(266) Hallquist, M.; Stewart, D. J.; Stephenson, S. K.; Cox, R. A. Hydrolysis of N_2O_5 on Sub-Micron Sulfate Aerosols. *Phys. Chem. Chem. Phys.* **2003**, *5*, 3453−3463.
(267) Brown, S. S.; Stutz, J. Nighttime Radical Observations and Chemistry. *Chem. Soc. Rev.* **2012**, *41*, 6405−6447.
(268) Brown, S. S.; Ryerson, T. B.; Wollny, A. G.; Brock, C. A.; Peltier, R.; Sullivan, A. P.; Weber, R. J.; Dube, W. P.; Trainer, M.; Meagher, J. F.; Fehsenfeld, F. C.; Ravishankara, A. R. Variability in Nocturnal Nitrogen Oxide Processing and Its Role in Regional Air Quality. *Science* **2006**, *311*, 67−70.
(269) Xue, J.; Yuan, Z. B.; Lau, A. K. H.; Yu, J. Z. Insights into Factors Affecting Nitrate in $PM_{2.5}$ in a Polluted High NO_x Environment through Hourly Observations and Size Distribution Measurements. *J. Geophys. Res.* **2014**, *119*, 4888−4902.
(270) Pathak, R. K.; Wang, T.; Wu, W. S. Nighttime Enhancement of $PM_{2.5}$ Nitrate in Ammonia-Poor Atmospheric Conditions in Beijing and Shanghai: Plausible Contributions of Heterogeneous Hydrolysis of N_2O_5 and HNO_3 Partitioning. *Atmos. Environ.* **2011**, *45*, 1183−1191.
(271) Formenti, P.; Schutz, L.; Balkanski, Y.; Desboeufs, K.; Ebert, M.; Kandler, K.; Petzold, A.; Scheuvens, D.; Weinbruch, S.; Zhang, D. Recent Progress in Understanding Physical and Chemical Properties of African and Asian Mineral Dust. *Atmos. Chem. Phys.* **2011**, *11*, 8231−8256.
(272) Liu, Y.; Gibson, E. R.; Cain, J. P.; Wang, H.; Grassian, V. H.; Laskin, A. Kinetics of Heterogeneous Reaction of $CaCO_3$ Particles with Gaseous HNO_3 over a Wide Range of Humidity. *J. Phys. Chem. A* **2008**, *112*, 1561−1571.
(273) Santschi, C.; Rossi, M. J. Uptake of CO_2, SO_2, HNO_3 and HCl on Calcite ($CaCO_3$) at 300 K: Mechanism and the Role of Adsorbed Water. *J. Phys. Chem. A* **2006**, *110*, 6789−6802.
(274) Sullivan, R. C.; Moore, M. J. K.; Petters, M. D.; Kreidenweis, S. M.; Roberts, G. C.; Prather, K. A. Timescale for Hygroscopic Conversion of Calcite Mineral Particles through Heterogeneous

DOI: 10.1021/acs.chemrev.5b00067
Chem. Rev. 2015, 115, 3803−3855

Reaction with Nitric Acid. *Phys. Chem. Chem. Phys.* **2009**, *11*, 7826−7837.
(275) Ziemba, L. D.; Dibb, J. E.; Griffin, R. J.; Anderson, C. H.; Whitlow, S. I.; Lefer, B. L.; Rappengluck, B.; Flynn, J. Heterogeneous Conversion of Nitric Acid to Nitrous Acid on the Surface of Primary Organic Aerosol in an Urban Atmosphere. *Atmos. Environ.* **2010**, *44*, 4081−4089.
(276) Ianniello, A.; Spataro, F.; Esposito, G.; Allegrini, I.; Hu, M.; Zhu, T. Chemical Characteristics of Inorganic Ammonium Salts in $PM_{2.5}$ in the Atmosphere of Beijing (China). *Atmos. Chem. Phys.* **2011**, *11*, 10803−10822.
(277) Wang, G. H.; Cheng, C. L.; Huang, Y.; Tao, J.; Ren, Y. Q.; Wu, F.; Meng, J. J.; Li, J. J.; Cheng, Y. T.; Cao, J. J.; Liu, S. X.; Zhang, T.; Zhang, R.; Chen, Y. B. Evolution of Aerosol Chemistry in Xi'an, Inland China, during the Dust Storm Period of 2013—Part 1: Sources, Chemical Forms and Formation Mechanisms of Nitrate and Sulfate. *Atmos. Chem. Phys.* **2014**, *14*, 11571−11585.
(278) Li, C.; Tsay, S.-C.; Fu, J. S.; Dickerson, R. R.; Ji, Q.; Bell, S. W.; Gao, Y.; Zhang, W.; Huang, J.; Li, Z.; Chen, H. Anthropogenic Air Pollution Observed near Dust Source Regions in Northwestern China during Springtime 2008. *J. Geophys. Res.* **2010**, *115*, DOI: 10.1029/2009JD013659.
(279) Gard, E. E.; Kleeman, M. J.; Gross, D. S.; Hughes, L. S.; Allen, J. O.; Morrical, B. D.; Fergenson, D. P.; Dienes, T.; M, E. G.; Johnson, R. J.; Cass, G. R.; Prather, K. A. Direct Observation of Heterogeneous Chemistry in the Atmosphere. *Science* **1998**, *279*, 1184−1187.
(280) Saul, T. D.; Tolocka, M. P.; Johnston, M. V. Reactive Uptake of Nitric Acid onto Sodium Chloride Aerosols across a Wide Range of Relative Humidities. *J. Phys. Chem. A* **2006**, *110*, 7614−7620.
(281) Perring, A. E.; Pusede, S. E.; Cohen, R. C. An Observational Perspective on the Atmospheric Impacts of Alkyl and Multifunctional Nitrates on Ozone and Secondary Organic Aerosol. *Chem. Rev.* **2013**, *113*, 5848−5870.
(282) Perraud, V.; Bruns, E. A.; Ezell, M. J.; Johnson, S. N.; Greaves, J.; Finlayson-Pitts, B. J. Identification of Organic Nitrates in the NO_3 Radical Initiated Oxidation of α-Pinene by Atmospheric Pressure Chemical Ionization Mass Spectrometry. *Environ. Sci. Technol.* **2010**, *44*, 5887−5893.
(283) Nguyen, T. B.; Laskin, J.; Laskin, A.; Nizkorodov, S. A. Nitrogen-Containing Organic Compounds and Oligomers in Secondary Organic Aerosol Formed by Photooxidation of Isoprene. *Environ. Sci. Technol.* **2011**, *45*, 6908−6918.
(284) Baker, J. W.; Neale, A. J. Importance of Ion Exchange with the Solvent in Kinetic Studies. *Nature* **1953**, *172*, 583−583.
(285) Hu, K. S.; Darer, A. I.; Elrod, M. J. Thermodynamics and Kinetics of the Hydrolysis of Atmospherically Relevant Organonitrates and Organosulfates. *Atmos. Chem. Phys.* **2011**, *11*, 8307−8320.
(286) Sato, K. Detection of Nitrooxypolyols in Secondary Organic Aerosol Formed from the Photooxidation of Conjugated Dienes under High-NO_x Conditions. *Atmos. Environ.* **2008**, *42*, 6851−6861.
(287) Rindelaub, J. D.; McAvey, K. M.; Shepson, P. B. The Photochemical Production of Organic Nitrates from α-Pinene and Loss via Acid-Dependent Particle Phase Hydrolysis. *Atmos. Environ.* **2015**, *100*, 193−201.
(288) Liu, S.; Shilling, J. E.; Song, C.; Hiranuma, N.; Zaveri, R. A.; Russell, L. M. Hydrolysis of Organonitrate Functional Groups in Aerosol Particles. *Aerosol Sci. Technol.* **2012**, *46*, 1359−1369.
(289) Khalizov, A. F.; Hogan, B.; Qiu, C.; Petersen, E. L.; Zhang, R. Y. Characterization of Soot Aerosol Produced from Combustion of Propane in a Shock Tube. *Aerosol Sci. Technol.* **2012**, *46*, 925−936.
(290) Qiu, C.; Khalizov, A. F.; Hogan, B.; Petersen, E. L.; Zhang, R. Y. High Sensitivity of Diesel Soot Morphological and Optical Properties to Combustion Temperature in a Shock Tube. *Environ. Sci. Technol.* **2014**, *48*, 6444−6452.
(291) Xue, H. X.; Khalizov, A. F.; Wang, L.; Zheng, J.; Zhang, R. Y. Effects of Coating of Dicarboxylic Acids on the Mass−Mobility Relationship of Soot Particles. *Environ. Sci. Technol.* **2009**, *43*, 2787−2792.
(292) Ranjan, M.; Presto, A. A.; May, A. A.; Robinson, A. L. Temperature Dependence of Gas-Particle Partitioning of Primary Organic Aerosol Emissions from a Small Diesel Engine. *Aerosol Sci. Technol.* **2012**, *46*, 13−21.
(293) Khalizov, A. F.; Lin, Y.; Qiu, C.; Guo, S.; Collins, D.; Zhang, R. Y. Role of OH-Initiated Oxidation of Isoprene in Aging of Combustion Soot. *Environ. Sci. Technol.* **2013**, *47*, 2254−2263.
(294) May, A. A.; Presto, A. A.; Hennigan, C. J.; Nguyen, N. T.; Gordon, T. D.; Robinson, A. L. Gas-Particle Partitioning of Primary Organic Aerosol Emissions: (2) Diesel Vehicles. *Environ. Sci. Technol.* **2013**, *47*, 8288−8296.
(295) Liu, Y. C.; Liu, C.; Ma, J. Z.; Ma, Q. X.; He, H. Structural and Hygroscopic Changes of Soot during Heterogeneous Reaction with O^{3-}. *Phys. Chem. Chem. Phys.* **2010**, *12*, 10896−10903.
(296) Zhang, D.; Zhang, R. Y. Laboratory Investigation of Heterogeneous Interaction of Sulfuric Acid with Soot. *Environ. Sci. Technol.* **2005**, *39*, 5722−5728.
(297) Levitt, N. P.; Zhang, R. Y.; Xue, H. X.; Chen, J. M. Heterogeneous Chemistry of Organic Acids on Soot Surfaces. *J. Phys. Chem. A* **2007**, *111*, 4804−4814.
(298) Adachi, K.; Buseck, P. R. Internally Mixed Soot, Sulfates, and Organic Matter in Aerosol Particles from Mexico City. *Atmos. Chem. Phys.* **2008**, *8*, 6469−6481.
(299) Kamens, R. M.; Coe, D. L. A Large Gas-Phase Stripping Device To Investigate Rates of PAH Evaporation from Airborne Diesel Soot Particles. *Environ. Sci. Technol.* **1997**, *31*, 1830−1833.
(300) Khalizov, A. F.; Xue, H. X.; Wang, L.; Zheng, J.; Zhang, R. Y. Enhanced Light Absorption and Scattering by Carbon Soot Aerosol Internally Mixed with Sulfuric Acid. *J. Phys. Chem. A* **2009**, *113*, 1066−1074.
(301) Khalizov, A. F.; Zhang, R. Y.; Zhang, D.; Xue, H. X.; Pagels, J.; McMurry, P. H. Formation of Highly Hygroscopic Soot Aerosols upon Internal Mixing with Sulfuric Acid Vapor. *J. Geophys. Res.* **2009**, *114*, DOI: 10.1029/2008jd010595, D05208.
(302) Xue, H. X.; Khalizov, A. F.; Wang, L.; Zheng, J.; Zhang, R. Y. Effects of Dicarboxylic Acid Coating on the Optical Properties of Soot. *Phys. Chem. Chem. Phys.* **2009**, *11*, 7869−7875.
(303) Adam, T. W.; Chirico, R.; Clairotte, M.; Elsasser, M.; Manfredi, U.; Martini, G.; Sklorz, M.; Streibel, T.; Heringa, M. F.; DeCarlo, P. F.; Baltensperger, U.; De Santi, G.; Krasenbrink, A.; Zimmermann, R.; Prevot, A. S. H.; Astorga, C. Application of Modern Online Instrumentation for Chemical Analysis of Gas and Particulate Phases of Exhaust at the European Commission Heavy-Duty Vehicle Emission Laboratory. *Anal. Chem.* **2011**, *83*, 67−76.
(304) Dewulf, J.; Van Langenhove, H. Anthropogenic Volatile Organic Compounds in Ambient Air and Natural Waters: A Review on Recent Developments of Analytical Methodology, Performance and Interpretation of Field Measurements. *J. Chromatogr. A* **1999**, *843*, 163−177.
(305) Molina, M. J.; Molina, L. T.; Zhang, R.; Meads, R. F.; Spencer, D. D. The Reaction of $ClONO_2$ with HCl on Aluminum Oxide. *Geophys. Res. Lett.* **1997**, *24*, 1619−1622.
(306) Zhao, J.; Zhang, R. Y.; Fortner, E. C.; North, S. W. Quantification of Hydroxycarbonyls from OH−Isoprene Reactions. *J. Am. Chem. Soc.* **2004**, *126*, 2686−2687.
(307) Fortner, E. C.; Zhao, J.; Zhang, R. Y. Development of Ion Drift-Chemical Ionization Mass Spectrometry. *Anal. Chem.* **2004**, *76*, 5436−5440.
(308) Zheng, J.; Khalizov, A.; Wang, L.; Zhang, R. Y. Atmospheric Pressure-Ion Drift Chemical Ionization Mass Spectrometry for Detection of Trace Gas Species. *Anal. Chem.* **2010**, *82*, 7302−7308.
(309) Lindinger, W.; Hansel, A.; Jordan, A. On-line Monitoring of Volatile Organic Compounds at pptv Levels by Means of Proton-Transfer-Reaction Mass Spectrometry (PTR-MS) - Medical Applications, Food Control and Environmental Research. *Int. J. Mass Spectrom.* **1998**, *173*, 191−241.
(310) Su, T.; Bowers, M. T. Theory of Ion-Polar Molecule Collisions. Comparison with Experimental Charge Transfer Reactions of Rare Gas Ions to Geometric Isomers of Difluorobenzene and Dichloroethylene. *J. Chem. Phys.* **1973**, *58*, 3027−3037.

DOI: 10.1021/acs.chemrev.5b00067
Chem. Rev. 2015, 115, 3803−3855

(311) Zhang, R. Y.; Lei, W. F. Reactions of O_2^+ with OH-Isoprene Adduct Isomers: Exothermicity, Product Ions, and Rate Constants. *J. Chem. Phys.* **2000**, *113*, 8574−8579.
(312) Warneke, C.; van der Veen, C.; Luxembourg, S.; de Gouw, J. A.; Kok, A. Measurements of Benzene and Toluene in Ambient Air Using Proton-Transfer-Reaction Mass Spectrometry: Calibration, Humidity Dependence, and Field Intercomparison. *Int. J. Mass Spectrom.* **2001**, *207*, 167−182.
(313) Zhao, J.; Zhang, R. Y. Proton Transfer Reaction Rate Constants between Hydronium Ion (H_3O^+) and Volatile Organic Compounds. *Atmos. Environ.* **2004**, *38*, 2177−2185.
(314) Yue, D. L.; Hu, M.; Zhang, R. Y.; Wang, Z. B.; Zheng, J.; Wu, Z. J.; Wiedensohler, A.; He, L. Y.; Huang, X. F.; Zhu, T. The Roles of Sulfuric Acid in New Particle Formation and Growth in the Mega-City of Beijing. *Atmos. Chem. Phys.* **2010**, *10*, 4953−4960.
(315) Zheng, J.; Hu, M.; Zhang, R.; Yue, D.; Wang, Z.; Guo, S.; Li, X.; Bohn, B.; Shao, M.; He, L.; Huang, X.; Wiedensohler, A.; Zhu, T. Measurements of Gaseous H_2SO_4 by AP-ID-CIMS during CAREBeijing 2008 Campaign. *Atmos. Chem. Phys.* **2011**, *11*, 7755−7765.
(316) Levy, M.; Zhang, R.; Zheng, J.; Zhang, A. L.; Xu, W.; Gomez-Hernandez, M.; Wang, Y.; Olaguer, E. Measurements of Nitrous Acid (HONO) Using Ion Drift-Chemical Ionization Mass Spectrometry during the 2009 SHARP Field Campaign. *Atmos. Environ.* **2014**, *94*, 231−240.
(317) Wiedensohler, A.; Birmili, W.; Nowak, A.; Sonntag, A.; Weinhold, K.; Merkel, M.; Wehner, B.; Tuch, T.; Pfeifer, S.; Fiebig, M.; Fjaraa, A. M.; Asmi, E.; Sellegri, K.; Depuy, R.; Venzac, H.; Villani, P.; Laj, P.; Aalto, P.; Ogren, J. A.; Swietlicki, E.; Williams, P.; Roldin, P.; Quincey, P.; Huglin, C.; Fierz-Schmidhauser, R.; Gysel, M.; Weingartner, E.; Riccobono, F.; Santos, S.; Gruning, C.; Faloon, K.; Beddows, D.; Harrison, R. M.; Monahan, C.; Jennings, S. G.; O'Dowd, C. D.; Marinoni, A.; Horn, H. G.; Keck, L.; Jiang, J.; Scheckman, J.; McMurry, P. H.; Deng, Z.; Zhao, C. S.; Moerman, M.; Henzing, B.; de Leeuw, G.; Loschau, G.; Bastian, S. Mobility Particle Size Spectrometers: Harmonization of Technical Standards and Data Structure To Facilitate High Quality Long-Term Observations of Atmospheric Particle Number Size Distributions. *Atmos. Meas. Technol.* **2012**, *5*, 657−685.
(318) Vanhanen, J.; Mikkila, J.; Lehtipalo, K.; Sipila, M.; Manninen, H. E.; Siivola, E.; Petaja, T.; Kulmala, M. Particle Size Magnifier for Nano-CN Detection. *Aerosol Sci. Technol.* **2011**, *45*, 533−542.
(319) Asmi, E.; Sipila, M.; Manninen, H. E.; Vanhanen, J.; Lehtipalo, K.; Gagne, S.; Neitola, K.; Mirme, A.; Mirme, S.; Tamm, E.; Uin, J.; Komsaare, K.; Attoui, M.; Kulmala, M. Results of the First Air Ion Spectrometer Calibration and Intercomparison Workshop. *Atmos. Chem. Phys.* **2009**, *9*, 141−154.
(320) Chow, J. C. Measurement Methods To Determine Compliance with Ambient Air-Quality Standards for Suspended Particles. *J. Air Waste Manage. Assoc.* **1995**, *45*, 320−382.
(321) Niu, J. J.; Rasmussen, P. E.; Wheeler, A.; Williams, R.; Chenier, M. Evaluation of Airborne Particulate Matter and Metals Data in Personal, Indoor and Outdoor Environments Using ED-XRF and ICP-MS and Co-Located Duplicate Samples. *Atmos. Environ.* **2010**, *44*, 235−245.
(322) Chow, J. C.; Watson, J. G.; Crow, D.; Lowenthal, D. H.; Merrifield, T. Comparison of IMPROVE and NIOSH Carbon Measurements. *Aerosol Sci. Technol.* **2001**, *34*, 23−34.
(323) Turpin, B. J.; Cary, R. A.; Huntzicker, J. J. An in Situ, Time-Resolved Analyzer for Aerosol Organic and Elemental Carbon. *Aerosol Sci. Technol.* **1990**, *12*, 161−171.
(324) Maria, S. F.; Russell, L. M.; Turpin, B. J.; Porcja, R. J. FTIR Measurements of Functional Groups and Organic Mass in Aerosol Samples over the Caribbean. *Atmos. Environ.* **2002**, *36*, 5185−5196.
(325) Rogge, W. F.; Mazurek, M. A.; Hildemann, L. M.; Cass, G. R.; Simoneit, B. R. T. Quantification of Urban Organic Aerosols at a Molecular-Level—Identification, Abundance and Seasonal-Variation. *Atmos. Environ.* **1993**, *27*, 1309−1330.
(326) Kleindienst, T. E.; Jaoui, M.; Lewandowski, M.; Offenberg, J. H.; Lewis, C. W.; Bhave, P. V.; Edney, E. O. Estimates of the Contributions of Biogenic and Anthropogenic Hydrocarbons to Secondary Organic Aerosol at a Southeastern US Location. *Atmos. Environ.* **2007**, *41*, 8288−8300.
(327) Takahama, S.; Johnson, A.; Morales, J. G.; Russell, L. M.; Duran, R.; Rodriguez, G.; Zheng, J.; Zhang, R.; Toom-Sauntry, D.; Leaitch, W. R. Submicron Organic Aerosol in Tijuana, Mexico, from Local and Southern California Sources during the CalMex Campaign. *Atmos. Environ.* **2013**, *70*, 500−512.
(328) Takahama, S.; Russell, L. M.; Shores, C. A.; Marr, L. C.; Zheng, J.; Levy, M.; Zhang, R.; Castillo, E.; Rodriguez-Ventura, J. G.; Quintana, P. J. E.; Subramanian, R.; Zavala, M.; Molina, L. T. Diesel Vehicle and Urban Burning Contributions to Black Carbon Concentrations and Size Distributions in Tijuana, Mexico, during the Cal-Mex 2010 Campaign. *Atmos. Environ.* **2014**, *88*, 341−352.
(329) Levy, M. E.; Zhang, R.; Zheng, J.; Tan, H.; Wang, Y.; Molina, L. T.; Takahama, S.; Russell, L. M.; Li, G. Measurements of Submicron Aerosols at the California−Mexico Border during the Cal−Mex 2010 Field Campaign. *Atmos. Environ.* **2014**, *88*, 308−319.
(330) Arnott, W. P.; Moosmuller, H.; Abbott, R. E.; Ossofsky, M. D. Thermoacoustic Enhancement of Photoacoustic-Spectroscopy—Theory and Measurements of the Signal-to-Noise Ratio. *Rev. Sci. Instrum.* **1995**, *66*, 4827−4833.
(331) Slanina, J.; ten Brink, H. M.; Otjes, R. P.; Even, A.; Jongejan, P.; Khlystov, A.; Waijers-Ijpelaan, A.; Hu, M. The Continuous Analysis of Nitrate and Ammonium in Aerosols by the Steam Jet Aerosol Collector (SJAC): Extension and Validation of the Methodology. *Atmos. Environ.* **2001**, *35*, 2319−2330.
(332) ten Brink, H.; Otjes, R.; Jongejan, P.; Slanina, S. An Instrument for Semi-Continuous Monitoring of the Size-Distribution of Nitrate, Ammonium, Sulphate and Chloride in Aerosol. *Atmos. Environ.* **2007**, *41*, 2768−2779.
(333) Weber, R. J.; Orsini, D.; Daun, Y.; Lee, Y. N.; Klotz, P. J.; Brechtel, F. A Particle-into-Liquid Collector for Rapid Measurement of Aerosol Bulk Chemical Composition. *Aerosol Sci. Technol.* **2001**, *35*, 718−727.
(334) Lee, S. H.; Allen, H. C. Analytical Measurements of Atmospheric Urban Aerosol. *Anal. Chem.* **2012**, *84*, 1196−1201.
(335) Murphy, D. M. The Design of Single Particle Laser Mass Spectrometers. *Mass Spectrom. Rev.* **2007**, *26*, 150−165.
(336) Johnston, M. V. Sampling and Analysis of Individual Particles by Aerosol Mass Spectrometry. *J. Mass Spectrom.* **2000**, *35*, 585−595.
(337) Nash, D. G.; Baer, T.; Johnston, M. V. Aerosol Mass Spectrometry: An Introductory Review. *Int. J. Mass Spectrom.* **2006**, *258*, 2−12.
(338) Wexler, A. S.; Johnston, M. V. What Have We Learned from Highly Time-Resolved Measurements during EPA's Supersites Program, and Related Studies? *J. Air Waste Manage. Assoc.* **2008**, *58*, 303−319.
(339) Prather, K. A.; Hatch, C. D.; Grassian, V. H. Analysis of Atmospheric Aerosols. *Annu. Rev. Anal. Chem.* **2008**, *1*, 485−514.
(340) Zelenyuk, A.; Imre, D. Single Particle Laser Ablation Time-of-Flight Mass Spectrometer: An Introduction to SPLAT. *Aerosol Sci. Technol.* **2005**, *39*, 554−568.
(341) Drewnick, F. Speciation Analysis in On-Line Aerosol Mass Spectrometry. *Anal. Bioanal. Chem.* **2012**, *404*, 2127−2131.
(342) Jayne, J. T.; Leard, D. C.; Zhang, X. F.; Davidovits, P.; Smith, K. A.; Kolb, C. E.; Worsnop, D. R. Development of an Aerosol Mass Spectrometer for Size and Composition Analysis of Submicron Particles. *Aerosol Sci. Technol.* **2000**, *33*, 49−70.
(343) Aiken, A. C.; de Foy, B.; Wiedinmyer, C.; DeCarlo, P. F.; Ulbrich, I. M.; Wehrli, M. N.; Szidat, S.; Prevot, A. S. H.; Noda, J.; Wacker, L.; Volkamer, R.; Fortner, E.; Wang, J.; Laskin, A.; Shutthanandan, V.; Zheng, J.; Zhang, R.; Paredes-Miranda, G.; Arnott, W. P.; Molina, L. T.; Sosa, G.; Querol, X.; Jimenez, J. L. Mexico City Aerosol Analysis during MILAGRO Using High Resolution Aerosol Mass Spectrometry at the Urban Supersite (T0)—Part 2: Analysis of the Biomass Burning Contribution and the Non-Fossil Carbon Fraction. *Atmos. Chem. Phys.* **2010**, *10*, 5315−5341.

DOI: 10.1021/acs.chemrev.5b00067
Chem. Rev. 2015, 115, 3803−3855

(344) He, L. Y.; Huang, X. F.; Xue, L.; Hu, M.; Lin, Y.; Zheng, J.; Zhang, R. Y.; Zhang, Y. H. Submicron Aerosol Analysis and Organic Source Apportionment in an Urban Atmosphere in Pearl River Delta of China Using High-Resolution Aerosol Mass Spectrometry. *J. Geophys. Res.* **2011**, *116*, DOI: 10.1029/2010JD014566, D12304.
(345) Canagaratna, M. R.; Jayne, J. T.; Jimenez, J. L.; Allan, J. D.; Alfarra, M. R.; Zhang, Q.; Onasch, T. B.; Drewnick, F.; Coe, H.; Middlebrook, A.; Delia, A.; Williams, L. R.; Trimborn, A. M.; Northway, M. J.; DeCarlo, P. F.; Kolb, C. E.; Davidovits, P.; Worsnop, D. R. Chemical and Microphysical Characterization of Ambient Aerosols with the Aerodyne Aerosol Mass Spectrometer. *Mass Spectrom. Rev.* **2007**, *26*, 185−222.
(346) Williams, B. J.; Goldstein, A. H.; Kreisberg, N. M.; Hering, S. V. An In-Situ Instrument for Speciated Organic Composition of Atmospheric Aerosols: Thermal Desorption Aerosol GC/MS-FID (TAG). *Aerosol Sci. Technol.* **2006**, *40*, 627−638.
(347) Smith, J. N.; Rathbone, G. J. Carboxylic Acid Characterization in Nanoparticles by Thermal Desorption Chemical Ionization Mass Spectrometry. *Int. J. Mass Spectrom.* **2008**, *274*, 8−13.
(348) Yatavelli, R. L. N.; Thornton, J. A. Particulate Organic Matter Detection Using a Micro-Orifice Volatilization Impactor Coupled to a Chemical Ionization Mass Spectrometer (MOVI-CIMS). *Aerosol Sci. Technol.* **2010**, *44*, 61−74.
(349) Denkenberger, K. A.; Moffet, R. C.; Holecek, J. C.; Rebotier, T. P.; Prather, K. A. Real-Time, Single-Particle Measurements of Oligomers in Aged Ambient Aerosol Particles. *Environ. Sci. Technol.* **2007**, *41*, 5439−5446.
(350) Hopke, P. K. *Receptor Modeling for Air Quality Management*; Elsevier: Amsterdam, 1991.
(351) Jolliffe, I. T. *Principal Component Analysis*; Springer Verlag: New York, 2002.
(352) Paatero, P. Least Squares Formulation of Robust Non-Negative Factor Analysis. *Chemom. Intell. Lab. Syst.* **1997**, *37*, 23−35.
(353) Turpin, B. J.; Huntzicker, J. J.; Larson, S. M.; Cass, G. R. Los Angeles Summer Midday Particulate Carbon: Primary and Secondary Aerosol. *Environ. Sci. Technol.* **1991**, *25*, 1788−1793.
(354) Millet, D. B.; Donahue, N. M.; Pandis, S. N.; Polidori, A.; Stanier, C. O.; Turpin, B. J.; Goldstein, A. H. Atmospheric Volatile Organic Compound Measurements during the Pittsburgh Air Quality Study: Results, Interpretation, and Quantification of Primary and Secondary Contributions. *J. Geophys. Res.* **2005**, *110*, DOI: 10.1029/2004jd004601.
(355) Stone, E. A.; Zhou, J. B.; Snyder, D. C.; Rutter, A. P.; Mieritz, M.; Schauer, J. J. A Comparison of Summertime Secondary Organic Aerosol Source Contributions at Contrasting Urban Locations. *Environ. Sci. Technol.* **2009**, *43*, 3448−3454.
(356) Zhang, Y.; Sheesley, R. J.; Schauer, J. J.; Lewandowski, M.; Jaoui, M.; Offenberg, J. H.; Kleindienst, T. E.; Edney, E. O. Source Apportionment of Primary and Secondary Organic Aerosols Using Positive Matrix Factorization (PMF) of Molecular Markers. *Atmos. Environ.* **2009**, *43*, 5567−5574.
(357) Zhang, Q.; Alfarra, M. R.; Worsnop, D. R.; Allan, J. D.; Coe, H.; Canagaratna, M. R.; Jimenez, J. L. Deconvolution and Quantification of Hydrocarbon-like and Oxygenated Organic Aerosols Based on Aerosol Mass Spectrometry. *Environ. Sci. Technol.* **2005**, *39*, 4938−4952.
(358) Lanz, V. A.; Alfarra, M. R.; Baltensperger, U.; Buchmann, B.; Hueglin, C.; Prevot, A. S. H. Source Apportionment of Submicron Organic Aerosols at an Urban Site by Factor Analytical Modelling of Aerosol Mass Spectra. *Atmos. Chem. Phys.* **2007**, *7*, 1503−1522.
(359) Jimenez, J. L.; Canagaratna, M. R.; Donahue, N. M.; Prevot, A. S. H.; Zhang, Q.; Kroll, J. H.; DeCarlo, P. F.; Allan, J. D.; Coe, H.; Ng, N. L.; Aiken, A. C.; Docherty, K. S.; Ulbrich, I. M.; Grieshop, A. P.; Robinson, A. L.; Duplissy, J.; Smith, J. D.; Wilson, K. R.; Lanz, V. A.; Hueglin, C.; Sun, Y. L.; Tian, J.; Laaksonen, A.; Raatikainen, T.; Rautiainen, J.; Vaattovaara, P.; Ehn, M.; Kulmala, M.; Tomlinson, J. M.; Collins, D. R.; Cubison, M. J.; Dunlea, E. J.; Huffman, J. A.; Onasch, T. B.; Alfarra, M. R.; Williams, P. I.; Bower, K.; Kondo, Y.; Schneider, J.; Drewnick, F.; Borrmann, S.; Weimer, S.; Demerjian, K.; Salcedo, D.; Cottrell, L.; Griffin, R.; Takami, A.; Miyoshi, T.; Hatakeyama, S.; Shimono, A.; Sun, J. Y.; Zhang, Y. M.; Dzepina, K.; Kimmel, J. R.; Sueper, D.; Jayne, J. T.; Herndon, S. C.; Trimborn, A. M.; Williams, L. R.; Wood, E. C.; Middlebrook, A. M.; Kolb, C. E.; Baltensperger, U.; Worsnop, D. R. Evolution of Organic Aerosols in the Atmosphere. *Science* **2009**, *326*, 1525−1529.
(360) Levy, M. E.; Zhang, R. Y.; Khalizov, A. F.; Zheng, J.; Collins, D. R.; Glen, C. R.; Wang, Y.; Yu, X. Y.; Luke, W.; Jayne, J. T.; Olaguer, E. Measurements of Submicron Aerosols in Houston, Texas during the 2009 SHARP Field Campaign. *J. Geophys. Res.* **2013**, *118*, 10518−10534.
(361) *AirData*; U.S. Environmental Protection Agency (EPA): Research Triangle Park, NC, 2014. http://www.epa.gov/airquality/airdata/ad_viz_plotval.html (accessed Jan 2, 2015).
(362) *Annual Estimates of the Population of Metropolitan and Micropolitan Statistical Areas: April 1, 2010 to July 1, 2011*; CBSA-EST2011-01; U.S. Census Bureau, Population Division: Washington, DC, 2012. http://www.census.gov/popest/data/metro/totals/2011/ (accessed Jan 2, 2015).
(363) Hayes, P. L.; Ortega, A. M.; Cubison, M. J.; Hu, W. W.; Toohey, D. W.; Flynn, J. H.; Grossberg, N.; Lefer, B. L.; Alvarez, S.; Rappengluck, B.; Allan, J. D.; Holloway, J. S.; Massoli, P.; Froyd, K. D.; Murphy, S. M.; Liu, J. M.; Weber, R. J.; Jimenez, J. L. Aerosol Composition in Los Angeles during the 2010 CalNex Campaign Studied by High Resolution Aerosol Mass Spectrometry. *Abstr. Pap.—Am. Chem. Soc.* **2011**, *242*, 1−1.
(364) Moore, K.; Krudysz, M.; Pakbin, P.; Hudda, N.; Sioutas, C. Intra-Community Variability in Total Particle Number Concentrations in the San Pedro Harbor Area (Los Angeles, California). *Aerosol Sci. Technol.* **2009**, *43*, 587−603.
(365) *Air Quality in the Mexico MegaCity: An Integrated Assessment*; Molina, L., Molina, M., Eds.; Kluwer Academic Publishers: Dordrecht, The Netherlands, 2002.
(366) Stephens, S.; Madronich, S.; Wu, F.; Olson, J. B.; Ramos, R.; Retama, A.; Muñoz, R. Weekly Patterns of México City's Surface Concentrations of CO, NO_x, PM_{10} and O_3 during 1986−2007. *Atmos. Chem. Phys.* **2008**, *8*, 5313−5325.
(367) Kalafut-Pettibone, A. J.; Wang, J.; Eichinger, W. E.; Clarke, A.; Vay, S. A.; Blake, D. R.; Stanier, C. O. Size-Resolved Aerosol Emission Factors and New Particle Formation/Growth Activity Occurring in Mexico City during the MILAGRO 2006 Campaign. *Atmos. Chem. Phys.* **2011**, *11*, 8861−8881.
(368) *Air Quality in Mexico City, 2010 Report, Mexico*; Ministry of Environment of the Federal District (Secretaria del Medio Ambiente del Gobierno del Distrito Federal, SEMARNAT): Mexico City, 2011. http://www.sedema.df.gob.mx/flippingbook/informe_anual_calidad_aire_2010/ (accessed Jan 2, 2015).
(369) *Promedios de 24 Horas de Dióxido Azufre*; Ministry of the Environment (Secretaría del Medio Ambiente, SEDEMA): Mexico City, 2014. http://www.aire.df.gob.mx/default.php?opc=%27aKBhnmI=%27&opcion=aQ (accessed Jan 2, 2015).
(370) Liu, Z.; Hu, B.; Wang, L.; Wu, F.; Gao, W.; Wang, Y. Seasonal and Diurnal Variation in Particulate Matter (PM_{10} and $PM_{2.5}$) at an Urban Site of Beijing: Analyses from a 9-Year Study. *Environ. Sci. Pollut. Res.* **2015**, *22*, 627−642.
(371) Li, Z.; Chen, H.; Cribb, M.; Dickerson, R.; Holben, B.; Li, C.; Lu, D.; Luo, Y.; Maring, H.; Shi, G.; Tsay, S. C.; Wang, P.; Wang, Y.; Xia, X.; Zheng, Y.; Yuan, T.; Zhao, F. Preface to Special Section on East Asian Studies of Tropospheric Aerosols: An International Regional Experiment (EAST-AIRE). *J. Geophys. Res.* **2007**, *112*, DOI: 10.1029/2007JD008853.
(372) Cowling, E. B.; Furiness, C.; Dimitriades, B.; Parrish, D. D. *Final Rapid Science Synthesis Report: Findings from the Second Texas Air Quality Study (TexAQS II)*; Texas Commission on Environmental Quality (TCEQ): Austin, TX, 2007. http://www.tceq.state.tx.us/assets/public/implementation/air/texaqs/doc/rsst_final_report.pdf (accessed Jan 2, 2015).
(373) Zhang, R. Y.; Lei, W. F.; Tie, X. X.; Hess, P. Industrial Emissions Cause Extreme Diurnal Urban Ozone Variability. *Proc. Natl. Acad. Sci. U.S.A.* **2004**, *101*, 6346−6350.

DOI: 10.1021/acs.chemrev.5b00067
Chem. Rev. 2015, 115, 3803−3855

(374) Lei, W. F.; Zhang, R. Y.; Tie, X. X.; Hess, P. Chemical Characterization of Ozone Formation in the Houston-Galveston Area: A Chemical Transport Model Study. *J. Geophys. Res.* **2004**, *109*, DOI: 10.1029/2003jd004219, D12301.
(375) Brock, C. A.; Trainer, M.; Ryerson, T. B.; Neuman, J. A.; Parrish, D. D.; Holloway, J. S.; Nicks, D. K.; Frost, G. J.; Hübler, G.; Fehsenfeld, F. C.; Wilson, J. C.; Reeves, J. M.; Lafleur, B. G.; Hilbert, H.; Atlas, E. L.; Donnelly, S. G.; Schauffler, S. M.; Stroud, V. R.; Wiedinmyer, C. Particle Growth in Urban and Industrial Plumes in Texas. *J. Geophys. Res.* **2003**, *108*, DOI: 10.1029/2002JD002746.
(376) Gasparini, R.; Li, R.; Collins, D. R. Integration of Size Distributions and Size-Resolved Hygroscopicity Measured during the Houston Supersite for Compositional Categorization of the Aerosol. *Atmos. Environ.* **2004**, *38*, 3285−3303.
(377) Zhang, Q.; Parworth, C.; Lechner, M.; Jimenez, J. L. Aerosol Mass Spectrometry (AMS) Global Database, 2006. https://sites.google.com/site/amsglobaldatabase/urban (accessed Jan 2, 2015).
(378) Russell, M.; Allen, D. T.; Collins, D. R.; Fraser, M. P. Daily, Seasonal, and Spatial Trends in $PM_{2.5}$ Mass and Composition in Southeast Texas. *Aerosol Sci. Technol.* **2004**, *38*, 14−26 (Special Issue on Findings from the Fine Particulate Matter Supersites Program).
(379) Fan, J.; Zhang, R.; Li, G.; Nielsen-Gammon, J.; Li, Z. Simulations of Fine Particulate Matter ($PM_{2.5}$) in Houston, Texas. *J. Geophys. Res.* **2005**, *110*, DOI: 10.1029/2005JD005805, D16203.
(380) Lee, S. H.; Murphy, D. M.; Thomson, D. S.; Middlebrook, A. M. Chemical Components of Single Particles Measured with Particle Analysis by Laser Mass Spectrometry (PALMS) during the Atlanta Supersite Project: Focus on Organic/Sulfate, Lead, Soot, and Mineral Particles. *J. Geophys. Res.* **2002**, *107*, DOI: 10.1029/2000jd000011.
(381) Ryerson, T. B.; Andrews, A. E.; Angevine, W. M.; Bates, T. S.; Brock, C. A.; Cairns, B.; Cohen, R. C.; Cooper, O. R.; de Gouw, J. A.; Fehsenfeld, F. C.; Ferrare, R. A.; Fischer, M. L.; Flagan, R. C.; Goldstein, A. H.; Hair, J. W.; Hardesty, R. M.; Hostetler, C. A.; Jimenez, J. L.; Langford, A. O.; McCauley, E.; McKeen, S. A.; Molina, L. T.; Nenes, A.; Oltmans, S. J.; Parrish, D. D.; Pederson, J. R.; Pierce, R. B.; Prather, K.; Quinn, P. K.; Seinfeld, J. H.; Senff, C. J.; Sorooshian, A.; Stutz, J.; Surratt, J. D.; Trainer, M.; Volkamer, R.; Williams, E. J.; Wofsy, S. C. The 2010 California Research at the Nexus of Air Quality and Climate Change (CalNex) Field Study. *J. Geophys. Res.* **2013**, *118*, 5830−5866.
(382) Hersey, S. P.; Craven, J. S.; Schilling, K. A.; Metcalf, A. R.; Sorooshian, A.; Chan, M. N.; Flagan, R. C.; Seinfeld, J. H. The Pasadena Aerosol Characterization Observatory (PACO): Chemical and Physical Analysis of the Western Los Angeles Basin Aerosol. *Atmos. Chem. Phys.* **2011**, *11*, 7417−7443.
(383) Pennington, M. R.; Klems, J. P.; Bzdek, B. R.; Johnston, M. V. Nanoparticle Chemical Composition and Diurnal Dependence at the CalNex Los Angeles Ground Site. *J. Geophys. Res.* **2012**, *117*, DOI: 10.1029/2011jd017061.
(384) Hudda, N.; Cheung, K.; Moore, K. F.; Sioutas, C. Inter-Community Variability in Total Particle Number Concentrations in the Eastern Los Angeles Air Basin. *Atmos. Chem. Phys.* **2010**, *10*, 11385−11399.
(385) Zhang, X. L.; Lin, Y. H.; Surratt, J. D.; Zotter, P.; Prevot, A. S. H.; Weber, R. J. Light-Absorbing Soluble Organic Aerosol in Los Angeles and Atlanta: A Contrast in Secondary Organic Aerosol. *Geophys. Res. Lett.* **2011**, *38*, DOI: 10.1029/2011gl049385.
(386) Fast, J. D.; de Foy, B.; Rosas, F. A.; Caetano, E.; Carmichael, G.; Emmons, L.; McKenna, D.; Mena, M.; Skamarock, W.; Tie, X.; Coulter, R. L.; Barnard, J. C.; Wiedinmyer, C.; Madronich, S. A Meteorological Overview of the MILAGRO Field Campaigns. *Atmos. Chem. Phys.* **2007**, *7*, 2233−2257.
(387) Dunn, M. J.; Jimenez, J. L.; Baumgardner, D.; Castro, T.; McMurry, P. H.; Smith, J. N. Measurements of Mexico City Nanoparticle Size Distributions: Observations of New Particle Formation and Growth. *Geophys. Res. Lett.* **2004**, *31*, DOI: 10.1029/2004gl019483.
(388) Molina, L. T.; Kolb, C. E.; de Foy, B.; Lamb, B. K.; Brune, W. H.; Jimenez, J. L.; Ramos-Villegas, R.; Sarmiento, J.; Paramo-Figueroa, V. H.; Cardenas, B.; Gutierrez-Avedoy, V.; Molina, M. J. Air Quality in North America's Most Populous City—Overview of the MCMA-2003 Campaign. *Atmos. Chem. Phys.* **2007**, *7*, 2447−2473.
(389) Molina, L. T.; Madronich, S.; Gaffney, J. S.; Apel, E.; de Foy, B.; Fast, J.; Ferrare, R.; Herndon, S.; Jimenez, J. L.; Lamb, B.; Osornio-Vargas, A. R.; Russell, P.; Schauer, J. J.; Stevens, P. S.; Volkamer, R.; Zavala, M. An Overview of the MILAGRO 2006 Campaign: Mexico City Emissions and Their Transport and Transformation. *Atmos. Chem. Phys.* **2010**, *10*, 8697−8760.
(390) Smith, J. N.; Dunn, M. J.; VanReken, T. M.; Iida, K.; Stolzenburg, M. R.; McMurry, P. H.; Huey, L. G. Chemical Composition of Atmospheric Nanoparticles Formed from Nucleation in Tecamac, Mexico: Evidence for an Important Role for Organic Species in Nanoparticle Growth. *Geophys. Res. Lett.* **2008**, *35*, DOI: 10.1029/2007gl032523.
(391) Paredes-Miranda, G.; Arnott, W. P.; Jimenez, J. L.; Aiken, A. C.; Gaffney, J. S.; Marley, N. A. Primary and Secondary Contributions to Aerosol Light Scattering and Absorption in Mexico City during the MILAGRO 2006 Campaign. *Atmos. Chem. Phys.* **2009**, *9*, 3721−3730.
(392) Moffet, R. C.; Qin, X. Y.; Rebotier, T.; Furutani, H.; Prather, K. A. Chemically Segregated Optical and Microphysical Properties of Ambient Aerosols Measured in a Single-Particle Mass Spectrometer. *J. Geophys. Res.* **2008**, *113*, DOI: 10.1029/2007jd009393.
(393) Wu, Z. J.; Hu, M.; Liu, S.; Wehner, B.; Bauer, S.; Ssling, A. M.; Wiedensohler, A.; Petaja, T.; Dal Maso, M.; Kulmala, M. New Particle Formation in Beijing, China: Statistical Analysis of a 1-Year Data Set. *J. Geophys. Res.* **2007**, *112*, DOI: 10.1029/2006jd007406.
(394) Kulmala, M.; Vehkamaki, H.; Petaja, T.; Dal Maso, M.; Lauri, A.; Kerminen, V. M.; Birmili, W.; McMurry, P. H. Formation and Growth Rates of Ultrafine Atmospheric Particles: A Review of Observations. *J. Aerosol Sci.* **2004**, *35*, 143−176.
(395) Lee, K. H.; Li, Z. Q.; Wong, M. S.; Xin, J. Y.; Wang, Y. S.; Hao, W. M.; Zhao, F. S. Aerosol Single Scattering Albedo Estimated across China from a Combination of Ground and Satellite Measurements. *J. Geophys. Res.* **2007**, *112*, DOI: 10.1029/2007jd009077.
(396) Yang, X.; Yao, Z. Y.; Li, Z. Q.; Fan, T. Y. Heavy Air Pollution Suppresses Summer Thunderstorms in Central China. *J. Atmos. Sol.-Terr. Phys.* **2013**, *95*−*96*, 28−40.
(397) Zhang, R. Y.; Tie, X. X.; Bond, D. W. Impacts of Anthropogenic and Natural NO_x Sources over the U.S. on Tropospheric Chemistry. *Proc. Natl. Acad. Sci. U.S.A.* **2003**, *100*, 1505−1509.
(398) Ying, Q.; Krishnan, A. Source Contributions of Volatile Organic Compounds to Ozone Formation in Southeast Texas. *J. Geophys. Res.* **2010**, *115*, DOI: 10.1029/2010jd013931.
(399) Zhang, H.; Ying, Q. Source Apportionment of Airborne Particulate Matter in Southeast Texas Using a Source-Oriented 3D Air Quality Model. *Atmos. Environ.* **2010**, *44*, 3547−3557.
(400) Ying, Q.; Kleeman, M. J. Source Contributions to the Regional Distribution of Secondary Particulate Matter in California. *Atmos. Environ.* **2006**, *40*, 736−752.
(401) Zhang, H.; Ying, Q. Contributions of Local and Regional Sources of NO_x to Ozone Concentrations in Southeast Texas. *Atmos. Environ.* **2011**, *45*, 2877−2887.
(402) Gamas, E. D.; Diaz, L.; Rodriguez, R.; López-Salinas, E.; Schifter, I.; Ontiveros, L. Exhaust Emissions from Gasoline- and LPG-Powered Vehicles Operating at the Altitude of Mexico City. *J. Air Waste Manage. Assoc.* **1999**, *49*, 1179−1189.
(403) Zhang, H.; Li, J.; Ying, Q.; Yu, J. Z.; Wu, D.; Cheng, Y.; He, K.; Jiang, J. Source Apportionment of $PM_{2.5}$ Nitrate and Sulfate in China Using a Source-Oriented Chemical Transport Model. *Atmos. Environ.* **2012**, *62*, 228−242.
(404) Ying, Q.; Wu, L.; Zhang, H. Local and Inter-Regional Contributions to $PM_{2.5}$ Nitrate and Sulfate in China. *Atmos. Environ.* **2014**, *94*, 582−592.
(405) Streets, D. G.; Bond, T. C.; Carmichael, G. R.; Fernandes, S. D.; Fu, Q.; He, D.; Klimont, Z.; Nelson, S. M.; Tsai, N. Y.; Wang, M. Q.; Woo, J. H.; Yarber, K. F. An Inventory of Gaseous and Primary Aerosol Emissions in Asia in the Year 2000. *J. Geophys. Res.* **2003**, *108*, DOI: 10.1029/2002jd003093.

DOI: 10.1021/acs.chemrev.5b00067
Chem. Rev. 2015, 115, 3803−3855

(406) Zhang, Q.; Streets, D. G.; Carmichael, G. R.; He, K. B.; Huo, H.; Kannari, A.; Klimont, Z.; Park, I. S.; Reddy, S.; Fu, J. S.; Chen, D.; Duan, L.; Lei, Y.; Wang, L. T.; Yao, Z. L. Asian Emissions in 2006 for the NASA INTEX-B Mission. *Atmos. Chem. Phys.* **2009**, *9*, 5131−5153.
(407) Ohara, T.; Akimoto, H.; Kurokawa, J.; Horii, N.; Yamaji, K.; Yan, X.; Hayasaka, T. An Asian Emission Inventory of Anthropogenic Emission Sources for the Period 1980−2020. *Atmos. Chem. Phys. Discuss.* **2007**, *7*, 6843−6902.
(408) Kurokawa, J.; Ohara, T.; Morikawa, T.; Hanayama, S.; Janssens-Maenhout, G.; Fukui, T.; Kawashima, K.; Akimoto, H. Emissions of Air Pollutants and Greenhouse Gases over Asian Regions during 2000−2008: Regional Emission Inventory in Asia (REAS) Version 2. *Atmos. Chem. Phys.* **2013**, *13*, 11019−11058.
(409) Mijling, B.; van der A, R. J.; Zhang, Q. Regional Nitrogen Oxides Emission Trends in East Asia Observed from Space. *Atmos. Chem. Phys.* **2013**, *13*, 12003−12012.
(410) Stavrakou, T.; Mueller, J. F.; Boersma, K. F.; van der A, R. J.; Kurokawa, J.; Ohara, T.; Zhang, Q. Key Chemical NO_x Sink Uncertainties and How They Influence Top-Down Emissions of Nitrogen Oxides. *Atmos. Chem. Phys.* **2013**, *13*, 9057−9082.
(411) Wang, L. T.; Wei, Z.; Yang, J.; Zhang, Y.; Zhang, F. F.; Su, J.; Meng, C. C.; Zhang, Q. The 2013 Severe Haze over Southern Hebei, China: Model Evaluation, Source Apportionment, and Policy Implications. *Atmos. Chem. Phys.* **2014**, *14*, 3151−3173.
(412) Kleeman, M. J.; Schauer, J. J.; Cass, G. R. Size and Composition Distribution of Fine Particulate Matter Emitted from Motor Vehicles. *Environ. Sci. Technol.* **2000**, *34*, 1132−1142.
(413) Schauer, J. J.; Kleeman, M. J.; Cass, G. R.; Simoneit, B. R. T. Measurement of Emissions from Air Pollution Sources. 5. C_1−C_{32} Organic Compounds from Gasoline-Powered Motor Vehicles. *Environ. Sci. Technol.* **2002**, *36*, 1169−1180.
(414) Kleeman, M. J.; Schauer, J. J.; Cass, G. R. Size and Composition Distribution of Fine Particulate Matter Emitted from Wood Burning, Meat Charbroiling, and Cigarettes. *Environ. Sci. Technol.* **1999**, *33*, 3516−3523.
(415) Schauer, J. J.; Kleeman, M. J.; Cass, G. R.; Simoneit, B. R. T. Measurement of Emissions from Air Pollution Sources. 3. C_1−C_{29} Organic Compounds from Fireplace Combustion of Wood. *Environ. Sci. Technol.* **2001**, *35*, 1716−1728.
(416) Li, G. H.; Zhang, R. Y.; Fan, J. W.; Tie, X. X. Impacts of Biogenic Emissions on Photochemical Ozone Production in Houston, Texas. *J. Geophys. Res.* **2007**, *112*, DOI: 10.1029/2006jd007924, D10309.
(417) Guenther, A.; Karl, T.; Harley, P.; Wiedinmyer, C.; Palmer, P. I.; Geron, C. Estimates of Global Terrestrial Isoprene Emissions Using MEGAN (Model of Emissions of Gases and Aerosols from Nature). *Atmos. Chem. Phys.* **2006**, *6*, 3181−3210.
(418) Guenther, A. B.; Jiang, X.; Heald, C. L.; Sakulyanontvittaya, T.; Duhl, T.; Emmons, L. K.; Wang, X. The Model of Emissions of Gases and Aerosols from Nature Version 2.1 (MEGAN2.1): An Extended and Updated Framework for Modeling Biogenic Emissions. *Geosci. Model Dev.* **2012**, *5*, 1471−1492.
(419) Efstathiou, C.; Isukapalli, S.; Georgopoulos, P. A Mechanistic Modeling System for Estimating Large-Scale Emissions and Transport of Pollen and Co-Allergens. *Atmos. Environ.* **2011**, *45*, 2260−2276.
(420) Choi, Y. J.; Fernando, H. J. S. Implementation of a Windblown Dust Parameterization into MODELS-3/CMAQ: Application to Episodic PM Events in the US/Mexico Border. *Atmos. Environ.* **2008**, *42*, 6039−6046.
(421) Gillette, D. A.; Passi, R. Modeling Dust Emission Caused by Wind Erosion. *J. Geophys. Res.* **1988**, *93*, 14233−14242.
(422) Shaw, W. J.; Allwine, K. J.; Fritz, B. G.; Rutz, F. C.; Rishel, J. P.; Chapman, E. G. Evaluation of the Wind Erosion Module in DUSTRAN. *Atmos. Environ.* **2008**, *42*, 1907−1921.
(423) Atkinson, R.; Baulch, D. L.; Cox, R. A.; Crowley, J. N.; Hampson, R. F.; Hynes, R. G.; Jenkin, M. E.; Rossi, M. J.; Troe, J. Evaluated Kinetic and Photochemical Data for Atmospheric Chemistry: Volume I—Gas Phase Reactions of O_x, HO_x, NO_x and SO_x Species. *Atmos. Chem. Phys.* **2004**, *4*, 1461−1738.
(424) Atkinson, R.; Arey, J. Atmospheric Degradation of Volatile Organic Compounds. *Chem. Rev.* **2003**, *103*, 4605−4638.
(425) Atkinson, R. Atmospheric Chemistry of VOCs and NO_x. *Atmos. Environ.* **2000**, *34*, 2063−2101.
(426) Gery, M. W.; Whitten, G. Z.; Killus, J. P.; Dodge, M. C. A Photochemical Kinetics Mechanism for Urban and Regional Scale Computer Modeling. *J. Geophys. Res.* **1989**, *94*, 12925−12956.
(427) Yarwood, G.; Rao, S.; Yocke, M.; Whitten, G. Z. *Updates to the Carbon Bond Chemical Mechanism: CB05*; Final Report RT-0400675 to the U.S. EPA; U.S. EPA: Research Triangle Park, NC, 2005. http://www.camx.com/publ/pdfs/CB05_Final_Report_120805.pdf (accessed Jan 2, 2015).
(428) Sarwar, G.; Luecken, D.; Yarwood, G.; Whitten, G. Z.; Carter, W. P. L. Impact of an Updated Carbon Bond Mechanism on Predictions from the CMAQ Modeling System: Preliminary Assessment. *J. Appl. Meteorol. Climatol.* **2008**, *47*, 3−14.
(429) Stockwell, W. R.; Middleton, P.; Chang, J. S.; Tang, X. The Second Generation Regional Acid Deposition Model Chemical Mechanism for Regional Air Quality Modeling. *J. Geophys. Res.* **1990**, *95*, 16343−16367.
(430) Stockwell, W. R.; Kirchner, F.; Kuhn, M.; Seefeld, S. A New Mechanism for Regional Atmospheric Chemistry Modeling. *J. Geophys. Res.* **1997**, *102*, 25847−25879.
(431) Carter, W. P. L. *Documentation of the SAPRC-99 Chemical Mechanism for VOC Reactivity Assessment*; Report to the California Air Resources Board; Center for Environmental Research & Technology, University of California—Riverside (UCR): Riverside, CA, 2000. http://cert.ucr.edu/~carter/absts.htm#saprc99 and http://www.cert.ucr.edu/~carter/reactdat.htm (accessed Jan 2, 2015).
(432) Carter, W. P. L. Development of the SAPRC-07 Chemical Mechanism. *Atmos. Environ.* **2010**, *44*, 5324−5335.
(433) Carter, W. P. L. Development of a Condensed SAPRC-07 Chemical Mechanism. *Atmos. Environ.* **2010**, *44*, 5336−5345.
(434) Carter, W. P. L.; Heo, G. *Development of Revised SAPRC Aromatics Mechanisms*; Final Report to the California Air Resources Board, Contracts No. 07-730 and 08-326; 2012. http://www.engr.ucr.edu/~carter/SAPRC/saprc11.pdf (accessed Jan 2, 2015).
(435) Jenkin, M. E.; Saunders, S. M.; Pilling, M. J. The Tropospheric Degradation of Volatile Organic Compounds: A Protocol for Mechanism Development. *Atmos. Environ.* **1997**, *31*, 81−104.
(436) Jenkin, M. E.; Saunders, S. M.; Wagner, V.; Pilling, M. J. Protocol for the Development of the Master Chemical Mechanism, MCM V3 (Part B): Tropospheric Degradation of Aromatic Volatile Organic Compounds. *Atmos. Chem. Phys.* **2003**, *3*, 181−193.
(437) Saunders, S. M.; Jenkin, M. E.; Derwent, R. G.; Pilling, M. J. Protocol for the Development of the Master Chemical Mechanism, MCM v3 (Part A): Tropospheric Degradation of Non-Aromatic Volatile Organic Compounds. *Atmos. Chem. Phys.* **2003**, *3*, 161−180.
(438) Jimenez, P.; Baldasano, J. M.; Dabdub, D. Comparison of Photochemical Mechanisms for Air Quality Modeling. *Atmos. Environ.* **2003**, *37*, 4179−4194.
(439) Li, J.; Zhang, H.; Ying, Q. Comparison of the SAPRC07 and SAPRC99 Photochemical Mechanisms during a High Ozone Episode in Texas: Differences in Concentrations, OH Budget and Relative Response Factors. *Atmos. Environ.* **2012**, *54*, 25−35.
(440) Ying, Q.; Li, J. Implementation and Initial Application of the Near-Explicit Master Chemical Mechanism in the 3D Community Multiscale Air Quality (CMAQ) Model. *Atmos. Environ.* **2011**, *45*, 3244−3256.
(441) Zaveri, R. A.; Easter, R. C.; Fast, J. D.; Peters, L. K. Model for Simulating Aerosol Interactions and Chemistry (MOSAIC). *J. Geophys. Res.* **2008**, *113*, DOI: 10.1029/2007jd008782.
(442) Zhang, Y.; McMurry, P. H.; Yu, F.; Jacobson, M. Z. A Comparative Study of Nucleation Parameterizations: 1. Examination and Evaluation of the Formulations. *J. Geophys. Res.* **2010**, *115*, DOI: 10.1029/2010jd014150.
(443) Zhang, Y.; Liu, P.; Liu, X.-H.; Jacobson, M. Z.; McMurry, P. H.; Yu, F.; Yu, S.; Schere, K. L. A Comparative Study of Nucleation

DOI: 10.1021/acs.chemrev.5b00067
Chem. Rev. 2015, 115, 3803−3855

Parameterizations: 2. Three-Dimensional Model Application and Evaluation. *J. Geophys. Res.* **2010**, *115*, DOI: 10.1029/2010jd014151.
(444) Zhang, Y.; Seigneur, C.; Seinfeld, J. H.; Jacobson, M.; Clegg, S. L.; Binkowski, F. S. A Comparative Review of Inorganic Aerosol Thermodynamic Equilibrium Modules: Similarities, Differences, and Their Likely Causes. *Atmos. Environ.* **2000**, *34*, 117−137.
(445) Clegg, S. L.; Brimblecombe, P.; Wexler, A. S. Thermodynamic Model of the System H^+−NH_4^+−Na^+−SO_4^{2-}−NO_3^-−Cl^-−H_2O at 298.15 K. *J. Phys. Chem. A* **1998**, *102*, 2155−2171.
(446) Nenes, A.; Pandis, S. N.; Pilinis, C. ISORROPIA: A New Thermodynamic Equilibrium Model for Multiphase Multicomponent Inorganic Aerosols. *Aquat. Geochem.* **1998**, *4*, 123−152.
(447) Fountoukis, C.; Nenes, A. ISORROPIA II: A Computationally Efficient Thermodynamic Equilibrium Model for K^+−Ca^{2+}−Mg^{2+}−NH_4^+−Na^+−SO_4^{2-}−NO_3^-−Cl^-−H_2O Aerosols. *Atmos. Chem. Phys.* **2007**, *7*, 4639−4659.
(448) Robinson, R. A.; Stokes, R. H. *Electrolyte Solutions*, 2nd revised ed.; Dover Publications, Inc.: Mineola, NY, 2012.
(449) Zhang, M. G.; Uno, I.; Yoshida, Y.; Xu, Y. F.; Wang, Z. F.; Akimoto, H.; Bates, T.; Quinn, T.; Bandy, A.; Blomquist, B. Transport and Transformation of Sulfur Compounds over East Asia during the Trace-P and Ace-Asia Campaigns. *Atmos. Environ.* **2004**, *38*, 6947−6959.
(450) Evans, M. J.; Jacob, D. J. Impact of New Laboratory Studies of N_2O_5 Hydrolysis on Global Model Budgets of Tropospheric Nitrogen Oxides, Ozone, and OH. *Geophys. Res. Lett.* **2005**, *32*, DOI: 10.1029/2005gl022469.
(451) Ying, Q.; Lu, J.; Kleeman, M. J. Modeling Air Quality during the California Regional $PM_{10}/PM_{2.5}$ Air Quality Study (CRPAQS) Using the UCD/CIT Sourceoriented Air Quality Model—Part III. Regional Source Apportionment of Secondary and Total Airborne Particulate Matter. *Atmos. Environ.* **2009**, *43*, 419−430.
(452) Bertram, T. H.; Thornton, J. A. Toward a General Parameterization of N_2O_5 Reactivity on Aqueous Particles: The Competing Effects of Particle Liquid Water, Nitrate and Chloride. *Atmos. Chem. Phys.* **2009**, *9*, 8351−8363.
(453) Davis, J. M.; Bhave, P. V.; Foley, K. M. Parameterization of N_2O_5 Reaction Probabilities on the Surface of Particles Containing Ammonium, Sulfate, and Nitrate. *Atmos. Chem. Phys.* **2008**, *8*, 5295−5311.
(454) Riemer, N.; Vogel, H.; Vogel, B.; Schell, B.; Ackermann, I.; Kessler, C.; Hass, H. Impact of the Heterogeneous Hydrolysis of N_2O_5 on Chemistry and Nitrate Aerosol Formation in the Lower Troposphere under Photosmog Conditions. *J. Geophys. Res.* **2003**, *108*, 4144.
(455) Vogel, B.; Vogel, H.; Kleffmann, J.; Kurtenbach, R. Measured and Simulated Vertical Profiles of Nitrous Acid—Part II. Model Simulations and Indications for a Photolytic Source. *Atmos. Environ.* **2003**, *37*, 2957−2966.
(456) Zheng, B.; Zhang, Q.; Zhang, Y.; He, K. B.; Wang, K.; Zheng, G. J.; Duan, F. K.; Ma, Y. L.; Kimoto, T. Heterogeneous Chemistry: A Mechanism Missing in Current Models To Explain Secondary Inorganic Aerosol Formation during the January 2013 Haze Episode in North China. *Atmos. Chem. Phys. Discuss.* **2014**, *14*, 16731−16776.
(457) Wang, K.; Zhang, Y.; Nenes, A.; Fountoukis, C. Implementation of Dust Emission and Chemistry into the Community Multiscale Air Quality Modeling System and Initial Application to an Asian Dust Storm Episode. *Atmos. Chem. Phys.* **2012**, *12*, 10209−10237.
(458) Li, J.; Ying, Q.; Yi, B.; Yang, P. Role of Stabilized Criegee Intermediates in the Formation of Atmospheric Sulfate in Eastern United States. *Atmos. Environ.* **2013**, *79*, 442−447.
(459) Sarwar, G.; Fahey, K.; Kwok, R.; Gilliam, R. C.; Roselle, S. J.; Mathur, R.; Xue, J.; Yu, J.; Carter, W. P. L. Potential Impacts of Two SO_2 Oxidation Pathways on Regional Sulfate Concentrations: Aqueous-Phase Oxidation by NO_2 and Gas-Phase Oxidation by Stabilized Criegee Intermediates. *Atmos. Environ.* **2013**, *68*, 186−197.
(460) Ying, Q.; Cureño, I. V.; Chen, G.; Ali, S.; Zhang, H.; Malloy, M.; Bravo, H. A.; Sosa, R. Impacts of Stabilized Criegee Intermediates, Surface Uptake Processes and Higher Aromatic Secondary Organic Aerosol Yields on Predicted $PM_{2.5}$ Concentrations in the Mexico City Metropolitan Zone. *Atmos. Environ.* **2014**, *94*, 438−447.
(461) Pandis, S. N.; Wexler, A. S.; Seinfeld, J. H. Secondary Organic Aerosol Formation and Transport-II. Predicting the Ambient Secondary Organic Aerosol-Size Distribution. *Atmos. Environ., A: Gen. Top.* **1993**, *27*, 2403−2416.
(462) Carlton, A. G.; Bhave, P. V.; Napelenok, S. L.; Edney, E. O.; Sarwar, G.; Pinder, R. W.; Pouliot, G. A.; Houyoux, M. Model Representation of Secondary Organic Aerosol in CMAQ v4.7. *Environ. Sci. Technol.* **2010**, *44*, 8553−8560.
(463) Liao, H.; Henze, D. K.; Seinfeld, J. H.; Wu, S. L.; Mickley, L. J. Biogenic Secondary Organic Aerosol over the United States: Comparison of Climatological Simulations with Observations. *J. Geophys. Res.* **2007**, *112*, DOI: 10.1029/2006jd007813.
(464) Topping, D.; Barley, M.; McFiggans, G. Including Phase Separation in a Unified Model To Calculate Partitioning of Vapours to Mixed Inorganic-Organic Aerosol Particles. *Faraday Discuss.* **2013**, *165*, 273−288.
(465) Zuend, A.; Seinfeld, J. H. Modeling the Gas-Particle Partitioning of Secondary Organic Aerosol: The Importance of Liquid-Liquid Phase Separation. *Atmos. Chem. Phys.* **2012**, *12*, 3857−3882.
(466) Griffin, R. J.; Dabdub, D.; Kleeman, M. J.; Fraser, M. P.; Cass, G. R.; Seinfeld, J. H. Secondary Organic Aerosol—3. Urban/Regional Scale Model of Size- and Composition-Resolved Aerosols. *J. Geophys. Res.* **2002**, *107*, 4334.
(467) Chen, J. J.; Ying, Q.; Kleeman, M. J. Source Apportionment of Wintertime Secondary Organic Aerosol during the California Regional $PM_{10}/PM_{2.5}$ Air Quality Study. *Atmos. Environ.* **2010**, *44*, 1331−1340.
(468) Robinson, A. L.; Donahue, N. M.; Shrivastava, M. K.; Weitkamp, E. A.; Sage, A. M.; Grieshop, A. P.; Lane, T. E.; Pierce, J. R.; Pandis, S. N. Rethinking Organic Aerosols: Semivolatile Emissions and Photochemical Aging. *Science* **2007**, *315*, 1259−1262.
(469) Johnson, D.; Utembe, S. R.; Jenkin, M. E. Simulating the Detailed Chemical Composition of Secondary Organic Aerosol Formed on a Regional Scale during the TORCH 2003 Campaign in the Southern UK. *Atmos. Chem. Phys.* **2006**, *6*, 419−431.
(470) Lee-Taylor, J.; Madronich, S.; Aumont, B.; Baker, A.; Camredon, M.; Hodzic, A.; Tyndall, G. S.; Apel, E.; Zaveri, R. A. Explicit Modeling of Organic Chemistry and Secondary Organic Aerosol Partitioning for Mexico City and Its Outflow Plume. *Atmos. Chem. Phys.* **2011**, *11*, 13219−13241.
(471) Li, J.; Cleveland, M.; Ziemba, L. D.; Griffin, R. J.; Barsanti, K. C.; Pankow, J. F.; Ying, Q. Modeling Regional Secondary Organic Aerosol Using the Master Chemical Mechanism. *Atmos. Environ.* **2015**, *102*, 52−61.
(472) Ervens, B.; Volkamer, R. Glyoxal Processing by Aerosol Multiphase Chemistry: Towards a Kinetic Modeling Framework of Secondary Organic Aerosol Formation in Aqueous Particles. *Atmos. Chem. Phys.* **2010**, *10*, 8219−8244.
(473) Karambelas, A.; Pye, H. O. T.; Budisulistiorini, S. H.; Surratt, J. D.; Pinder, R. W. Contribution of Isoprene Epoxydiol to Urban Organic Aerosol: Evidence from Modeling and Measurements. *Environ. Sci. Technol. Lett.* **2014**, *1*, 278−283.
(474) Knote, C.; Hodzic, A.; Jimenez, J. L.; Volkamer, R.; Orlando, J. J.; Baidar, S.; Brioude, J.; Fast, J.; Gentner, D. R.; Goldstein, A. H.; Hayes, P. L.; Knighton, W. B.; Oetjen, H.; Setyan, A.; Stark, H.; Thalman, R.; Tyndall, G.; Washenfelder, R.; Waxman, E.; Zhang, Q. Simulation of Semi-Explicit Mechanisms of SOA Formation from Glyoxal in Aerosol in a 3-D Model. *Atmos. Chem. Phys.* **2014**, *14*, 6213−6239.
(475) Ying, Q.; Kleeman, M. Regional Contributions to Airborne Particulate Matter in Central California during a Severe Pollution Episode. *Atmos. Environ.* **2009**, *43*, 1218−1228.
(476) Almanza, V. H.; Molina, L. T.; Li, G.; Fast, J.; Sosa, G. Impact of External Industrial Sources on the Regional and Local SO_2 and O_3 Levels of the Mexico Megacity. *Atmos. Chem. Phys.* **2014**, *14*, 8483−8499.
(477) Hodzic, A.; Aumont, B.; Knote, C.; Lee-Taylor, J.; Madronich, S.; Tyndall, G. Volatility Dependence of Henry's Law Constants of

DOI: 10.1021/acs.chemrev.5b00067
Chem. Rev. 2015, 115, 3803−3855

Condensable Organics: Application To Estimate Depositional Loss of Secondary Organic Aerosols. *Geophys. Res. Lett.* **2014**, *41*, 4795−4804.
(478) Venkatram, A.; Pleim, J. The Electrical Analogy Does Not Apply to Modeling Dry Deposition of Particles. *Atmos. Environ.* **1999**, *33*, 3075−3076.
(479) Zhang, L. M.; Gong, S. L.; Padro, J.; Barrie, L. A. A Size-Segregated Particle Dry Depostion Scheme for an Atmospheric Aerosol Module. *Atmos. Environ.* **2001**, *35*, 549−560.
(480) Cherin, N.; Roustan, Y.; Musson-Genon, L.; Seigneur, C. Modelling Atmospheric Dry Deposition in Urban Areas Using an Urban Canopy Approach. *Geosci. Model Dev. Discuss.* **2014**, *7*, 8703−8756.
(481) Ramanathan, V.; Li, F.; Ramana, M. V.; Praveen, P. S.; Kim, D.; Corrigan, C. E.; Nguyen, H.; Stone, E. A.; Schauer, J. J.; Carmichael, G. R.; Adhikary, B.; Yoon, S. C. Atmospheric Brown Clouds: Hemispherical and Regional Variations in Long-Range Transport, Absorption, and Radiative Forcing. *J. Geophys. Res.* **2007**, *112*, DOI: 10.1029/2006jd008124.
(482) Ramanathan, V.; Carmichael, G. Global and regional climate changes due to black carbon. *Nat. Geosci.* **2008**, *1*, 221−227.
(483) Lee-Taylor, J.; Hodzic, A.; Madronich, S.; Aumont, B.; Camredon, M.; Valorso, R. Multiday Production of Condensing Organic Aerosol Mass in Urban and Forest Outflow. *Atmos. Chem. Phys.* **2015**, *15*, 595−615.
(484) Li, Z.; Schwier, A. N.; Sareen, N.; McNeill, V. F. Reactive processing of formaldehyde and acetaldehyde in aqueous aerosol mimics: surface tension depression and secondary organic products. *Amos. Chem. Phys.* **2011**, *11*, 11617−11629.
(485) Zhu, T.; Melamed, M. L.; Parrish, D.; Gauss, M.; Klenner, L. G.; Lawrence, M. G.; Konare, A.; Liousse, C. *WMO/IGAC Impacts of Megacities on Air Pollution and Climate*; GAW Report No. 205; World Meteorological Organization (WMO)/International Global Atmospheric Chemistry (IGAC): Geneva, Switzerland, 2012. http://www.wmo.int/pages/prog/arep/gaw/documents/Final_GAW_205.pdf (accessed Jan 2, 2015).

DOI: 10.1021/acs.chemrev.5b00067
Chem. Rev. 2015, 115, 3803−3855